Design and engineering of electrospun fibres for oil spill clean-up

A thesis submitted to

University College London

For the degree of

Doctor of Philosophy

By

Muftau Jide Akanbi

Department of Mechanical Engineering

University College London

July, 2018

Declaration

I, Muftau Jide Akanbi confirm that the work in this thesis is mine and where information has been derived from other sources, I confirm that this has been duly referenced in this thesis.

Abstract

The superior oil sorption performance of electrospun polystyrene (PS)/PS-based fibres has rendered its use more competitive than the commercial melt blown polypropylene (PP) fibres. However, on a microscale level, the oil - sorbent interaction and its effect on the sorption behaviour is yet to be fully understood; considering PP polymer is known to have a lower surface energy than polystyrene. Furthermore, the commercialisation of electrospun PS sorbent has been hindered due to the poor mechanical strength of the fibre mats particularly after oil sorption. Therefore, the aim of this thesis is to (1) enhance the understanding of the oil sorption behaviour of electrospun PS fibres (single filament level) and (2) to explore ways to effectively enhance the mechanical properties of the PS fibre mat.

The oil adherence potential of filaments of electrospun PS and subsequent comparison with filaments of the commercial melt blown PP sorbent was quantitatively evaluated using drop-on-fibre micro-sorption technique. This was preceded by a systematic optimisation of the electrospinning process, 20% w/w concentration of PS dissolved in DMF/THF (4:1) gave fibres with the best morphology for the micro-sorption test. Further experiments showed single filaments of electrospun PS to exhibit the strongest affinity to the two oils tested, with a mean adhesive energy of 18.0×10^{-13}J and 26.2×10^{-13}J for sunflower and motor oil respectively. This represents values $3 - 6$ times higher than those recorded for single filaments of the PP counterparts. The superior oil adsorptivity of PS fibre was attributed to its chemical structure i.e. the presence of aromatic phenyl group in its structure.

For the second aim of this thesis, a single step electrospinning method of blending PS and thermoplastic polyurethane PU polymers in different weight ratio of PSPU polymer blend was explored, using either a Flat Collector (FC) or a Drum Collector (DC) system. This was done in order to enhance the mechanical properties of PS fibres. The method is a simple, cost-effective engineering approach and exhibits great potential. The ultimate tensile strength (UTS) and elongation at UTS were seen to rise with increased PU content. Samples of PSPU ratio 6:4 fabricated using a DC system (PSPU_DC 6:4) and those fabricated using the FC system (PSPU_FC 6:4) recorded a 600% and 1000% increase in tensile strength respectively, in comparison to the pure PS mat. The oil sorption and retention capacities was seen to be dependent on several variables including the fibre collection system. Post treatment of the fibre mat using heat treatment around the polymer glass transition temperature (110ºC) was seen to induce inter-fibre bonds, with the amount of bonds seen to rise with increase in treatment temperature. This causes a simultaneous increase in tensile strength.

The work presented in this thesis has pioneered some key aspects that will take electrospinning of polymer fibres further. In terms of characterization, it is the first to quantitatively evaluate the oil adsorptivity of filaments of electrospun PS and melt blown polypropylene sorbents. This creates fundamental insight into the sorption mechanism at a micro-scale level to aid the design of future and improved electrospun sorbents. Also, the electrospinning of PS and PU presented in this thesis, is the first time polymer blend of both polymers is being electrospun for any application, with detailed characterisation of the bi-component fibres presented.

Research Impact Statement

This research investigates the potential of electrospun polymer fibres as sorbents for oil spill remediation. The abstract has summarised the major content and key findings of the study, this section however, highlights the potential academic, economic and industrial impact of the research.

The superior sorption performance of electrospun PS/PS-based mats over the commercial, melt blown PP sorbent has been well established in literature. These previous studies have been based on the macro-scale structure. The novelty of the study presented in this thesis lies in the microscale evaluation of the oil adsorptivity of single filaments of these mats. The research bridges the gap that exist in literature over the lack of data on the micro-scale level interactions between the oils and the fibres. It presents a quantitative means of estimating the oil adherence of fibres to selected oil types and also provides a basis for comparing the oil affinity of different polymer fibres down to the microscale level (of a single filament of the fibre). This will provide characterisation data for different polymer fibres and will help in the choice of polymers in the design of future electrospun sorbent. In this thesis, the superior oil adhesive energy reported for electrospun PS filaments, is an indication that in addition to the mat architecture, other factors such as polymer chemistry is a key consideration in the design of electrospun oil sorbents.

In addition, the wetting envelope presented in chapter 4, further elucidates the importance of polymer inherent properties (chemistry) in the design of these oil sorbents.

Despite the increasing research on the use of electrospun polymer fibres as a possible replacement for the commercial PP sorbent, one of the limiting factors to its commercialisation has been its poor mechanical strength. Electrospinning of blends of PS and PU polymers presented in chapter 5, represents a frugal approach at enhancing the mechanical properties of electrospun sorbents down to a single filament level. The method avoids the use of complex needle configuration, multiple voltage and pump systems, and also allow molecular interactions between both polymers. This makes it an economical and efficient approach than the multi-nozzle and coaxial electrospinning of both polymers reported in literature. This will saves time and cost associated with the use of a post treatment method to enhance the mechanical properties of these fibres.

Acknowledgement

Dedication

In loving memory of my parents; Alhaji Abdul-Kareem Akanbi and Alhaja Belawu

Akanbi

Table of Contents

List of Figures

List of Tables

Nomenclature

A	Cross sectional area
A_L	Liquid surface area
A_{SL}	Solid liquid interface area
a	Acceleartion
C	Conductivity
D	Diameter
d	Deformation
E	Electric field
E_{act}	Actual adhesive energy
E^r	Reduced adhesive energy
E_S	Sample modulus
E_{tip}	Cantilever tip modulus
E_*	Reduced modulus
F_{adh}	Adhesion force
F_{tip}	Force on cantilever tip
f_a	Fractional area in contact with air
f_s	Fractional solid surface area
g	Gravity
g/g	Grams per gram
H	Gap distance
J	Joules
K	Cell constant
L	Capillary tube length
L^r	Reduced drop length
m	Mass
n	Reduced drop height
P	Density
R	Radius
R_t	Electrical resistant

r	Roughness factor
T_d	Decomposition temperature
T_g	Glass transition temperature
T_m	Melting temperature
V	Volume
V_{act}	Actual drop volume
V_C	Critical Potential
V^r	Reduced drop volume
w/w	Weight by weight
w_1	Weight of sorbent after draining
w_o	Weight of dry sorbent
W_A	Work of Adhesion
w_w	Weight of water
θ	Static contact angle
θ_a	Intrinsic contact angle in air
θ_s	Intrinsic contact angle on solid
θ^*	Apparent contact angle
δ	Resistivity
q	Charge density
λ	Wavelength
γ	Surface tension
γ_L^d	Dispersive component of liquid surface tension
γ_S^d	Dispersive component of solid surface free energy
γ_L^p	Polar component of liquid surface tension
γ_S^P	Polar component of solid surface free energy
γ_S	Solid surface energy
γ_{SL}	Interfacial energy between the solid and liquid interface
γ_L	Liquid surface tension
v_s	Poisson ratio of sample
v_{tip}	Poisson ratio of tip

Abbreviations

AFD	Average fibre diameter
AFM	Atomic force microscopy
ATR	Attenuated total reflectance
BSE	Backscattered electrons
BP	British petroleum
CA	Contact angle
CD	Cross direction
DC	Drum collector
DMF	N`N Dimethylformamide
DMT	Derjaguin-Muller-Toporov
DSC	Differential scanning calorimetry
DWH	Deep water horizon
EDX	Energy dispersive x-ray spectroscopy
EtOH	Ethanol
EU	European Union
FC	Flat collector
FESEM	Field Emission Scanning Electron Microscope
FTIR	Fourier transform and infrared spectroscopy
HT	Heat treatment
IARC	International agency for research on cancer
MD	Machine direction
MO	Motor oil
OWRK	Owen wendt rabel kaebel
PAH	Polycyclic aromatic hydrocarbon
PAN	Poly acrylonitrile
PDLA	Poly (D, L-lactic) acid
PEO	Polyethylene oxide
PMMA	Poly (methyl methacrylate) acid

PP	Polypropylene
PS	Polystyrene
PU	Polyurethane
PVA	Poly (vinylalcohol)
PVC	poly vinylchloride
RPM	Rotation per minute
QNM	Quantitative nanomechanical
SC	Sorption capacity
SE	Secondary electrons
SEM	Scanning electron microscope
SFE	Surface free energy
SO	Sunflower oil
TCD	Tip to collector distance
TGA	Thermogravimetric analysis
THF	Tetrahydrofuran
TPE	Thermoplastic elastomer
TPU	Thermoplastic polyurethane
UT	Ultrasonic energy treatment
UTS	Ultimate tensile strength
WCA	Water contact angle
XRD	X-ray Diffraction

1 Introduction

1.1 Background and research motivation

Oil is one of the most important sources of energy and raw material for most industrial processes (chemical, petrochemical and pharmaceutical plants). A rising trend in its global consumption has been seen and attributed to the increasing world's population and the sudden rise of emerging economies [1]. Considering this, activities such as oil exploration, production, transportation and storage operations [2-4], will continue to make oil spill a potential risk to the environment. In 2013, the annual global petroleum-based and vegetable oil consumption was reported to be in excess of 100 and 92 million tonnes respectively [5]. Also, between 2010 and 2013, an estimation of global marine oil spill was 22,000 tonnes, forming an oil film covering over 12 km^2 per tonne [6] of ocean surface.

Though marine oil spills account for just a fraction of global incidences of oil spills, they have enormous economic and environmental impact; putting aquatic organism at risk. The Exxon Valdez oil disaster in Prince Williams Sound Alaska in 1989 was reported to have led to the death of over 250,000 marine birds, 2800 sea otters and 22 killer whales [7, 8]. In the BP deep water horizon (DWH) disaster of 2010; 2200 marine birds, fishes, sea weeds and shell were reported to have been affected in just two months following the spill, with clean-up cost, claims and litigation running to billions of dollars in both incidences [7]. Hence, it is imperative that when spills occur it is timely and effectively cleaned up.

Current strategies used in oil spill clean-up are categorized into chemical (in-situ burning and the use of dispersant), physical (skimmers, booms and sorbent) and biological methods (bioremediation techniques) [9-11]. In the event of an oil spill, these methods often complements one another, as no particular method best apply to all spill situations. However, the use of sorbent is regarded as one of the most economical and efficient ways of mopping up oil spills, due to its ability to facilitate oil recovery by concentrating and transforming the liquid oil into a semi-solid state [2, 8, 12]. Sorbents also have the ability to completely eradicate oil spills if timely and effectively deployed. It is a technique applicable on both land and water, could be used as coalescing filters for separating oil in water emulsions[13] and in mopping up Polycyclic Aromatic Hydrocarbon (PAH)[14]; - a material classified by the EU and IARC as having carcinogenic, mutagenic and teratogenic effects[15]. The material commercially available for use as sorbent is melt blown polypropylene fibres, but this material suffers from low oil sorption capacity of approximately 15 - 20g/g, due to large fibre diameter and inter-fibre void spaces [12, 16-18].

In a bid to develop a more efficient sorbent, electrospinning, a technology capable of producing fibres from polymer solution with fibre diameters in the range of tens of microns to sub-micron sizes, has been explored with polystyrene (PS) polymer [16, 19]. This novel fibrous material exhibits a better sorption capacity of 5 – 9 times those of the commercial PP sorbent. Despite its superior sorption performance, it exhibits low mechanical strength particularly after sorption [20]. For electrospun PS/PS-based mat to become commercially viable, there is the need to enhance its mechanical strength. Also, having a better understanding of the sorption mechanisms of this fibrous mat will help facilitate the design of a more efficient electrospun sorbent that will address some of the present limitations.

1.2   Thesis aims and objectives

Recent studies have shown the superior oil sorption performance of electrospun PS/PS based fibre mats over meltblown PP fibres [16, 19], with credit for this attributed to the mat architecture. The first part of this thesis aim to study the contributions of individual fibres of both sorbent to the oil sorption behaviour of the bulk (macroscale) fibre mats. This will be investigated through a microscale evaluation of the oil adsorptivity of individual filaments to selected oils, using the drop-on-fibre micro-sorption technique. This is a novel approach being used for the first time to compare the oil affinity of both electrospun polystyrene PS and meltblown polypropylene PP fibre. It is hoped that fundamental insights into the sorption behaviour of both materials will be obtained, this will aid material selectin in the design of future electrospun sorbents.

The second part of this thesis aim to explore different techniques that could enhance the mechanical behaviour of the electrospun fibre mat. Polymer blending with thermoplastic polyurethane (PU) will be explored, as this offers a simple approach that lacks the complexities of co-axial and multi-nozzle side-by-side electrospinning of both polymers previously reported in literature [21, 22]. Detailed physicochemical, thermal, mechanical and oil sorption characterisation of the resulting novel fibres will be presented.

Two post treatment techniques - heat and ultrasonic treatment will also be explored with detailed sorption and mechanical characterisation also presented.

1.3   Thesis outline

This thesis is comprised of seven chapters, with the **first chapter** (**Chapter 1**) detailing a brief background and motivation for the research, the novelty of the approach used and a more detailed thesis outline.

Chapter 2 gives a detailed literature review with the first part covering electrospinning, the technology used for the fibre production. A review of the theory governing the process and key parameters that could influence the process and morphology of the fibres produced are discussed. An overview of oil spills, the polymers used and some key theoretical background for the concepts used in this thesis.

Chapter 3 provides detailed materials and experimental methods. It describes parts fabricated for an experimental procedure and the characterisation studies carried out.

Chapter 4 details the optimisation study of electrospinning PS polymer solutions. It shows the drop-on-fibre micro-sorption experiment, with the evaluation of oil adsorptivity and adhesiveness of both electrospun PS and melt blown PP fibres.

Chapter 5 investigates the feasibility of enhancing the mechanical properties of electrospun fibres using polymer blend approach. Detailed physicochemical, thermal, mechanical and sorption characterisation of the novel composite fibre is presented.

Chapter 6 explores the feasibility of using heat and ultrasonic treatments as two separate post treatment strategies to enhance the mechanical properties of electrospun PS fibre mats previously optimised in chapter 4. Detailed physico-chemical, mechanical and sorption characterisation of the fibres are also presented.

Chapter 7 concludes the findings of this this study and recommendations for further studies are also proposed.

2 Literature Review

2.1 Introduction to electrospinning

Electrospinning is a fibre fabrication technique capable of producing continuous fibres using polymeric solution or molten polymers, with diameter ranging from tens of nanometres to micrometre scale range [23-25]. It is a technology that has been widely explored over the past two decades due to its versatility in producing fibres from a wide range of materials (mostly polymers), the low cost of setting up in the laboratory and the ease of altering the properties of the fibres produced [25]. Studies have shown that the morphological structure of fibres can easily be manipulated by altering the conditions under which the fibres are produced or by incorporating other materials into the polymer solution/melt. This alters the functionality of the nano/microfibers [26, 27] depending on the intended application. The technology is currently being used in a wide variety of disciplines/fields, ranging from tissue engineering, filtration, opto-electronics, photonics, and energy [25-27]. It is a technique that can be used for environmental applications as well, such as sorbents, as will be explored in this thesis.

Schematic diagram of a typical laboratory electrospinning setup is illustrated in figure 2-1. It comprises basically of four main components; a high voltage supply, a grounded or negatively charged collector, a spinneret which holds the polymer droplet and a syringe pump to maintain a constant polymer flow. It is important to note that due to the versatility of this technique and the quest to increase its productivity, a number of different variant of this process has been reported. Process such as coaxial

electrospinning, bubble electrospinning, melt electrospinning, multi-nozzle electrospinning and multi-jet needleless spinning[28].

The process often involves inducing a voltage on a polymer droplet held at the tip of a spinneret/needle by its surface tension, while the collector a short distance away remains grounded or oppositely charged. When the applied voltage reaches a critical value, the electrostatic repulsive force overcomes the surface tension of the polymer solution/melt and a spinning jet of polymer is seen to erupt from the tip of the spinneret towards the oppositely charged or grounded collector [29, 30]. The jet is characterised by a region of bending instability as in moves further away from the spinneret tip where an initial stable jetting occurs [31]. The whipping instability causes stretching and thinning of the polymer jet accompanied by solvent evaporation, while the polymer chain entanglement prevents the jet from breaking, leading to the collection of fine fibres on the collector surface.

Setting up an electrospinning process in the laboratory may seems quite easy but the process of producing fibres with the desired properties is quite a complex one, owing to the need to balance the effect the of different parameters such as solution properties (concentration, molecular weight, viscosity, surface tension, conductivity), process conditions (Tip to collector distance, flow rate, and applied voltage) and ambient conditions (humidity and temperature). Hence, careful understanding of the fundamental principles that governs electrospinning, its theory and the influence of various contributory factors to jet evolution, propagation and the eventual fibre morphology needs to be understood. A detailed discussion of the aforementioned is presented in subsequent sections.
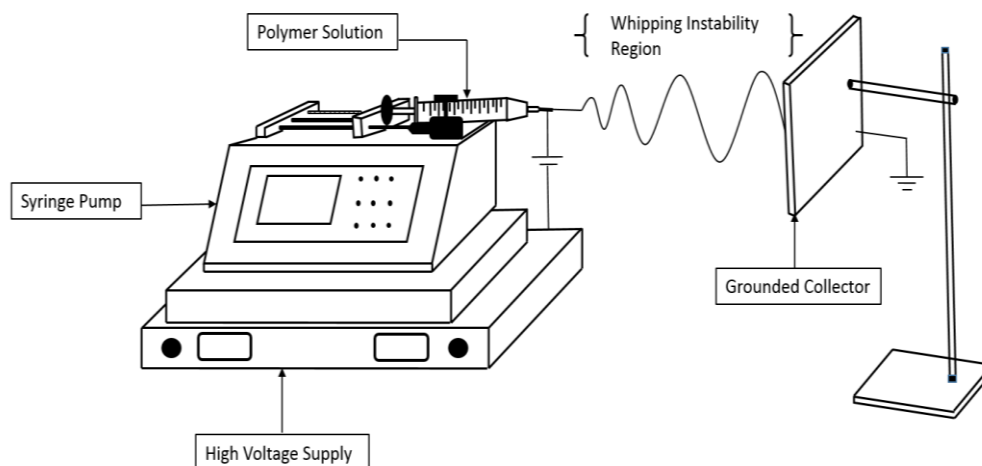
Figure 2-1: Schematic diagram of an electrospinning set-up showing the key components of a laboratory based horizontal configuration; i.e. high voltage supply, collector, continuous flow pump and polymeric solution

2.2 History of electrospinning

The term electrospinning is derived from the words "electrostatic spinning" and was first coined around 1994 [26, 29], but the principle behind the technology could be traced back to the late nineteenth and the beginning of the twentieth century.

One of the earliest detailed research on the excitation of liquids was carried out by Joseph Larmor in 1898 [32]. He derived an electrohydrodynamic theory that explains the excitation effect of an electric charge on a dielectric liquid. Four years later in 1902, two (2) US patents; patent no 692,631 and 705,691 by J.F Cooley [33] and W.J. Morton [34] respectively were filed. This inventions paved the way for further research into the principle of electrostatic spinning. Cooley in his patent described a phenomenon where a viscous polymer placed on a positively charge electrode and an electrode of opposite polarity (negatively charged) is placed in close proximity to it. This generates a cob web like collection of polymer on the negative electrode [33, 35].

Anton Formhal between 1934-1944, developed series of patent on electrospinning process and apparatus [36-39], with each successive patent being an improvement on the former. The first patent was on the production of polymer fibre on a movable collector from a solution of cellulose acetate, using acetone as solvent. Figure 2-2 shows a schematic diagram of a variant of Formhal`s invention, with the movable collector system clearly illustrated [36]. The invention demonstrated the need to allow fibres to dry before being collected on the substrate.  In the1960`s, Sir Geoffrey Taylor described what is today known as a Taylor Cone by observing the behaviour of a polymer droplet placed on a positive electrode, when subjected to an induced electric field [40, 41]. Peter Baumgartner, in 1971 [42] developed a device that could electrospin acrylic polymer with fibre diameters in the range of $0.05 – 1.1\mu m$, using a solution of acrylic copolymer dissolved in N`N-dimethyformamide. The experimental setup by Baumgarten includes; a positive displacement pump, a capillary tube to hold the polymer droplet, a grounded electrode and a high DC voltage supply. This creates the basis for the present day electrospinning set up.

Since the turn of the 21st century, there has been an upsurge in research on electrospinning, and it is estimated that there are over 200 research groups in different academic institutions and industries all over the world working on aspects of electrospinning technology [25, 30]. This could be attributed to the increasing popularity of nanotechnology and the acceptance of electrospinning as an important fibre fabrication technique, owing to its applicability in various fields of material research.

Fig. 6.   Fig. 7.   Fig. 8.

Fig. 9.

Fig. 10.
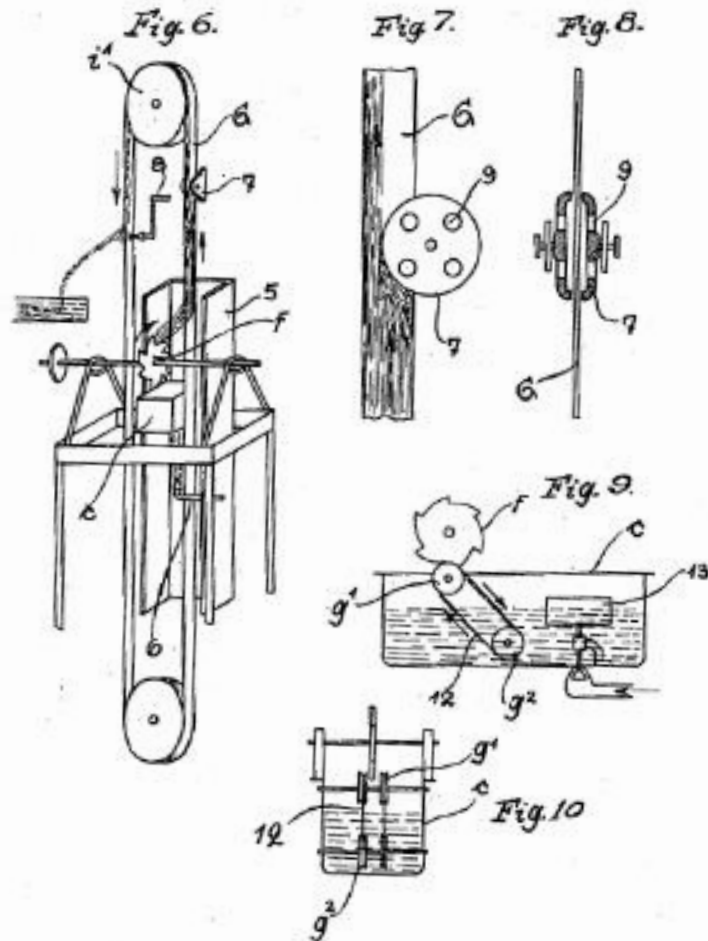
Figure 2-2: Anton Formhal patent describing the process and apparatus for preparing artificial thread. Taken from [36].

39

2.3 Theory of electrospinning process

Electrospinning as a process involves the complex interplay of rheological forces, electrical charges, temperature and mass transport, process and ambient conditions [43]. The process of jet formation to propagation and eventual solidification of the fibres, is an intricate electro-hydrodynamic process that needs to be carefully understood, in other to have control of the process for fibre morphology optimisation. It is a process that can be broadly categorized into three stages; jet initiation, jet elongation and jet solidification [44, 45].

2.3.1 Jet initiation

Polymeric solutions usually contains ions; both cations and anions in an electrically neutral state. The application of an external voltage to a polymer solution held in a spinneret/needle, causes the migration of ions of opposite polarity towards the electrode. This leads to a build-up of charges of same polarity as the induced voltage on any polymeric solution held in the spinneret and at the exit orifice of the spinneret. If the spinneret is charge with a negative voltage supply, cations in the polymer solution will be attracted towards the electrode while negative ions will move into the solution causing a build-up of anions on polymer droplet held at the spinneret tip. An opposite effect will occur in the case of an induced positive voltage (see Figure 2-3).
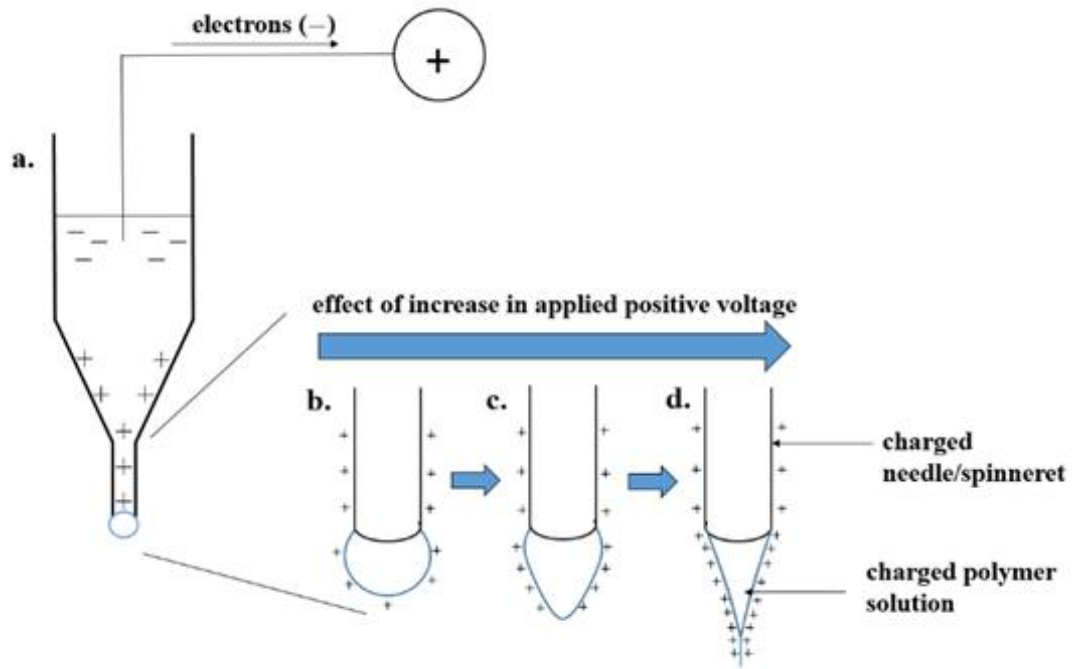
Figure 2-3: Schematic diagram; a.) Shows the effect of positively charged electrode on the charge build up in the polymer solution, (b-d) effect of increasing the positive voltage on polymer solution droplet held at the tip of the needle/spinneret. Note that an opposite effect will occur if negatively charge.

An increase in intensity of the induced voltage increases a charge build up on the polymer droplet at the tip of the spinneret, causing it to adopt a conical configuration, often called a Taylor cone [31, 44, 46]. The highest charge density is formed at the tip of the Taylor cone. When the applied voltage reaches a critical value, and able to overcome the inhibiting effect of surface tension and gravity, a spiral polymer jet erupts from the tip of the Taylor cone towards a collector, often grounded or charged with an opposite polarity. Sir Geoffrey Taylor, found the Taylor cone angle before jet initiation to be 49.3°[41], while the critical potential (V_C) that needs to be overcome for jet initiation was given by the below Equation[40];

$$V_C = \left[4 \left(\frac{H}{L} \right)^2 \left(\ln \frac{2L}{R} - 1.5 \right) 0.117\pi R\gamma \right]^{1/2}$$
(2-1)

41

where H represents the air gap distance, L is the capillary tube length (in this case the spinneret), R the radius of the capillary tube and γ the polymer surface tension in dyne/cm, while H, L and R measured in centimetres.

Over the years since Taylor found the angle prior to jet formation to be 49.3º, contradictory reports have been reported in literature, with Larrondo et al [47] independently verifying the angle to be 50º, while Yarin et al [48] had reported an angle 33.5º in a separate study.

It is worthy of note that after the jet initiation, the electrically driven jet travels in a straight line for a few centimetres[31] before spiralling radially into a conical jet during the jet elongation stage. During the straight jetting mode, the fibre diameter decreases monotonically with increasing distance from the tip [43] and this mode can occur with or without the formation of a Taylor cone depending on the process parameters employed.

2.3.2 Jet Elongation

This is the region where extensive jet thinning and instabilities (whipping or bending) occur and is characterised with a series of spiralling loops, with each successive loop having an increased circumferential diameter (conical envelop), while the cross sectional diameter of the jet thins out.

2.3.2.1 Jet Thinning

Electrical field and Coulombic forces created between the spinneret tip and the collector contributes to the stretching and jet thinning process[27], and the mass of polymer per unit time passing through any point remains the same. Dietzel el al [49] represented a volume element of an electrospinning jet, with a cylindrical geometry,

and presented a relationship between the jet radius and the volume as shown in Equation 2-2;

$$\frac{A}{V} = \frac{2}{R} \tag{2-2}$$

where A represents the cross sectional area, V the volume and R the jet radius.

This implies that the larger the jet radius of a specific volume element, the smaller the specific surface area associated with that volume element.

The relationship between the mass and charge density of a given volume element to the jet acceleration is given in Equation 2-3 below. This infers that an increase in the electrospinning jet radius causes a corresponding decrease in jet acceleration.

$$a = E\left(\frac{q}{m}\right) \tag{2-3}$$

where q and m represents the available charge and mass respectively of a given volume element, E the electric field strength and a the jet acceleration.

The cylindrical model reported by Dietzel et al[49], represents a simplified model of the jet thinning process, and only illustrates the interplay of applied voltage, solution feed rate and charge to mass ratio. A more detailed approach will consider solvent evaporation rate, viscoelastic responses and the charge relaxation time which will further complicates the process[44].

2.3.2.2 Jet instabilities

The existence of instabilities in electrically driven jets has been well recognised from the early works of Taylor[40]. They occurs as a result of coupling of the Coulombic forces in the spinning jet with the electrical field generated between the spinneret tip

and the collector, and has been attributed largely for the formation of sub-micron size fibres [50]. Electrical charges in the form of uncompensated ions are carried along with the polymer jet during jet initiation. In order to keep the interior of the polymer in equilibrium, excess charge moves radially outwards towards the surface of the spinning jet. The redistribution of these excess charges and the subsequent Coulombic repulsion of the charges causes jet stretching in the direction of its axis until jet solidification [43]. As the bending instability is initiated, the increasing spiralling loop diameters is a direct effect of the same Coulombic repulsion charge which thins out and elongates the jet.

Instabilities during electrospinning has been extensively researched by Hohman et al[50, 51] and Shin et al [52], and the possibilities of three modes of instabilities has been proposed, with the first two being the varicose (axisymmetric) instabilities and the third is the whipping instabilities. In the varicose instability, the jet remains axisymmetric about the jet centreline, while the radius is modulated. This instability comprises of the Rayleigh and the Conducting mode. The Rayleigh mode is the classical Rayleigh instability, which is the effect of opposing forces between the polymer surface tension which tends to have a cohesive effect on the jet surface area and the electrostatic repulsion which tries to increase its surface area [44, 53]. This is the instability responsible for droplet formation during electrospraying [54], due to low polymer chain entanglement and low applied electric field or surface charge density. In the case of sufficient viscosity or polymer chain entanglement with adequate fluid conductivity, the conducting mode instability or whipping instability will ensue and polymer fibres are formed. Hohman [50], described that the dominant instability will be a function of the fluid jet parameters (i.e dielectric strength, conductivity, solution viscosity) and the jet`s static charge density. The whipping

instability which is a non-asymmetrical mode as the jet centre line is kept modulated at this stage is also referred to as a conducting mode. It is the mode responsible for immense jet stretching prior to jet solidification. Figure 2-4, illustrates the conical jet path and the thinning process during whipping instability.
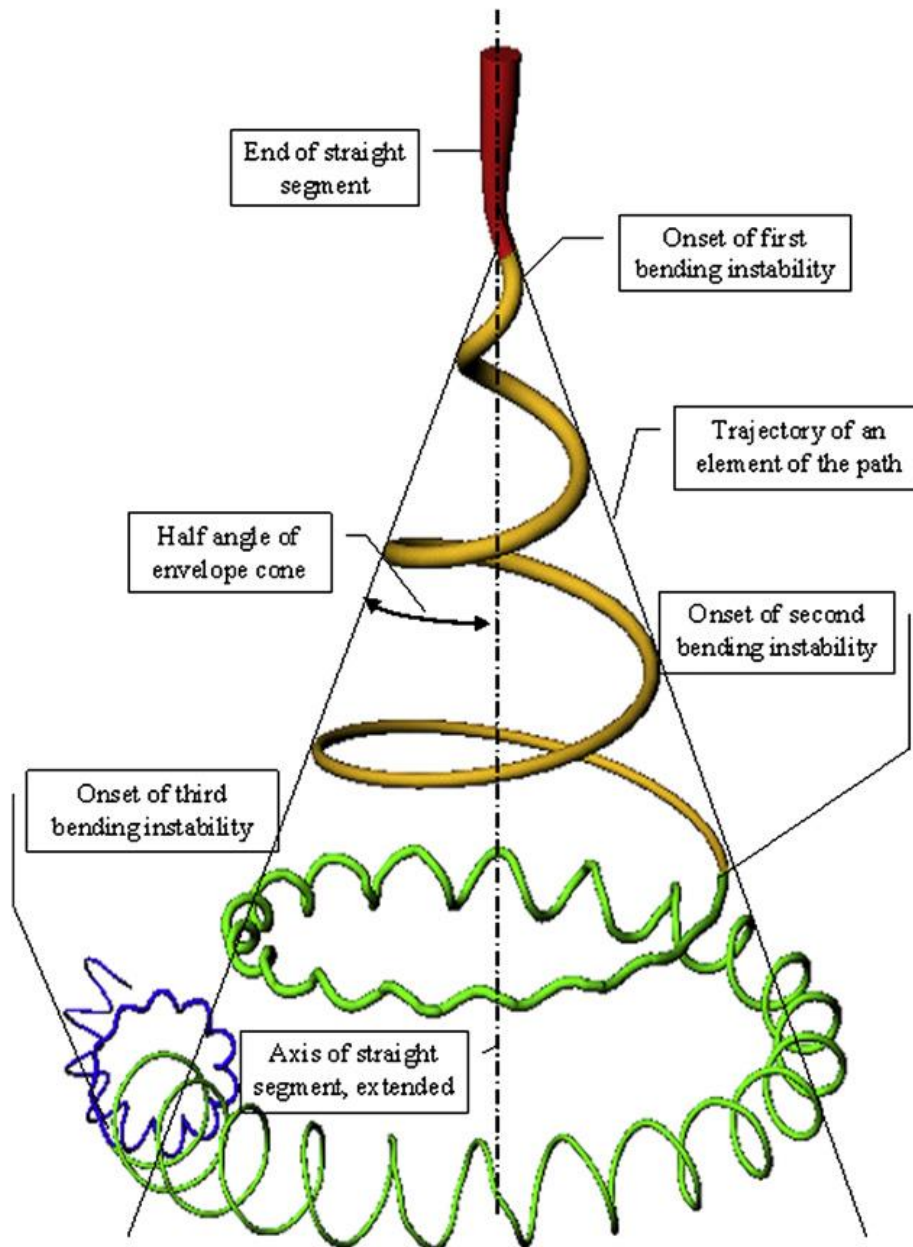
Figure 2-4: An illustration of electrospinning jet propagation phase showing the conical jet path and the bending instabilities. Taken from [43]. Copyright permission obtained from Elsevier

Another phenomenon that could occur during jet elongation stage is the splitting of the spiralling primary loop (whipping jet) into multiple secondary loops known as splaying, branching or splitting [51, 55]. This occur as a result of solvent evaporation and jet elongation, causing changes in the shape and charge per unit area of the jet. This leads to jet instability and to overcome the charge build up per unit area of the jet, a secondary jet is released [44, 55]. It is believed to have lesser influence compared to the whipping instability in the formation of thinner or nano-size fibres.

2.3.3 Jet solidification

At this stage, solidification of the jet occurs as a result of solvent evaporation and the dry fibre are subsequently deposited on the collector. The rate of fibre deposition is dependent on polymer concentration, applied electrical field and the tip to collector distance [44]. Other parameters such as ambient condition (temperature and humidity), solvent vapour pressure will also affect the jet solidification rate. Conglutination has been reported to occur prior to jet solidification in some electrospinning process. This is a process where partially wet jet intercepts mid-air during whipping instability stage and form bonded joints upon solidification. The existence of point bonded structure in fibre scaffolds enhances the mat stiffness and influences the overall mechanical properties of the fibre structure. A nonwoven fibre mat with a network of point bonded fibres are known as Garlands [56].

2.4 Electrospinning parameters/ parameters that influences electrospinning

The complexity of electrospinning is reflected in the number of different parameters that govern the morphology of fibres produced via the process. Studies have shown that by varying some of these parameters, it is possible to alter the morphology of the

fibres (from beaded to smooth ultrafine fibres or fibres with nano-structured surfaces) produced as may be required for different applications. The sensitivity of fibre morphology to variation in these parameter often differs from one polymer or polymer solution to another, hence optimisation of the process is important to achieve fibres of desired properties. These parameters can be broadly classified into; solution, process and environmental/ambient parameters [29]. Detailed breakdown and discussion of these parameters as it affects electrospinning is reviewed in this section.

2.4.1 Solution parameters

2.4.1.1 Molecular weight

Molecular weight of a polymer is an important solution parameter due to its effect on the viscosity, surface tension, dielectric property and conductivity of the solution. Polymers are made up of repeated chains of monomers and the molecular weight of the bulk can be expressed as a summation of the molecular weight of each monomer. The higher the molecular weight of a polymer, the higher the viscosity, and hence the more the ability of the polymer to form entanglement chains of its molecules during jet propagation [57].

In 2005, Guptal et al [58] demonstrated the effect of molecular weight on fibre structure, by electrospinning poly(methyl methacrylate) acid (PMMA) of different molecular weights. They found out that the higher the molecular weight the lower the number of bead and the more uniform the fibres produced. Casper et al[59], investigated the effect of molecular weight on intra-fibre pore formation, using PS polymers of 190,000g/mol and 560,900g/mol. Solution from the latter was seen to produce larger intra-fibre pore sizes when both polymers solutions of the same

concentration were electospun at the same relative humidity. This was attributed to either phase separation or difference in solution viscosity.

2.4.1.2 Concentration

Concentration of a polymer solution is closely linked to the viscosity and surface tension of the solution. It has been proven by various researchers that when a solution of low concentration is electrospun, they tend to produce beaded fibres. The shape of the beads formed changes from spherical to a spindle like structure with increased polymer concentration, while a further increase in the concentration will eventually lead to the formation of fine, uniform fibres with increased fibre diameter at the optimum concentration [29, 35, 57, 60, 61]. Dietzel et al in 2001 [62] in their study demonstrated the effect of concentration on fibre morphology by dissolving a 400,000g/mol polyethylene oxide (PEO) in water, to form different concentration ranging from 4 – 10% PEO solution. They observed that at low solution concentration beaded fibrous structures were produced and when the concentration was increased while keeping other parameters constant, the fibre morphology changes to a bead free, uniform structure with an increase in fibre diameter. However, it is important to note that increasing the concentration well beyond the optimum level could lead to needle/spinneret blockage during electrospinning, which could ultimately lead to production of defective fibres.

2.4.1.3 Viscosity

Viscosity of a polymer solution affects not only the quality of the fibres produced, but also the ability of the solution to be electrospun into fibres. It is closely related to the molecular weight and concentration of the polymer solution. At very low viscosity, jet propagation and formation of continuous fibres becomes difficult, due to poor

entanglement of the polymer molecules[29]. This is one of the factors responsible for the formation of micro beads in a process known as electrospraying, due to insufficient entanglement during the Rayleigh instability stage. On the other hand a high viscosity beyond the optimum, can lead to poor fluidity during jet propagation. Fong et al [63] studied different polyethylene oxide (PEO) solution with varying viscosity, and they

reported that the optimal viscosity to form uniform fibres for PEO solution is between 100 – 2000 centipoise, but it is important to note that the optimal viscosity required to produce uniform fibres varies from polymer to polymer. Figure 2-5 below illustrates the morphology of fibres produced at different solution viscosities as reported by Fong[63]. Similar effect of solution viscosity on fibre morphology has been reported in other literature studies [64-66].

2.4.1.4 Conductivity/surface charge density

Most polymers are conductive in nature with the exception of a few dielectric materials [29], and in solution, the polymer ions exists in an electrically neutral state if not excited. For jet initiation to occur during electrospinning, the polymer solution needs to be sufficiently conductive for the electrostatic repulsive charge to overcome the surface tension of the polymer, when induced with a voltage. The electrical conductivity of a polymer solution can be attributed to the solvent, the polymer and the presence of any ionisable salt in the solution. Electrospinning a polymer solution with enhanced conductivity increases the jet bending instability, leading to an increased flight path and a subsequent stretched fibre with reduced diameter. The fact that increasing the conductivity increases the charge density of polymer solution, reduces the critical voltage required for jet initiation. Zhong et al [67] demonstrated the effect of ionic salt addition on the morphology of electrospun poly (D, L-lactic)

acid (PDLA) using three different ionic salt of NaCl, NaH_2PO_4 and KH_2PO_4. A reduction in the fibre diameter was observed in all the solutions added with the 1%wt ionic salt, with the NaCl solution having fibres with the least diameter. This was attributed to its lower ionic radius giving it a higher charge density and increased mobility under an external charge. Similar effect was reported by Zhang et al [68] on PVA fibres, where the addition of NaCl to the polymer solution led to reduction in fibre diameter. This was ascribed to a higher electrical force being exerted on the polymer jet during electrospinning due to increased charge density with NaCl addition.
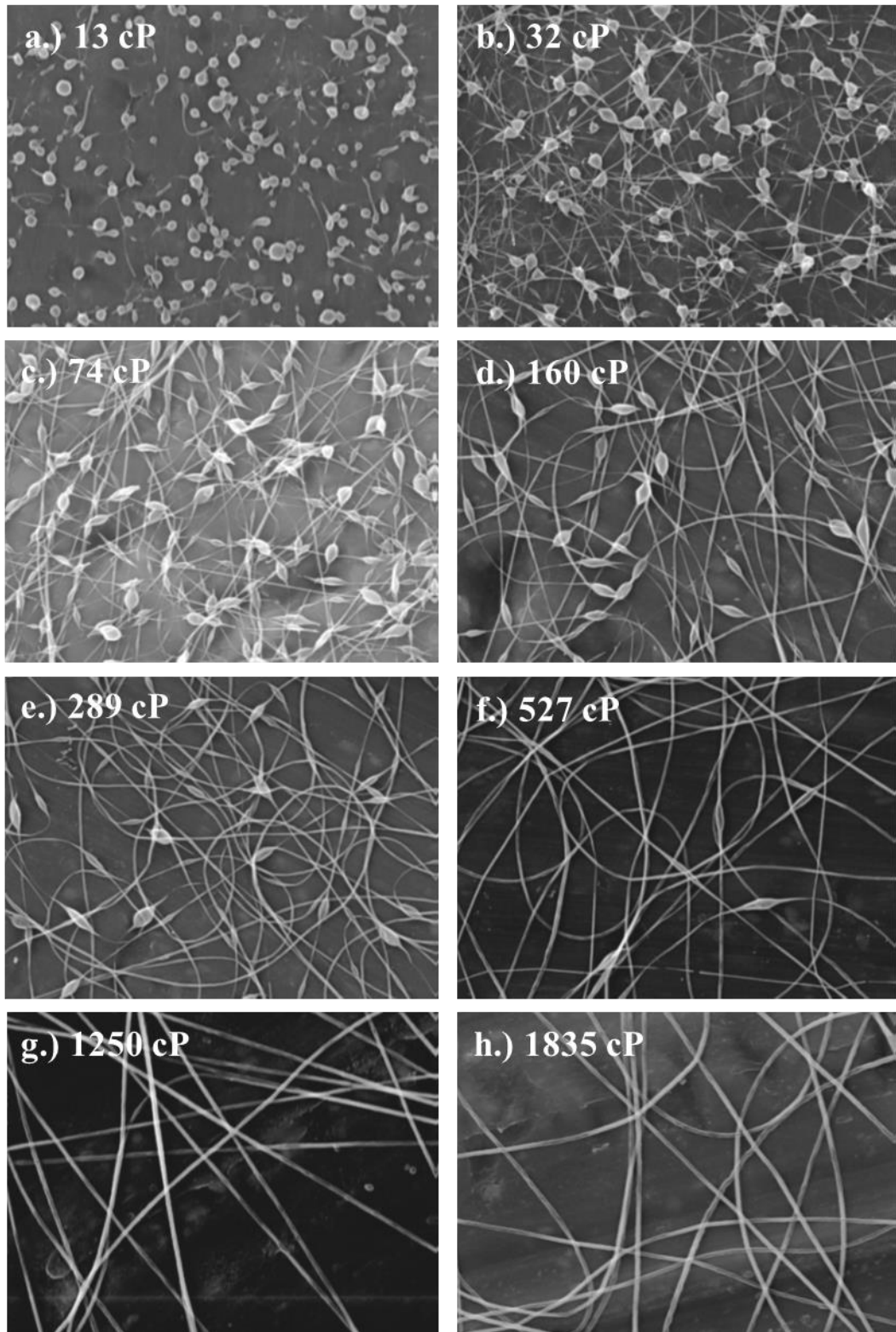
Figure 2-5: Effect of viscosity on fibre morphology of fibres electrospun with different PEO solution viscosity at 0.7kV/cm. Taken from [62]

2.4.1.5　Surface tension

Surface tension of a polymer solution is a function of the solvent used in making the solution. The surface tension of the solution needs to be overcome by the induced electrostatic charge, for the jet to propagate. It influences the formation of polymer droplet, production of either beads on string or uniform fibres [29, 57]. A high surface tension is undesirable in electrospinning as it enhances Rayleigh instability leading to droplet formation (electrospraying) [51]. Fong et al reported that decreasing the surface tension of a polymer solution increases the viscosity and hence leads to the production of a uniform fibre structure [63].

2.4.1.6　Dielectric strength of the solvent

The use of a solvent with a high dielectric constant such as N`N Dimethylformamide generally reduces beads formation and also leads to the production of small diameter fibres. The decrease in fibre diameter can be attributed to the increased bending instability of the jet which causes an increased flight time, hence a reduction in fibre diameter [18]. An increased deposition area also occurs as a result of the enhanced bending instability. Sun et al[69] in 2012, demonstrated that the use of solvents with low dielectric strength such as chloroform can be used to prevent bending instability during electrospinning process, hence can be used in generating aligned fibres with appropriate collectors system. Luo et al [70], investigated the effect of solvent dielectric constant on the electrospinning of PCL by creating a solvent mix of acetic acid and formic acid. They found the optimum dielectric constant required to generate nanofibers to be ~19 and above, at a solution temperature of 20°C, values below this was found to results in larger fibre diameters. They also reported that increase in

dielectric constant causes an increase in the electric field strength required for stable jetting of the electrospinning process.

2.4.2   Process parameters

2.4.2.1   Applied voltage

A minimum threshold voltage needs to be applied for electrospinning process to occur. The applied voltage need to be high enough to induce sufficient electrostatic charge in the polymer droplet to initiate jet propagation. There has been a number of variant to the effect of applied voltage on fibre formation. Zhang et al [68] in 2005 reported that increasing the applied voltage on a solution of poly (vinylalcohol) PVA, causes an increase in the amount of polymer ejected from the droplet, leading to the formation of fibres with increased diameter. Megelski et al [71] on the other hand reported that while electrospinning a solution of polystyrene, they observed that an increase in applied voltage causes a reduction in the diameter of the fibres produced. The reduced fibre diameter was attributed to increase stretching of the polymer jet due to a higher Coulombic forces. Zhao et al [72] also reported that an increase in applied voltage causes an increase in fibre diameter, while Dietzel et al [62] on its part reported that an increased voltage led to an increase in bead formation.

2.4.2.2   Flow rate

Flow rate determines the amount of polymer solution available per unit time for jet propagation. Megelski et al [71] demonstrated using polystyrene (PS) solution that a reduction in flow rate from 0.01ml/min to 0.07ml/min results in a reduction in beads formation as well as in the fibre diameter. Similar effect was observed by Zong et al [67] in an experiment conducted with 25% PDLA solution doped with 1%wt KH_2PO_4.

A high flow rate of 72µl/min was observed to result in large diameter fibres with large beaded structures, while a feed rate of 20µl/min led to smaller fibre diameters with spindle like beads. Zargham et al[73] in a separate study observed that increased flow rate could lead to the collection of wet, flattened fibres due to insufficient solvent evaporation.

2.4.2.3 Tip to collector distance (TCD)

This is the distance between the needle tip and the collector or substrate. Although it is believe to be of less significance when compared to other parameters, a minimum distance between the needle tip and the collector is required to allow adequate time for solvent evaporation, so as to prevent deposition of wet fibres on the collector. Also, an increase in the tip to collector distance may allow for an increased flight time thereby leading to the production of smaller diameter fibre [31, 72]. A short distance between the needle tip and the collector can cause the formation of inter-fibre bonds [74], thereby enhancing the strength of the fibre mat. Lee et al [75] reported the formation of beaded fibres at low TCD, and beyond the optimum TCD large diameter fibres were produced due to poor electrical field strength needed to cause jet stretching.

2.4.2.4 Collector

A collectors is any substrate on which fibres can be deposited during electrospinning process, usually a grounded or a charged (negative or positively) metallic surface. Traditionally, aluminium is utilized as a collector during electrospinning experiment as it is cheap, readily available and has a high conductivity. A major drawback in using flat aluminium foil as a collector is the difficulty in transferring the collected fibres and its inability to enhance the production of aligned fibres. To mitigate this drawback, different configurations of collectors have been utilized by researcher ranging from; rotating disk, rotating drum[62], split electrodes, conductive cloth, conductive paper, wire mesh [29, 76, 77]. Figure 2-6 shows examples of the different collector configuration that could be used for electrospinning.
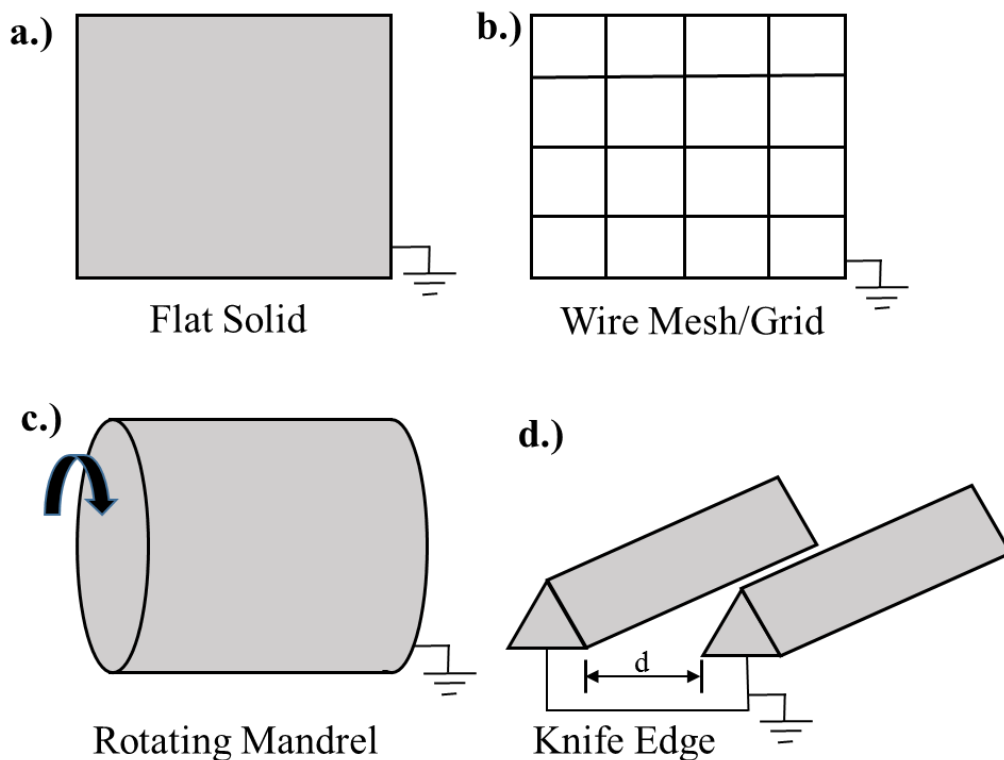
Figure 2-6: Schematic diagram illustrating some of the different electrospinning collector systems

2.4.3   Ambient Parameters

2.4.3.1   Humidity and temperature

Temperature and humidity are two (2) key environmental parameters that can affects the morphology of electrospun fibres, as they could influence the electrostatic field generated between the needle and the collector. A number of studies have shown that increasing the humidity of an electrospinning ambient condition will lead to the formation of intra fibre pores [21, 59]. In 2004, Caspers et al [59] demonstrated that electrospinning polystyrene polymer solution at a high ambient humidity will cause the formation of intra-fibre pores. The sizes of the pores were reported to increase with increasing humidity. Lin et al [21] in 2012 equally supports this claim, with the production of fibres with high intra fibre porosity at a relative humidity (RH) of 45%, when compared to the solid structures observed with fibres produced at 20% RH.

Mit-Uppathan et al [78] in 2004 was able to demonstrate the effect of temperature on fibre morphology with a solution of polyamide-6 dissolved in formic acid. They observed that an increase in the ambient temperature from $30 - 60^oC$ causes a reduction in fibre diameter. The decrease in fibre diameter was attributed to reduced in-flight jet viscosity and surface tension, with increased ambient temperature. Vrieze, et al [79] reported that ambient temperature creates two opposing effects; either an increased rate of solvent evaporation or an increase in jet viscosity, both of which affects the fibre diameter produced.

2.5   Application of Electrospinning

The application of electrospinning and its versatile nature can be seen in the amount of both on-going and proven research findings, which spans across different

disciplines, utilization a vast array of materials (polymers, metals and ceramics) and materials science skills. This could be attributed to the ease in which the process can be manipulated in achieving fibres of desired morphology and the different post treatment measures possible to enhance fibre functionality. Heat treatments, plasma treatment and chemical vapour deposition, and solvent processing [27, 80, 81] among others are some important post treatment methods that can be employed to enhance/modify fibre functions. An example is the use of solvent treatment to introduce porosity through selective dissolution of bi-component fibres. All of these techniques makes it possible to produce fibres with vast array of functionalities for different application areas ranging from defence and security, energy, healthcare to environment applications [30]. Prominent among these application area is health care where it has been extensively used in tissue engineering[82-84], wound healing [85] and drug delivery application[86]. Research into its use for environmental applications has been more into filtration, and affinity membrane generation, only recently has studies into its use for oil sorbent application been explored. Figure 2-7 below shows the categorization of the different research areas as it relates to electrospinning technology, with characterisation and processing being the most researched areas. This implies that a better understanding of this technology as it relates to the different application areas still remains an ongoing interest.
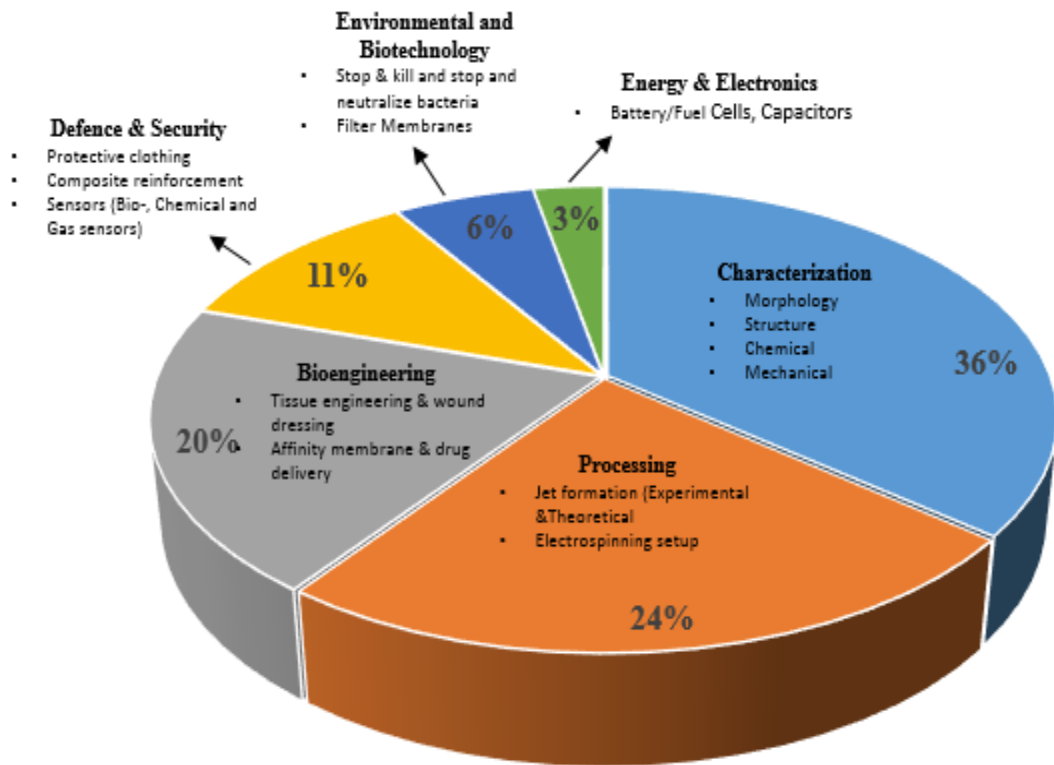
Figure 2-7: Chart illustrating the proportion of electrospinning research areas. Adapted and modified from [28]

2.6   Overview of oil spill

2.6.1   Oil spill and factors that influences spill clean-up

Incidences of oil spill can occur either on land or water, but spills over water do have more damaging impact due to the absence of natural vegetation or surface topographies, which often hinders its spread on land limiting its impact [87]. When spills occur on water, they often undergo some physicochemical changes due to a number of simultaneous processes known as weathering [3, 4]. Weathering processes such as spreading, dissolution, evaporation, photo-oxidation, emulsification and biodegradation; do have significant influence on how the oil behaves in the aftermath of a spill [7, 88]. Other factors such as ocean/sea current and wind movement often

increases the spread of oil spill on water. In order to better understand the limitation of the various oil spill clean-up techniques and how these techniques could be used to complement one another, there is the need to have an understanding of the transformation profile of the oil under the prevailing ocean or weather condition. These factors could favour the use of a particular technique over the others, which is why no particular clean up method could be deemed to be ideal in all oil spill situations[89].

Figure 2-8 below shows the relationship between all the different weathering processes in a marine oil spill. These processes affects the oil spill transport, the formation of emulsions and ultimately the overall fate of the spill. **Spreading** of the spilt oil starts almost immediately the spill occurs, and will depend largely on the volume and viscosity of the oil[90]. The rate of **evaporation** of the volatile components of oil will depend on the atmospheric condition and the wind speed. **Dispersion** on the other hand, can occur as a result of wave and sea turbulence breaking the oil spill into smaller droplets which can get dispersed and remain in the water column or coalesce on the surface as oil sheen[90]. Dissolution, pho-oxidation, biodegradation and emulsification are other key processes which can greatly affect the

fate of an oil spill and influences the choice of oil spill method that could be deployed [3, 17].
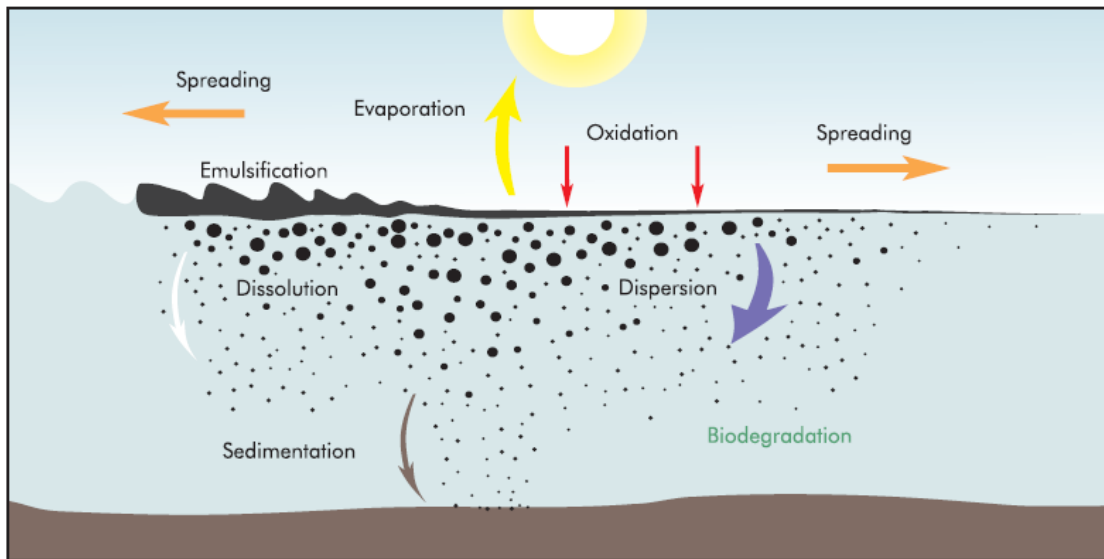
Figure 2-8: Illustration of weathering process undergone by oil spill at sea Taken from [84]

2.6.2   Methods of oil spill clean up

The choice of clean-up strategies used for a particular oil spill will depend on the oil type and the surface where the spill has occurred. Clean up methods can be broadly categorized into; mechanical/physical, chemical and biological/bioremediation methods. Chemical method comprises of in-situ burning and the use of dispersant, while mechanical methods are the use of sorbent, oil booms and skimmers. Bioremediation involves the use of microorganisms in degrading the oil spill in processes such as bio-augumentation, biostimulation etc. The literature review in this thesis will be on sorbent as it is a method known to be applicable for both land and sea oil spills, and can effectively recover all spilt oil if timely deployed. This is in addition to the fact that the technology being explored in this thesis is on the use of electrospun fibres as sorbent.

2.6.2.1 Sorbents

Sorbents are materials that uses process of adsorption, absorption, capillarity or combination of these mechanisms to recover other liquids. One major advantage of this method is the fact that it can be used on both land and water, and it is the most effective and economical means of cleaning up spills on shorelines; one of the most difficult spills to clean and that also has quite an enormous economic and environmental impact [91]. Since oils often have a lower density that water, sorbent used in marine oil spill clean-up should have a good buoyancy. Other properties of an ideal sorbent are; good oil sorption and retention capacity, excellent oil-water selectivity and good reusability and recyclability [2, 8, 12]. These sorbent are generally disperse on the surface of the oil for sorption to occur. The soaked sorbent is subsequently retrieved for the oil to be recovered and sorbent reused or for outright disposal [7]. Sorbents used in oil spill clean-up can be categorized into; inorganic minerals, synthetic organic materials and organic sorbents [2].

2.6.2.1.1 Inorganic mineral sorbent

Examples of inorganic minerals that have been used as sorbents for oil spill clean-up are diatomite, perlite, vermiculite, sorbent clay, zeolite, graphite and activated carbon [2, 12]. Classifying activated carbon is a bit tricky as it can also be derived from organic sources (wood and fruit seeds), synthetic organic product (polymers and rubber) as well as from mineral products (peat, coal and lignite) [7]. Most mineral sorbent have a low sorption capacity but activated carbon and organoclay have been shown to have a high sorption capacity, due to its excellent pore structure and high surface area. In the studies carried out by Carmody et al and Adebajo et al, they reported that despite organoclay having an excellent sorption capacity, it has the

downside of being, expensive, non-biodegradable and non-reusable [2, 91]. Activated carbon on the other hand has the issue of pore clogging and regeneration[7].

Major disadvantages in the use of inorganic sorbent is its dense nature and low oil retention capacity[2]. The density causes the sorbent to sink to the ocean floor, releasing the sorbed oil in the process. Having saturated mineral sorbent on the sea/ocean floor also poses great danger to aquatic organisms[7].

2.6.2.1.2 Natural Sorbent

There has been quite a number of research on the use of natural agricultural product (kenaf, milkweed, cotton, straw, rice husk) as sorbents for oil spill clean-up [3, 4, 12, 92]. These studies have shown that some of these materials have a higher sorption capacity when compared to the commercial polypropylene sorbent [93]. They are equally cheap and readily biodegradable. Annunciado et al in 2005 in their study of sorption behaviour of different vegetable fibres reported silk floss to have a high sorption capacity (85g/g), good oil retention capacity, excellent buoyancy and high oil/water selectivity [3]. However, limitations in the use of some of these natural sorbent such as straw is the cumbersome nature of broadcasting and retrieval in the case of marine spill clean-up. This makes the operation expensive and often limits its use to shoreline and small water bodies. They are also not readily available in the incident of an oil spill and most natural sorbent except a few (straw, silk floss and kapok) have low sorption behaviour [7].

2.6.2.1.3 Synthetic Organic Sorbent

The most widely used synthetic organic materials for oil spill clean-up are non-woven polypropylene fibres and polyurethane foams, largely due to their hydrophobic and

oleophilic nature. In 2003, Wei et al [17] evaluated the oil sorption behaviour of five different commercially available polypropylene fibres, with the difference being their method of fabrication. Each sample was tested in light crude oil as well as in 25% and 50% weathered oil samples. It was observed that stitch bonded polypropylene fibres exhibits the highest sorption of 15g/g in the 25% weathered oil, which they attributed to the high porosity of the fibre sample. Duong et al [89] in 2006, observed that Ultralight Instapak, a brand of polyurethane foam could sorb close to 100 times its weight in an experiment conducted with naphthenic based crude oil. Despite the high sorption capacity of this brand of polyurethane, non-woven polypropylene fibre still remain the most widely used sorbent in oil spill clean-up due to its compact nature.

Major limitation in the use of synthetic organic sorbent is low biodegradable nature of the polymer which had to be incinerated after use[2]. Creating a fibre or foam that could be reused will be a way in mitigating the short fall of this technique. Also despite the oleophilic nature of polyurethane foam and polypropylene fibre, they both exhibit poor hydrophobicity, while polypropylene sorbent generally have low sorption capacity [17, 19].

2.6.3 Use of electrospun fibres for oil spill clean-up

The aftermath of the BP Deep Water Horizon (DWH) oil spill disaster of 2010 saw the quest to develop new and effective materials for oil spill clean-up [94]. One of the new method explored is the use of electrospun fibres as sorbents for oil spill clean-up. This method offers an alternative sorbent to the widely used PP fibres, fabricated using melt blown technology. The first research in this field was reported in 2011 by Zhu et al[19], in an experiment performed using fibres electrospun from polymer blend of polyvinyl chloride (PVC) and polystyrene (PS). The resulting mat was reported to

exhibit a sorption capacity 2 - 9 times higher than those recorded for commercial PP sorbent, with a maximum sorption capacity of 146g/g reported for motor oil.

The use of electrospun pure PS polymers were recorded in three different studies [16, 95, 96] with all the works reporting a similar high sorption performance as earlier recorded by Zhu et al. In one of the works, Lin et al [16] used different molecular weight PS to demonstrate the effect of fibre diameter and fibre morphology on oil sorption. Wu et al [96] on their part studied the effect of fibre diameter and fibre surface porosity on oil sorption, by varying the needle gauge/sizes used for the electrospinning experiment. Thinner fibres obtained using the smaller needle size was observed to possess better oil/water selectivity and a superior sorption performance. Lin et al [95], in another study further demonstrated the effect of microstructural properties of PS fibre on its sorption performance, by tuning the fibre morphology through a control of the solvent composition, polymer molecular weight and concentration.

Despite the high sorption capacity of electrospun PS fibres, its poor strength and resiliency after oil sorption has been a major limitation to its commercialisation and reusability [94]. Methods such as polymer blending, coaxial and multi-nozzle side-by-side electrospinning have been explored in literature in mitigating this short fall. Peng et al [20] in 2015 reported the production of a composite blend of PS and poly acrylonitrile (PAN). Though an improvement in mechanical strength and high sorption capacity was achieved, the use of PAN being a hydrophilic polymer has the possibility of negatively impacting the oil-water selectivity of the mat. Jiang et al [97] in their study used a hydrophobic PVDF as a reinforcement polymer, while also incorporating iron oxide (Fe_3O_4) nanoparticles into the polymer matrix. They found the sorption

capacity to be between 35 – 45 g/g for the oils studied, with good mechanical strength recorded for the composite mats. The pioneering work of Zhu et al [19], which also created composite polymer blend fibre had no report of the mechanical properties of the mat.

Lin et al [21] created a composite fibre mat by incorporating PU fibres into the PS fibre mat using a multi-nozzle side-by-side electrospinning method. This approach further enhanced the elasticity and recoverability of the mat while also enabling its reusability. In another study, Lin et al[22] used a coaxial electrospinning approach with PS polymer forming the sheath and PU in the core, to improve the mechanical performance of the fibre mat. The composite mat showed good reusability even after five sorption iterations and exhibited a high sorption performance, with a maximum of 64.4 g/g recorded for motor oil. These two approaches [21, 22] involves the use of complex needle configuration, with the need for additional voltage supply and syringe pumps, thereby increasing the production cost of the fibres..

The above works elucidates the need for further studies to actualise the goal of commercialising electrospun fibres as oil sorbents. Table 2-1, shows a summary of previous literatures in this field and the sorption performance achieved.

Table 2-1: Summary of previous work on the use of electrospun fibre in oil spill clean-up

Author / Year	Polymer	Approach / Setup	Oil Type Investigated	Sorption Capacity (g/g)	Remark
Zhu et al (2011)[19]	PVC/PS (1:9)	Polymer blending / Single nozzle	Ethylene Glycol Peanut Oil Motor Oil Diesel	81 119 146 38	* Sorbent has a sorption capacity of about 5-9 times that of commercial PP sorbent. * No study was done using crude * No mechanical study
Li et al (2012)[16]	20% PS (M_w=350,000) 30% PS (M_w=208,000)	Pure PS / Single nozzle	Motor Oil Bean Oil Sunflower Oil Same as above	113.87 111.80 96.89	* Sorbent has a sorption capacity of 3-4times that of commercial PP sorbent * No study was done using crude * No mechanical study
Li et al (2012)[95]	30% PS (M_w=208,000)	Pure PS / Single nozzle	Motor Oil Sunflower	84.41 79.62	* Studied the effect of solvent composition , polymer concentration and molecular weight on fibre porosity and sorption * No study was done using crude * No mechanical study
Wu et al (2012)[96]	20% PS in DMF	Pure PS / Single nozzle	Motor Oil Peanut Oil Silicon Oil Diesel	131.63 112.30 81.40 7.13	* Studied effect of fibre morphology and porosity * No study was done using crude oil * No mechanical study
Li et al (2012)[21]	20% PS (M_w=350,000) 50 %PU resin 30% PS (M_w=208,000) 50 % PU resin in DMF	Multi-nozzle spinning of PS/PU(4:1)	Motor Oil Sunflower Oil Motor Oil Sunflower Oil	27.75 23.84 30.81 24.36	* Studied the effect of relative humidity on fibre porosity * Multi-nozzle spinning using different nozzle ratio of PS and PU * No study was done using crude oil
Li et al (2013)[22]	20% PS (M_w=350,000) 100 %PU resin	Coaxial / PS Sheath, PU Core	Motor Oil Sunflower Oil	64.40 47.48	* Studied coaxial spinning of PS/PU polymers. * No study was done using crude oil
Peng et al (2015)[20]	18%PS/PAN (1:1) in DMF	Polymer blend / Single nozzle	Pump oil Peanut Oil Diesel Gasoline	194.85 131.7 66.75 43.38	* Polymer blending with hydrophilic PAN * No report on the mechanical strength of the fibre * No study was done using crude oil
Jiang et al (2015)[97]	20% PS/PVDF/Fe_3O_4	Multi-nozzle spinning PS/ Fe_3O_4 and PVDF	Motor oil Sunflower oil Soybean oil Diesel	35 – 46	* Fibre blending with magnetic properties * No study was done using crude oil * No mechanical study

2.7   Polymers

Polymers are macromolecules made up of repeating units of monomers linked together by covalent bonds. A good example of this is polystyrene polymer, which is made up polymerized styrene ($C_6H_5CH=CH_2$) monomers. The ability of polymers to form entanglement in solution makes it one of the few materials aside ceramics that can be electrospun[27].   There are large number of polymers and the choice of polymer selected for electrospinning will often depend on the intended application.

Polymers used in electrospinning could be natural or synthetic polymers [98-102]. Natural polymers as the name implies are from natural sources (i.e chitin, chitosan, gelatine). They are often used in situations where biocompatibility and biodegradability is of high importance, particularly for tissue engineering and other biological applications [98]. Synthetic polymers on the other hand are man-made polymers, synthesized through chemical processes, such as; polyethylene, polystyrene, polypropylene, Poly (vinyl chloride) etc. They are classified based on their response to heat into thermoplastic and thermoset polymers[27, 103]. Thermoplastics polymers melts on application of heat and can be reversibly melted and dissolved, while thermosets are polymers that cannot be melted or dissolved and on application of heat or chemicals can undergo chemical reaction to form insoluble material [103].

The choice of polymer to be electrospun will depend primarily on the application, the morphological structure of fibres/fibre mat desired as well as the ready accessibility of the polymer. For the production of fibre mat for oil sorption applications, polymer availability, low surface free energy polymer, and ability to be electrospun from solution were some of the factors considered in polymer selection [16, 104].

2.7.1 Polystyrene (PS)

Polystyrene one of the most widely used thermoplastic polymers due to its low cost and good processing properties is produced from the polymerization of styrene monomers. It exists either in a glassy like solid form or as an extruded foam material. The chemical structure of polystyrene consist of a backbone of carbon atoms with attached phenyl group (benzene ring), the arrangement of the benzene ring attachment about the carbon atom determines the tacticity of the polystyrene polymer. The tacticity on the other hand determines the physical properties of the polymer. Depending on the processing method, three different tacticity of polystyrene exist; the atactic (amorphous) polystyrene and the crystalline; isotactic and syndiotactic molecular structures. Atactic polystyrene which is amorphous in nature has a stereochemical structure with the phenyl group randomly placed on both sides of the carbon chain. Most commercially available polystyrene are atactic in nature. Isotactic and syndiotactic PS on the other hand both have ordered spatial arrangement of the benzene ring, giving it a crystalline structure, with the degree of crystallinity determining the physical properties of the PS polymer. One of the major difference between the two crystalline forms of PS is its melting temperatures (T_m) and the degree and rate of crystallization, with isotactic PS having a melting temperature of 250º and syndiotactic being 270ºC. Syndiotactic PS also crystallizes at a much faster rate and to a level over 50% more than isotactic[105]. Figure 2-9 shows the different tacticity of polystyrene.

The form of polystyrene used in this thesis is the commercial "amorphous" atactic PS, due to its low cost, low surface energy and ready availability. Its low surface energy has seen it being explored for the production of superhydrophobic surfaces by a number of researchers [101, 104, 106]

Atactic

Isotactic
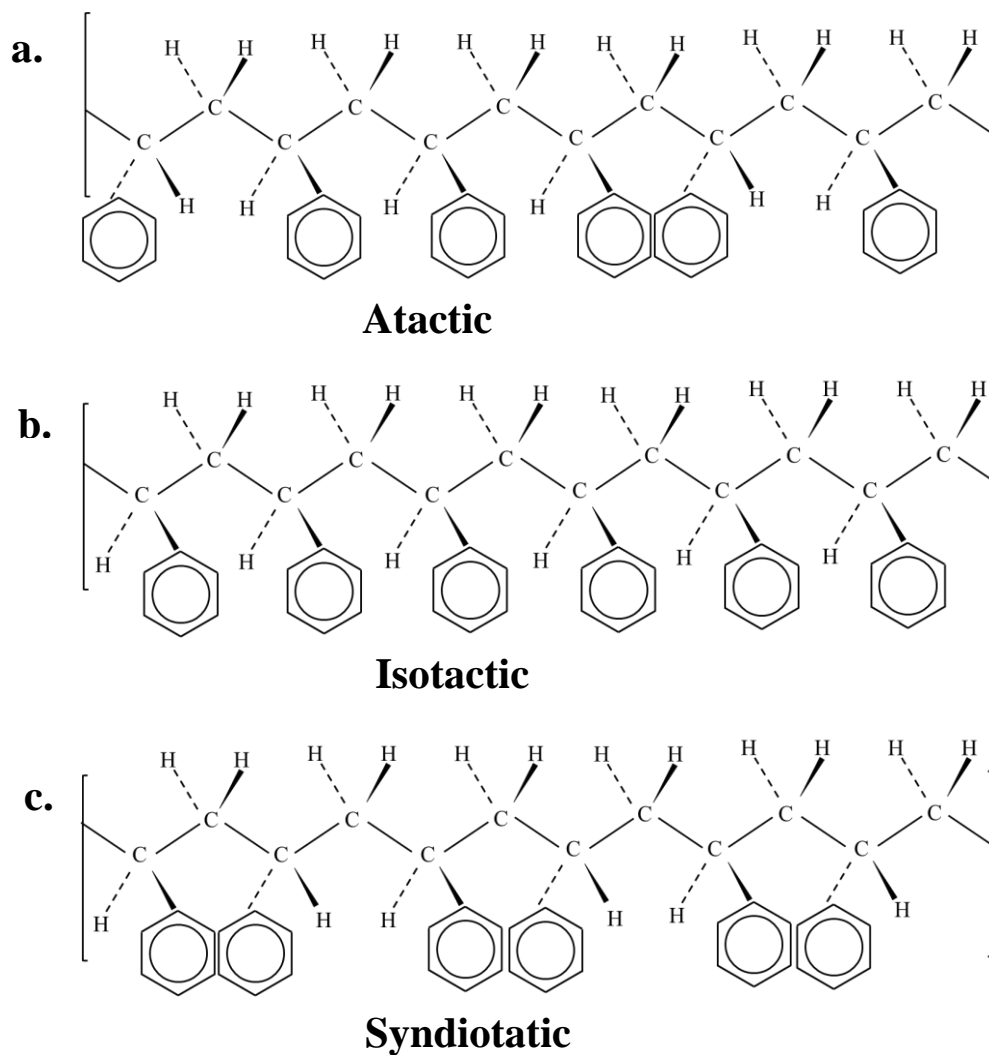
Syndiotatic

Figure 2-9: Chemical structure of Atactic, Isotactic and Syndiotactic polystyrene

2.7.2 Thermoplastic Polyurethane (PU)

Thermoplastic polyurethane are segmented block copolymer composed of alternating hard and soft segment and belong to the family of thermoplastic elastomers (TPE) [107, 108]. They are synthesized using poly diol as the soft segment and diisocynate and chain extender as the hard segment, while recent studies have shown that it can also be synthesized using diisocynate free methods[109]. The hard segment act as a

69

physical crosslink below their melting point and offer TPU its elastomeric properties, while at temperatures above its melting point, it makes it possible for TPU to be processed [109, 110]. As a result of the chemical structure of TPU, they exhibit similar level of elasticity as cross linked elastomer (rubber), as well as the same level of process-ability and recyclability as regular thermoplastic polymers. They also have a glass transition temperature below 0ºC, and exhibit a wide range of properties from excellent abrasion resistance, biocompatibility, hydrolytic stability and tuneable mechanical properties. The properties of the resulting TPU can be tuned during synthesis by modulating the ratio of hard and soft segment present in the polymer[111]. Based on this, they have been used in a wide range of applications in several fields, automobile, biomedical devices, food packaging, cables and building materials etc.

TPUs can be broadly classified into three based on the polyol type used in its synthesis; 1.) Polyester-based; 2.) Polyether-based, and 3.) Polycaprolactone-based TPU. Polyether based TPU exhibits good hydrolysis resistant[112] making it hydrophobic and ideal for use in marine oil sorbent application as will be explored in this thesis. Figure 2-10 shows the chemical structure of typical thermoplastic polyurethane used in this research. In the rest of this thesis the abbreviation "PU" is used for thermoplastic polyurethane (TPU).
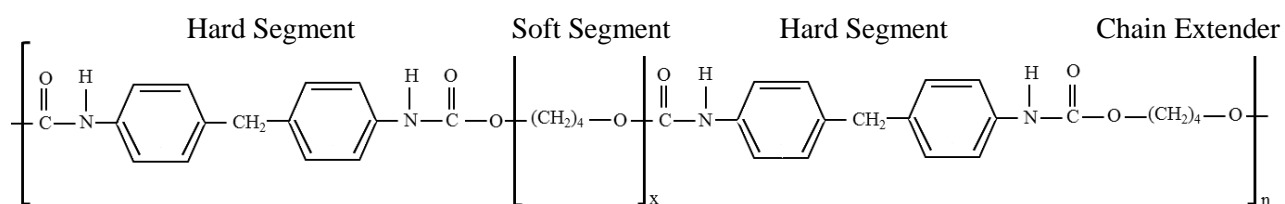
Figure 2-10: Chemical structure of polyether-based polyurethane

2.7.3 Polymer Blending: Post treatment technique

Polymer blending is the mechanical mixing of two or more polymers to form a polymer with a different or distinct physicochemical properties[113] from those of the homopolymers. It is the physical mixture of structurally different polymers or copolymers which interact with one another through secondary forces (hydrogen boding, dipole-dipole forces etc) without covalently bonding[114]. Blending offers an economical way of tailoring the properties of an existing polymer rather than synthesizing new monomers for polymerization, thereby achieving improvement cost savings and property maximization[114]. The properties and performance of the blend will depend on the properties of the homopolymers, their morphology and ratio in the blend. It is often done for specific property enhancement or modification such as tensile strength, modulus, improve process-ability or recyclability etc[113]. Polymer blends are classified according to the level of miscibility of the polymers, and this has a strong influence on the mechanical, thermal, rheological and other properties of the blend. These classification categories are; immiscible, miscible, compatible and compatibilized polymer blends[113].

Immiscible polymer blends consist of large size domains of dispersed phase with no or poor adhesion between the domains. In a case of a binary polymer blend, thermal analysis will reveal two separate glass transition temperatures of the constituent polymers. In miscible blends, just a single glass transition temperature will be observed under thermal analysis and these are cases where the polymers are homogeneously mixed to form a single-phase structure[115, 116]. Compatible blends are technically immiscible blends with strong interface interaction between the polymers[113, 117]. Macroscopically they exhibit uniform properties. Compatibilized polymer blends, on the other hand are another form of immiscible blends in which the

microstructural and physical properties can be stabilized, through the addition of surface active agents to aid the processes of deformation, breakup and coalescing of the polymer droplet[113].

For electrospinning of polymer blends, it is important that the constituent polymers are both soluble in the same solvent system in order to create the best form of miscibility possible and also to ensure the electrospinnability of the polymer solution[115].

2.8   Contact Angle, Wenzel and Cassie-Baxter Theory/Equations

Contact Angle is the angle formed by a line tangential to the liquid at the three point solid, liquid and gas interface, when a liquid droplet is place on the surface of a solid material. It is used to quantitatively determine the wettability of a solid material. When water is used as the probe liquid, it is a measure of the hydrophobicity/hydrophilicity of the surface. Thomas-Young derive a governing equation for the interfacial equilibrium force at the three phase boundary, known as the young equation.

$$\gamma_S - \gamma_{SL} = \gamma_L \cos\theta \qquad (2\text{-}4)$$

where; γ_S, represents the solid surface energy, γ_{SL} the interfacial energy between the solid and the liquid; and γ_L represents the surface tension of the liquid, while angle θ is the angle at the three point interface[118].

This equation represents the contact angle in an idealized chemical and structurally homogeneous surface, and hence not applicable in the case of a rough, heterogeneous surface. Wenzel in his equation factored in the roughness profile of surfaces in his expression for the apparent contact angle[118, 119].

$$\cos\theta^* = r\cos\theta \qquad\qquad (2\text{-}5)$$

Where; θ^* is the apparent contact angle, θ the intrinsic contact angle and r the roughness factor; which is the ratio of the actual surface to the geometric surface. This equation is on the assumption that the wetting liquid penetrates through the grooves, which gives a value of r >1. Marmur et al,[120] proposes that for Wenzel equation to be applicable, the size of the liquid droplet must be 2-3 fold the roughness scale.

However, in situation where the liquid seats right on top of the rough surface, the Cassie-Baxter equation becomes more applicable [118]. In 1944, Cassie and Baxter et al [121], extended the findings of Wenzel to porous surfaces and came up with an expression for the apparent contact angle;

$$\cos\theta^* = f_s\cos\theta_s + f_a\cos\theta_a \qquad\qquad (2\text{-}6)$$

f_s and θ_s; represents the fractional surface area of the solid and intrinsic contact angle on an homogeneous solid surface, while contact angle for a liquid droplet suspended in air θ_a will be 180º and f_a second fractional area in contact with air on the surface of the porous material.

where; $f_s + f_a = 1$;

$$cos\theta^* = f_s(cos\theta_s + 1) - 1 \qquad\qquad (2\text{-}7)$$

Hence, surface modification makes an hydrophobic surface more hydrophobic and an hydrophilic surface more hydrophilic [118]. A separate study has shown that making a surface more hydrophobic could also increases the oleophilicity of the material [122]. Generally material with a water contact angle (WCA) above 90º, are termed as hydrophobic while those with WCA below 90º are hydrophilic surfaces. Superhydrophobic surfaces have a WCA above 150º.

The schematics in Figure 2-11 shows the difference between contact angle measurement on a smooth homogeneous, surface with both Wenzel and Cassie-Baxter models.
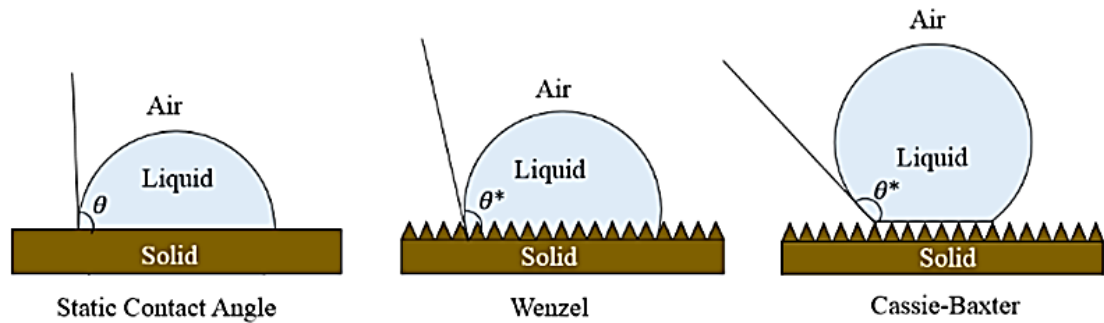
Figure 2-11: Illustrates contact angle of a liquid droplet and the difference between Wenzel and Cassie-Baxter models

2.9   Surface Free Energy (SFE)

The interaction at a solid-liquid interface is an interplay between the forces of adhesion and cohesion. This interaction enables the determination of the surface free energy (SFE) of a solid, which is often determined empirically by measuring the contact angle of different probe liquids on the surface [123]. The SFE is referred to as the work required to increase the length of a surface (wetting); expressed as the energy required per unit area in mJ/m^2. The term SFE is used for solids while surface tension is used for liquids. The terms are often used interchangeably due to the fact that they both have same units. The contact angle measures the ability of a liquid to wet a surface and equally enables the discrimination between polar and dispersive interactions [123]. Fowkes [124], Owen [125], Neuman et al [126], have all proposed different methods of measuring the surface free energy (SFE) of solids. Owen et al [125]proposed a method for determining the SFE of polymers, using a pair of polar

(water) and non-polar (diiodomethane) liquid. The result obtained by Owen et al was found to be in good agreement with previous and more laborious methods; such Zissman and Fowkes methods[125]. Hence, this method has been widely used by researchers across different fields, as the knowledge of SFE and wetting is important in several industries such as; used in painting, bonding surface, surface coating, cleaning surface [127] etc.

2.10 Theoretical Background

2.10.1 Owens Wendt Rabel Kaebel (OWRK)

A method widely used for measuring the SFE of polymers is the Owen Wendt Rabel Kaebel (OWRK) method[123]. It is derived from the classical Young`s equation which expresses the interfacial equilibrium force at the three point interface of a liquid droplet formed on a flat solid surface.

$$\gamma_S = \gamma_{SL} + \gamma_L \cos\theta \qquad (2\text{-}8)$$

where γ_S is the surface free energy of the solid, γ_L the surface tension of the liquid, γ_{SL} represents the interfacial tension between the solid and the liquid, and θ is the contact angle at the three point interface between the solid, liquid and air.

Expressing the interfacial energy γ_{SL} as the sum of the surface tension/energy minus the work of adhesion W_A; W_A could then be expressed as;

$$W_A = \gamma_L(1 + \cos\theta) \qquad (2\text{-}9)$$

According to Fowkes [124] and Owen et al[125], the total SFE on the surface of a liquid or solid is a sum of different intermolecular forces and can be categorized into polar (p) and dispersive (d) components. Hence, both γ_S and γ_L can be expressed as;

75

$$\gamma_L = \gamma_L^d + \gamma_L^p \tag{2-10}$$

$$\gamma_S = \gamma_S^d + \gamma_S^P \tag{2-11}$$

Owens [125] further expresses the W_A in a reversible form using the geometrical mean as;

$$W_A = 2\left(\sqrt{\gamma_L^d \gamma_S^d} + \sqrt{\gamma_L^p \gamma_S^p}\right) \tag{2-12}$$

From both equations 2-9 and 2-12, we have the OWRK expression as;

$$\frac{(1 + \cos\theta)\gamma_L}{2\sqrt{\gamma_L^d}} = \sqrt{\gamma_S^p}\sqrt{\frac{\gamma_L^p}{\gamma_L^d}} + \sqrt{\gamma_S^d} \tag{2-13}$$

Equation 2-13 above exhibits a linear relationship. This enables the determination of the SFE component (dispersive and polar) of solids, when two or more liquids or known SFE components are used.

2.10.2 Drop-on-fibre theory

The drop on fibre theory developed by B.J Carrol [128] in 1976 was based on the barrel-shaped liquid droplet on a single fibre/filament. It states that in the event of an insignificant influence of gravity on a liquid droplet, its equilibrium on the fibre is determined by the Laplace excess pressure ΔP acting on the liquid-air interface, and
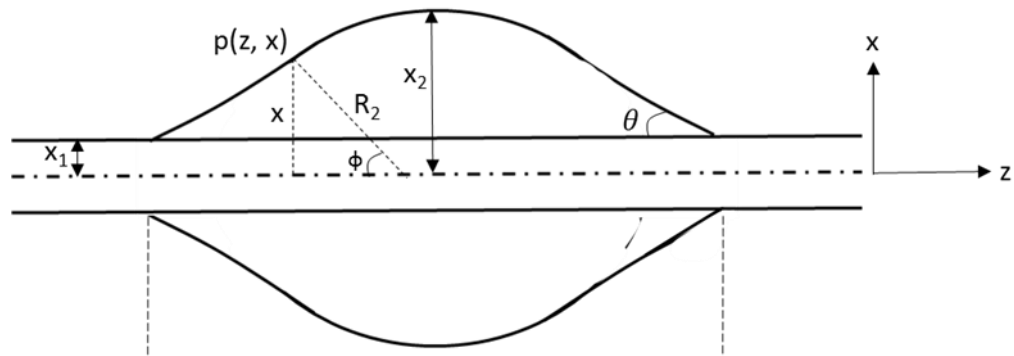
Figure 2-12: Schematic diagram and symbol definition for barrel-shaped drop-on-fibre model

should be constant everywhere across the interface. Carrol then developed the following equations for the reduced drop length (L^r) and reduced drop volume(V^r). Figure 2-12 shows schematics of a barrel drop conformation on a single fibre filament.

2.10.2.1 Reduced drop length

If $n = \frac{x_2}{x_1}$; $a = \frac{n\cos\theta - 1}{n - \cos\theta}$; and $k^2 = \left(1 - \frac{a^2}{n^2}\right)$, then the **reduced drop length** (L^r) can be obtained as follows;

$$L^r = 2[aF(u_1, k) + nE(u_1, k)] = \frac{L}{x_1} \tag{2-14}$$

where $u_1 = \frac{n^2 - 1}{a^2 n^2}$, and $F(u_1, k)$ and $E(u_1, k)$ are elliptical integral of the first and second kind respectively. x_1 is the fibre radius; x_2 the maximum drop height in the plane normal to the fibre axis; n the reduced drop height and θ being the contact angle.

2.10.2.2 Reduced drop volume

The **reduced drop volume** (V^r) can also be determined with the below expression;

$$V^r = \frac{2}{3}\pi n \left[(2a^2 + 3na + 2n^2)E(u_1, k) - a^2 F(u_1, k) - \frac{1}{n}\{(1 - a^2)(n^2 - 1)\}^{\frac{1}{2}}\right] - \pi L = \frac{V_{act}}{x_1^3} \tag{2-15}$$

where V_{act} and V^r represents the actual and reduced drop volume respectively.

2.10.2.3 Reduced adhesive energy

McHale et al in 2002/1997 [129, 130], used a mathematical expression similar to the Cassie-Baxter [121] definition of net energy on porous fibre to define the **reduced adhesive energy** (E^r) on a single fibre filament as;

$$E^r = \gamma_L A_L + (\gamma_{SL} - \gamma_S)A_{SL} = \gamma_L(A_L - A_{SL}\cos\theta) \qquad (2\text{-}16)$$

where A_{SL} being the area interface between the liquid droplet and the fibre; and A_L the liquid surface area, both expressions can be calculated using the below equations;

$$A_L = 4\pi n(a + n)E(u_1, k) \qquad (2\text{-}17)$$
$$A_{SL} = 2\pi L^r \qquad (2\text{-}18)$$

The above equation offers a means to quantitatively evaluate the oil adsorptivity of different filaments to selected oil types. It can also provide a basis for material selection based on filaments microscale oil affinity as will be explored in Chapter 4.

3 Materials and Methods

This chapter provides an in-depth description of the common materials, experimental methods and analytical techniques utilized in this thesis. In cases where the method used in a particular result chapter differs, details of such method is further described in such chapter.

3.1 Materials

All chemicals and reagents used in this study were of the highest purity available and were either procured from VWR, (Leicestershire, UK) or Sigma Aldrich, (Dorset, UK). Polystyrene (PS) polymer pellets with molecular weight 3.5 x 10^5g/mol was purchased from Sigma Aldrich (Dorset, UK). The thermoplastic polyurethane; pellethane 2363 80AE, used for the polymer blend study was kindly provided by Lubrizol Advanced Materials (Flintsbach am Inn, Germany). The Pennsylvania light crude oil with an API gravity of 46.7° was purchased from Onta, (Ontario Canada). Shell Helix motor oil 15W-40 with a viscosity of 287.23 mPas.s was procured locally from a Shell gas station, while both the vegetable (Sunpride brand) and sunflower oils (Tesco brand) were procured from a local Tesco stores.

3.2 Fibre Mat Fabrication

3.2.1 Solution Preparation

American Chemical Society (ACS) grade solvents; N`N dimethylformamide (DMF) and tetrahydrofuran (THF) were used to dissolve the polystyrene and polyurethane

polymer pellets used in this study, and both solvents were purchased from Sigma Aldrich, (Dorset, UK).

Preliminary electrospinning experiments were carried out to determine the optimum PS concentration and solvent mix. 10%, 15%, 20% and 25% w/w PS concentrations dissolved in DMF/THF (4:1 ratio) respectively, while different DMF/THF weight ratios; 5:0; 4:1; 3:2; 2:3; 1:4 and 0:5 respectively were also studied. The optimum concentration and solvent mix were subsequently used as a basis for the polymer blend experiment. To fabricate the PSPU polymer blend fibres, different weight ratios of PS and PU pellets (10:0, 9:1, 8:2, 7:3 and 6:4) were dissolved in DMF/THF (4:1), with the polymer concentration kept constant at 20%w/w in all the polymer blend solutions. The solutions were stirred on a Stuart CB 302 magnetic stirrer (Staffordshire, UK) at room temperature, for a minimum of 24hrs. Prior to electrospinning, the solutions were subsequently agitated on a Stuart vortex mixer (Staffordshire, UK) for approximately 2mins before electrospinning to ensure a homogenous mix of the solution. Composition of all polymer solutions prepared is shown in Tables 3-1 and 3-2.

Table 3-1: Composition of polystyrene solution used for preliminary electrospinning experiments

Polymer Solution	Polymer Conc. (%) w/w	Polymer Weight (g)	Solvent Weight (g)		Solvent Ratio (DMF:THF)
		PS	DMF	THF	
PS	10	4	28.8	7.2	4:1
PS	15	6	27.2	6.8	4:1
PS	20	8	25.6	6.4	4:1
PS	25	10	24.0	6.0	4:1
PS	20	8	32.0	-	5:0
PS	20	8	19.2	12.8	3:2
PS	20	8	12.8	19.2	2:3
PS	20	8	6.4	25.6	1:4
PS	20	8	-	32.0	0:5

Table 3-2: Composition of PSPU polymer blend solution

Polymer Solution / Polymer Ratio	Polymer Conc. (%) w/w	Polymer Weight (g)		Solvent Weight (g)		Solvent Ratio (DMF:THF)
		PS	PU	DMF	THF	
PS	20	8	-	25.6	6.4	4:1
PSPU 9:1	20	7.2	0.8	25.6	6.4	4:1
PSPU 8:2	20	6.4	1.6	25.6	6.4	4:1
PSPU 7:3	20	5.6	2.4	25.6	6.4	4:1
PSPU 6:4	20	4.8	3.2	25.6	6.4	4:1
PSPU 4:6	20	3.2	4.8	25.6	6.4	4:1
PSPU 2:8	20	0.8	7.2	25.6	6.4	4:1
PU	20	-	8	25.6	6.4	4:1

3.2.2 Density

The density of the oils were determined by first pipetting a 100ml of oil (using a borosilicate glass pipette and a Mettler Toledo pipette gun) into a glass beaker. The mass of the 100ml oil was subsequently measured on a digital Mettler Toledo scale and the density value calculated using the equation below;

$$\rho = \frac{m}{V} \qquad (3\text{-}1)$$

where m and V represents the measured mass and volume of measured oil respectively, and ρ the calculated density.

Prior to the test, the oils were heated in a water bath to a temperature of 20°C and the temperature confirmed using an Oakton pH 6+ meter. All density values represents the mean value for 3 different measurements.

3.2.3 Electrospinning Process

The polymer solutions described in Section 3.2.1 were electrospun using either a conventional horizontal electrospinning setup or an electrospinning cabinet that was

designed in the course of this research, which is equipped with a rotating drum system and programmable linear actuator that carries the electrospinning nozzle head. Both setups are described in Section 3.2.2.1 and 3.2.2.2 respectively.

3.2.3.1 Horizontal Electrospinning Setup

Figure 2.1 shows the horizontal electrospinning configuration used in this study. This is tagged the flat collector (FC) system in this thesis. The setup comprises of a FC series high voltage supply; model PS/FC30R04.0-22 from Glassman Europe Limited (Hampshire, UK). A programmable syringe pump model 4400PSI from Harvard Apparatus (Cambridge, UK), a 21G needle connected to a 10ml plastic syringe both from Becton Dickinson (Oxfordshire, UK), and a stainless steel flat collector covered with aluminium foil. The needle tip to collector distance, flow rate and voltage were varied to obtain a stable jet propagation between the needle and the collector. All fibres were air dried in ambient condition before characterisation or further processing.

3.2.3.2 Electrospinning Cabinet: Design and Fabrication

An electrospinning cabinet equipped with a fully detachable rotating drum system and an actuator carrying the electrospinning nozzle head was designed and fabricated with the help of the UCL Mechanical Engineering workshop. The cabinet is to help prevent external interference on the electrospinning process, while the drum will ensure the production of a uniform, continuous fibre mat. The cabinet is made with a Nylon 6 material and has a dimension of 490 x 550x 750mm (L x W x H), with a wall thickness of 30mm. For easy visual access to the electrospinning process, the front cover was made with a 10mm thick transparent acrylic material.

The modular rotating drum system is made fully detachable and a drum or mandrel system of different configuration can be attached, depending on the intended

application. The drum is driven by a brushless DC motor, with a variable speed control range between 80 – 4000rpm, procured from Oriental Motors (Basingstoke, UK). Figure 3-1 shows a picture of the electrospinning cabinet with the fabricated modular rotating drum setup.

3.2.3.3 Electrospinning Parameters

Since PS can be electrospun over a wide range of parameters. For studies carried out in Section 4.2.1, a flow rate of 0.5ml/hr, tip to collector distance of 15cm and voltage of 15kV was used. For the polymer blend a flow rate of 2-3ml/hr, tip to collector distance of 15cm and a voltage 15kV was maintained in all the experiment, as these set of parameters gave a stable jet for all the polymer blend ratio. All experiment were carried out at room temperature of 21 ± 2 ºC and a relative humidity $50 \pm 5\%$.
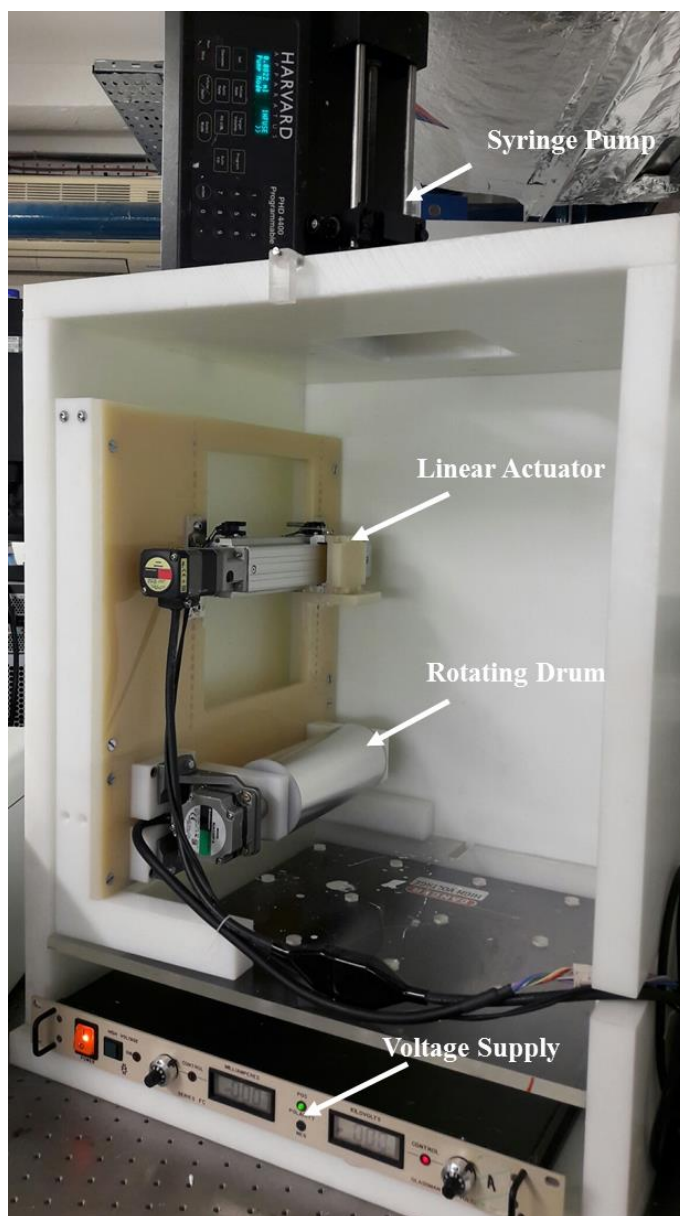
Figure 3-1: Picture of the electrospinning cabinet showing the rotating drum collector setup with the programmable linear actuator, the syringe pump and the voltage supply

3.3   Solution Testing/Characterisation

3.3.1   Conductivity

The ability of the polymer solutions to conduct electrical current was measured using a SevenGo Duo pH/Conductivity meter by Mettler Toledo (Leicester, UK). The device was fitted with a 738-ISM conductivity probe with a conductivity range of 0.01 – 500mS/cm. The probe comprises of a conductivity cell with a pair of fixed parallel

plates, which has an area (A) and distance (L) between the electrodes[131]. The probe prior to each experiment, was calibrated with a known standard. The conductivity (C) is derived using the expression below, with (δ) being the resistivity;

$$C = \frac{1}{\delta} = \frac{K}{R_t}$$

(3-2)

where K is the cell constant and is define as;

$$K = \frac{L}{A}$$

(3-3)

3.3.2 Surface Tension

Surface tension were estimated using the capillary rise method [132]. The experiment was performed using a thin borosilicate glass tube by World Precision Instrument (Hitchin, UK), with internal diameter of 0.86mm. Immersing the tube into the polymer solution, the height (h) rise after an equilibrium period of approximately 10 mins was recorded. Prior to this, the density (ρ) of the solution was estimated using Equation 3-3, from the mass (m) of 1ml of the polymer solution. The surface tension was subsequently calculated using the below equation;

$$\gamma = \frac{\rho g h r}{2}$$

(3-4)

where γ is the surface tension, ρ the density of the polymer solution, h the height rise and r the internal radius of the capillary tube.

3.3.3 Viscosity

Viscosity were measured using a Kinexus Lab$^+$ rheometer by Malvern Instruments Ltd (Worcestershire, UK). The equipment is fitted with an appropriate measuring geometry, either a parallel plate (PU-50 or PU-20) or a cone and plate system,

depending on the expected viscosity of the measured fluid. For all the tests, a sample volume of 0.5ml was applied on the lower plate and using the system`s rSpace software a standard operating procedure was set. Measurements were carried out at a set temperature of 25°C and the shear rate varied between 100 – 1000rpm, to determine the rheological properties of the liquid. Viscosity recorded at the shear rate of 100 rpm was reported in this thesis.

3.3.4   Porosity and Specific Surface Area (SSA)

Porosity of the fibre mats were estimated using a method previously described in literature [133, 134]. For fibres electrospun using the horizontal flat collector (FC) system (Section 3.2.2.1), the fibres were loosely packed into a column box of approximately 80cm^3, without compression. The density of the fibres was subsequently evaluated using Equation (3-3). For the PP sorbent and PS fibres electrospun using the rotating drum collector (DC) system (Section 3.2.2.3), the density was estimated through the mass and volume of a cut sample of the mat, with dimension 3.0 x 3.0 x 0.3cm for the PP mat and 3.0 x 3.0 x 0.1cm for electrospun PS mat. A bulk density value of 1.05g/cm^3 and 1.2g/cm^3 was used for the PS and PP polymers respectively, while the blend was evaluated based on the ratio of both polymers in the blend. The porosity was the estimated using the Equation (3-5) below;

$$\text{Porosity} = \frac{\rho_{\text{fibre}}}{\rho_{\text{bulk polymer}}} \qquad (3\text{-}5)$$

Where ρ_{fibre} represents the measured density of the fibre and $\rho_{bulk\ polymer}$ density of the bulk polymer.

The specific surface area (SSA) was measured using an expression derived by lin et al[95], for a non-porous, circular cross section fibres of infinite length. The mean (average) fibre diameter (AFD) was used with the equation for SSA below;

$$SSA = \frac{4}{\rho_{bulk\ polymer} \times D} \hspace{3cm} (3\text{-}6)$$

where D represents the mean fibre diameter and $\rho_{bulk\ polymer}$ the polymer bulk density.

3.4 Polymer Fibre/Mat Characterisation

3.4.1 Fibre morphological and chemical analysis

3.4.1.1 Scanning Electron Microscopy (SEM)

Morphological characterisation of the fibres were carried out using a Field Emission Scanning Electron Microscopy (FESEM) model JSM-7401F manufactured by (JEOL limited, Japan). Scanning electron microscopy is an imaging technique capable of producing high resolution images of samples with resolution several order of magnitude greater than an optical light microscope. Images are generated through the interaction of an incident high energy electron beam and atoms at or close to the surface of a sample often coated with a conductive layer. This interaction generates several signals; secondary electrons (SE), backscattered electrons (BSE) and X-ray signals which are used for morphological, microstructural and chemical composition analysis of a sample [135]. The SEs are mainly used for morphological characterisation due to the high resolution of images produced.

In this research, the FESEM model JSM-7401F manufactured by (JEOL limited, Japan) was used for the morphological study. All electrospun samples were left to completely dry and made free of residual solvent by drying under ambient condition,

before subsequently secured on an aluminium stub with a leit adhesive carbon tabs. Sputter coating of samples with Gold-Palladium (Au-Pd) film was done with a high resolution beam coater Model 681 (Gatan, USA). Scanning was done using a low accelerating voltage of 2-3 kV to prevent sample charging and for high resolution imaging. Image processing was done with ImageJ a free online software by NIH, USA. Due to equipment availability Hitachi (S3400) was used in some analysis and this is duly stated in such chapter.

3.4.1.2 Attenuated Total Reflectance-Fourier Transform and Infrared Spectroscopy (ATR-FTIR)

Fourier Transform and Infrared Spectroscopy (FTIR) is an analytical technique capable of identifying the chemical bonds (functional group) present in organic or inorganic compounds. It works on the principle that every poly-atomic molecule exhibits a unique fingerprint in the form of an infrared spectra when irradiated with an infrared signal [136]. The IR spectra peaks are formed as a result of molecular vibration between the atoms, which is dependent on the bond strength, the inter- and intramolecular attractions as well as the atomic masses of the constituent elements[136].

A Spectrum Two IR spectroscopy by Perkin Elmer (Buckinghamshire, UK), equipped with an attenuated total reflectance (ATR) accessory was used to characterise the electrospun fibres produce in this study. Samples were placed on a composite zinc selenide (ZnSe)-diamond crystal, with an applied force gauge of 80. Sample scans were done in the mid infrared region of $400 - 4000 \text{cm}^{-1}$ and each IR spectra was produced from an average of 20 scans at a resolution of 4cm^{-1}.

3.4.1.3　X-Ray Diffraction (XRD) Spectroscopy

X-ray Diffraction (XRD) pattern of the fibre samples were obtained using a benchtop x-ray diffraction instrument; the MiniFlex Diffractometer by Rigaku (Tokyo, Japan). Analysis was carried out using a Cu-Kα radiation source, at 40kV and 40mA. All data were obtained under a scan range of ~3° to 70° 2θ.

The X-ray diffraction provides data for quick identification of the structure (amorphous or crystalline nature) of a material. It works basically on the principle of Braggs Law; which is described by Equation 3-7 below;

$$n\lambda = 2d \sin \theta \qquad (3\text{-}7)$$

where n is a positive integer representing the order of diffraction, λ is the wavelength of the incident X-ray beam, θ , the angle of incident or diffraction of the beam, while d represents the inter-planar spacing between successive planes.

Figure 3-2 shows a schematic representation of Bragg`s law and the diffraction process.
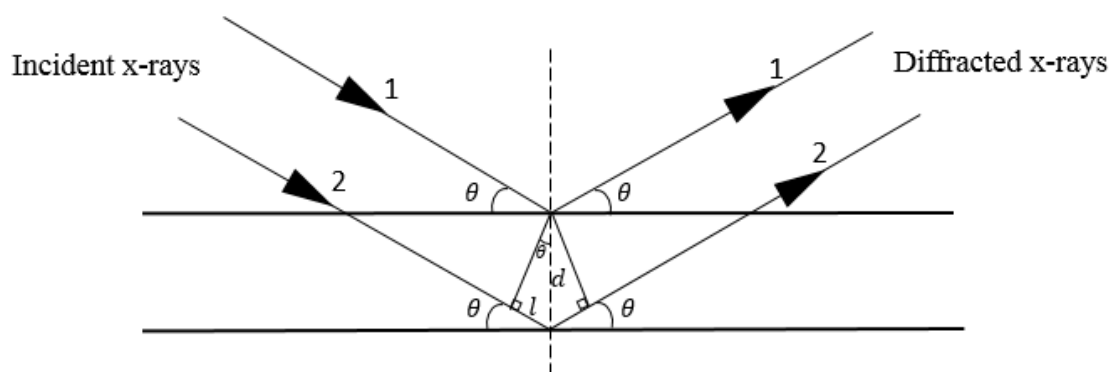
Figure 3-2: Schematic diagram illustrating Bragg`s Law

3.4.1.4　Energy Dispersive X-ray (EDX) Spectroscopy

Energy Dispersive X-Ray (EDX) Spectroscopy attached to a Hitachi S3400 scanning electron microscopy was used for elemental analysis of the electrospun polymer fibre

blend. Spot scan at three different positions along a single filament was carried out. Element identification and quantification of the fibres was done with the aid of an INCA energy software installed on an accompanying workstation. Prior to EDX analysis, all samples were affixed on an aluminium stub with a leit adhesive carbon tabs, and sputter coated with a carbon layer using a Turbo-pumped thermal evaporator K975X by Quorum Technologies (East Sussex, UK).

3.4.1.5   Water Contact Angle (WCA)

Contact angle measurements of the fibre and polymer thin films were measured using a DSA MK-10 contact angle measuring device. A 4 – 6µl droplet of the probe liquid was dispensed on the samples surface, and the reported value represents an mean of seven measurements at different points on the sample.

3.4.2   Thermal Testing

3.4.2.1   Thermogravimetric Analysis (TGA)

Thermogravimetric analysis (TGA) measurements of the electrospun fibres (both pure and polymer blend fibres) were performed using a TGA 7 Thermogravimetric analyser by Perkin-Elmer (USA). Samples size of approximately 10mg was used for each analysis and were carried out under a nitrogen blanket at a temperature range of 50^oC - 800^oC, using a heating rate of $20^oC/min$. Data for the TGA were plotted as weight % versus temperature to obtain the onset and final decomposition temperatures. Thermograph of temperature versus derivative weight % was used to determine the decomposition temperatures.

3.4.2.2   Differential Scanning Calorimetry (DSC)

The glass transition temperature of the composite PSPU fibres, as well as those of the pristine polymer fibres were measured using a differential scanning calorimeter DSC Q2000 by TA Instrument (Delaware, USA). The measurements were done in a nitrogen atmosphere at a temperature range of -80 and 150°C and a heat scan rate of 10°C/min. Prior to the DSC analysis, a sample size of approximately 7mg was placed in a hermetic crucible (TA Instrument) and securely sealed on a hydraulic press with a matching hermetic lid. A pin hole slit was made at the top of each sample to allow the escape of any volatile vapour that may be emitted during the heating scan. In DSC analysis, results obtained are often sensitive to the scan rate, the pan type, the type of gas used and the sample weight [137]. All analyses were carried out in duplicates.

3.4.3   Fibre/Mat Mechanical Property Evaluation/Testing

3.4.3.1   Tensile Testing

Mechanical properties of the fibre mats were evaluated with slight modification to ASTM D882 test method [138].

The tests were conducting on a bench top uniaxial tensile testing machine, model H5KS by Hounsfield Test Equipment (Surrey, UK). All data were recorded and exported through the device software (a product of Tinus Olsen) to plot the stress-strain curve. The Young's modulus, tensile strength, yield strength and elongation at ultimate tensile strength were subsequently determined from the stress strain curve. To determine the yield strength, a 0.2 % offset was applied to the elastic region. All data reported represents a mean from five specimens. Table 3-3 shows the settings used for the tensile test experiment.

Table 3-3*: Experimental setting used in all tensile test*

Tensile Test Setting	
Load Cell	100N
Gauge Length	20mm
Strain Rate	2mm/min
Specimen Dimension	60mm x 10mm

For the specimen and test preparation, a pair of "U - channel" test grip; with two inner parallel plates was fabricated to securely hold the specimen during testing (see Figure 3-3). For each fibre mat a sample size of 60mm x 10mm was prepared and placed on a special three part, cardboard test frame with dimensions as shown in Figure 3-4. The test frame holds the sample securely on the test grips and help prevent damage to the mat prior to testing. The mat thickness was determined from an average of five measurement taken at different position on the sample using a fabric thickness gauge.
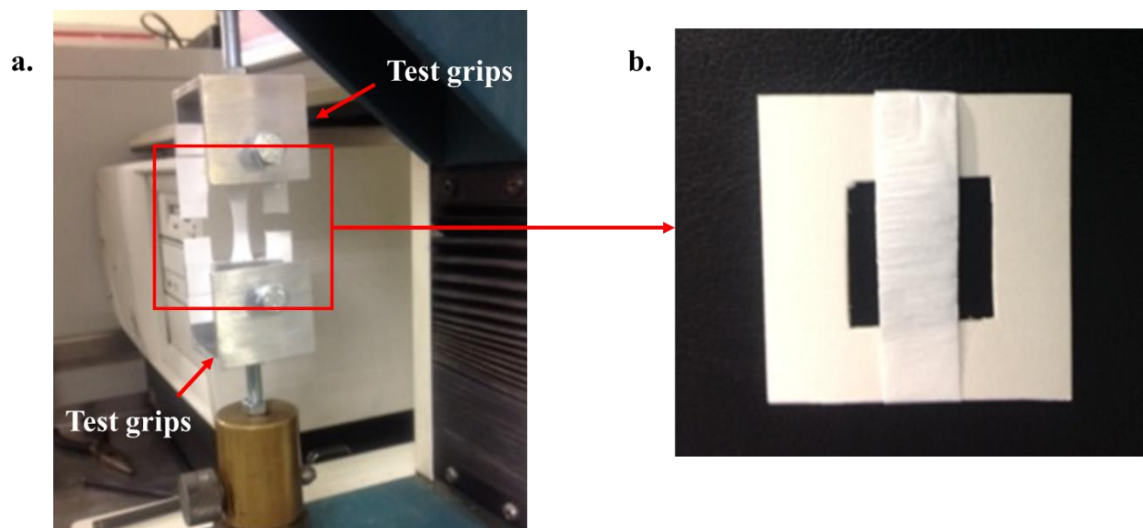
Figure 3-3: Photograph of the tensile test setup, showing the sample mounted on the test grips.
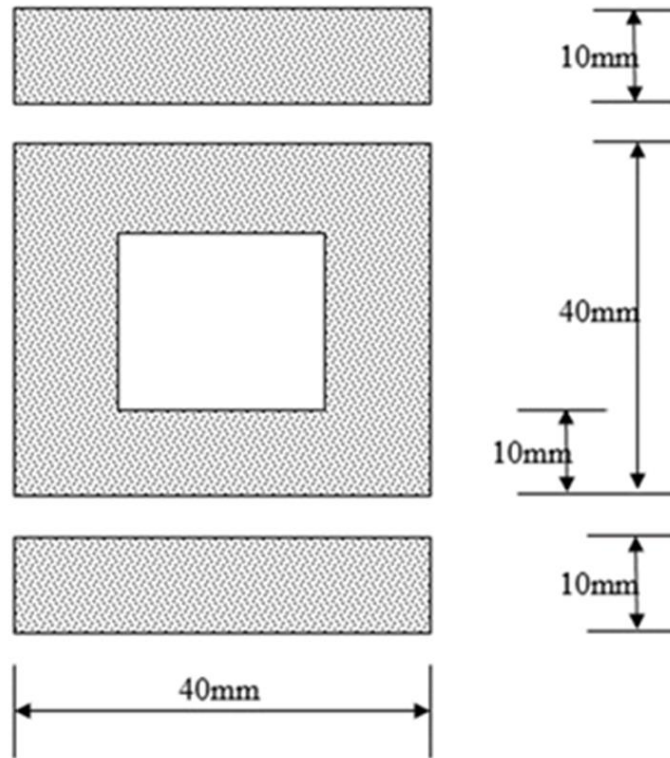
Figure 3-4: *Dimensions of the tensile test frame*

3.4.3.2 Peak Force Quantitative Nano Mechanical (QNM) Testing

The variation in modulus of elasticity and adhesion property of the polymer blend fibres with the polymer ratio, was evaluated using the AFM Peakforce QNM method. The test was carried out on a single filament of each blend using a Bruker Multimode 8 AFM (Coventry, UK). For each analysis a scan area of 1um x 1um was aimed at the top of the fibre filament at a measuring pixel of 256 x 256. In situation where a smaller scan area was utilized due to fibre size has been acknowledge in the appropriate chapter. Prior to measurement the cantilever tip was calibrated through an iterative process using a known reference sample.

Peakforce QNM measures the Young's modulus using the Derjaguin-Muller-Toporov (DMT) model; a modified form of the Hertzian model and takes into account the adhesion between the tip of the cantilever and the sample [139, 140] using the equations below;

93

$$F_{tip} - F_{adh} = \frac{4}{3}E_*\sqrt{R(d^3)} \qquad \text{(3-8)}$$

where $F_{tip} - F_{adh}$ represents the force on the cantilever relative to the adhesion force, R the radius of the cantilever tip; d is the sample deformation and E_* the reduced modulus. The relationship between the reduced and sample modulus is expressed in the equation below;

$$E_* = \left[\frac{1-v_s^2}{E_S} - \frac{1-V_{tip}^2}{E_{tip}}\right] \qquad \text{(3-9)}$$

E_{tip} and E_S are the modulus of the cantilever tip an sample respectively, while v_s and v_{tip} represents the corresponding poisson ratio.

3.4.4 Oil Sorption Evaluation of Fibre Mats

All static and dynamic sorption tests were performed with slight modification to ASTM F726-12 test standards [141]. To analyse the oil-water selectivity under static and dynamic conditions, 20g of oil was added to a 250ml glass beaker containing 150ml of seawater to form an oil layer of approximately 8mm thickness. Approximately 0.1g of the fibre mat was placed on the oil-water medium for 30 mins, after which the wet mat was removed, drained for another 1min before weighing. For dynamic sorption analysis, the system was agitated at 250rpm. The sorption capacity was evaluated using the Equation below[19];

$$\text{Sorption Capacity (SC)} = \frac{w_1 - (w_o + w_w)}{w_o} \qquad \text{(3-10)}$$

where W_1 is the weight of the wet sorbent after draining, W_0 is the initial weight of the dry sorbent and W_w represents the weight of any sorbed water. In all the test, the amount of water sorbed was found to be negligible, hence W_w was taken as zero.

For oil only system, the fibre mat was placed in a beaker containing 150ml of the test oil, while all other steps as stated above for the oil-water system was followed. For comparison of the oil sorption capacity of the polyblend mat with previous works, the test procedure reported in literature was used [22].

Physical properties of the oils used for sorption analysis in this thesis is as shown in the Table 3-4 below;

Table 3-4: Physical characteristic of the studied oils

Oil Sample	Viscosity (mPa.s)	Density (g/cm³)
Pennsylvania Light Crude	0.13	0.794
Vegetable Oil	28	0.861
Sunflower Oil	37	0.894
Motor Oil	95	0.812

3.4.5   Buoyancy test

The buoyancy of the fibre mats was simulated under both static and dynamic (500rpm) conditions. For the static test, a sorbent of ~1.5g was gently placed in a 250ml beaker containing 10ml of motor oil layered on a 150ml water. The sorbent was subsequently monitored over a period 30mins. The dynamic test was conducted on the basis of the static test but agitated at ~500rpm using magnetic stirrer.

3.5   Surface Free Energy Measurement

Surface free energy (SFE) evaluations was done using OWRK method described in Section 2.10.1. Two different probe liquids; water and diiodomethane were used. The static contact angle the probe liquid makes with the surface of the solid material (fibre or cast) were measured using the sessile drop method. The data were recorded and analysed on a Drop Shape Analyser-DSA MK10 by Kruss GmbH (Hamburg,

Germany). The reported static contact angle represents an average of at least 5 measurements taken at approximately 4s of exposure to the test liquid. This value was subsequently used for SFE measurement using Owen Wendt Kaebel Rabel (OWRK) method.

3.5.1   Sample preparation

The polymer film used for the SFE measurement was drop cast from a 5% w/w PS dissolved in THF. The PP thin film was prepared from a PP sorbent melt. The sorbent was sandwiched between two polished aluminium sheet and heated to a temperature of approximately 250ºC, with a 10kg weight placed on the sample for approximately 2mins. The fibres used in this study were the commercial PP sorbent and PS fibres electrospun using the horizontal flat collector system at the optimised parameter stated in Section 3.2.2.3.

3.6   Drop on fibre analysis

Drop-on-fibre analysis was performed on a DSA-MK 10 device. A single fibre filament was suspended on a special test jig designed for this experiments. Optical image of the test jig is as shown in Figure 3-5, below. Using the device syringe needle (Ø 650µm), approximately 6µl droplet of oil was allowed to drop through the suspended filament. Images of the interaction between the oil and the fibre was obtained via the device CCD camera. NIH free online software, ImageJ was used for image processing to obtain the drop contact angle, experimental drop length and reduced drop height. Further data processing (using Equation 2-14, 2-15 and 2-16 obtain in section 2.10.2) to determine the theoretical reduced drop length, drop volume and adhesive energy, using a matlab codes. Analysis of each oil type was made using

measurements obtained from 50 barrel-shaped droplets on each fibre type. The matlab code used for the data processing is presented in the Appendix.
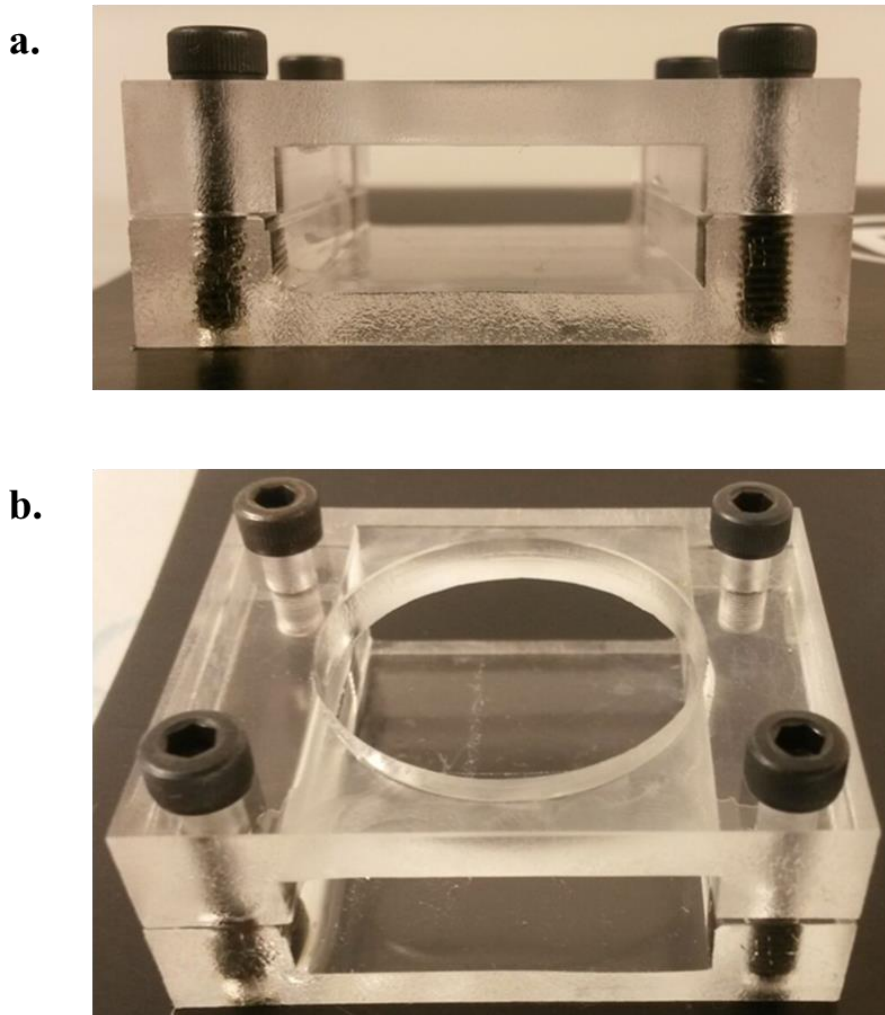
Figure 3-5: *Photograph of the test jig fabricated for the drop-on-fibre test.*

3.7   Heat Treatment

Thermal treatment of the electrospun fibre mats were performed using a Nabertherm Oven (Lilienthal, Germany). PS fibre mats with dimensions 240mm x 200mm were secured to the aluminium foil across the width of the mat, to prevent mat shrinkage. The treatments were carried out at temperatures around the polymer glass transition temperature and were done with air circulation. Heating temperatures of 90, 100, 110, 120 and 130ºC were used for 5 mins to investigate the effect of treatment temperature

on the mat. The effect of treatment time was evaluated at a treated temperature of 90ºC and at 5, 10 and 5mins heat treatment duration.

3.8 Ultrasonic Treatment

Ultrasonic treatment of the PS fibre mats were carried out by immersing a cut fibre mat secured at both ends into a 50% ethanol concentration in an ultrasonic bath CD 4820. Treatment were carried out at approximately 65ºC for 5 and 10 mins, and fibre were removed and allowed to dry in ambient condition for at least 7 days before further use.

4 Microscale oil adsorptivity evaluation

4.1 Introduction

Sorbents as material commonly used in oil spill remediation has proven to be an effective method of completely eradicating such spills, if timely and effectively deployed [7, 91]. The ability of fibrous sorbent to adsorb and retained oil pollutant is often attributed to its physicochemical properties (fibre/mat morphology, chemical composition of the fibre) as well as the properties of the oil (viscosity, surface tension and density) [142]. Recent studies have shown polystyrene (PS) fibres fabricated using electrospinning technique to possess better sorption performance than the commercially available melt blown polypropylene (PP) sorbent [19]. On a microscale level, the oil – sorbent (fibre) interaction and its effect on the sorption behaviour is yet to be fully understood; considering PP bulk material is known to have a lower surface energy than polystyrene.

PP is a very unreactive polymer and insoluble in solvents at room temperature and therefore cannot be electrospun from solution[143]. Existing literatures on electrospinning PP was done via melting electrospinning, which involves complex electrospinning setup as fibre production has to been done at elevated temperatures [134, 143, 144] and in some cases involves the use of viscosity reducing additives [144]. This extra complexity and cost makes it an undesirable process, hence commercial PP sorbent used in oil spill clean-up is fabricated using melt blown technology

The primary aim of this chapter is to employ the drop-on-fibre micro sorption technique based on B.J Carroll's theory [128], to quantitatively evaluate the adsorptivity and adhesive energy of a single electrospun PS fibre filament to selected oil types. This will be further compared with commercial melt-blown PP fibres, using the droplet sizes and adhesive energy distribution of the oils on the fibres. As a prelude to carrying out this study, an evaluation of the factors that could affect the morphology of electrospun PS fibres were studied, to ensure fibres produced for the micro sorption experiment were of the desired morphology and global geometry. Consequently this chapter will be in two parts; first is optimising the electrospinning process followed by investigating the oil adsorptivity of electrospun PS fibres and PP fibres. In achieving the above, the specific objectives of this chapter are as follows;

- To optimise the electrospinning of polystyrene fibre and investigate the effect of polymer concentration, solvent type, solvent mix ratio and flow rate on fibre morphology.

- To investigate the water contact angle (WCA), wettability and surface energy of melt blown PP and electrospun PS fibres and the respective polymer thin films.

- To evaluate the experimental drop length from the drop-on-fibre micro sorption experiment and compared to the theoretically derived values.

- To evaluate the droplet size and adhesive energy distribution of both electrospun PS and melt-blown PP fibre.

- To study the oil droplet size distribution on single the PS and PP filaments, and relate micro-sorption behaviour of the fibres to the macroscale mat sorption behaviour.

4.2 Optimisation of electrospun PS fibre fabrication

This section looks at electrospinning experiment by evaluating the effect of polymer concentration, solvent type/mix ratio of DMF and THF, and the effect of flow rate on the morphology of the resulting fibres. Previous studies have shown these factors as some of the key parameters that could effects the morphological structure of electrospun fibres [145-147]. The subsequent sub-section details the solution properties and the optimisation experiments conducted using set up described in Section 3.2.2.1

4.2.1 Investigating the effect of concentration on fibre morphology

The effect of increasing polymer concentration on solution properties is shown in Figure 4-1, where the viscosity is seen to increase from 35.1 mPa.s at PS 10% w/w concentration to 1130 mPas.s as the concentration was increased to 25%. This effect could be attributed to an increase in polymer chain entanglement [148, 149]. Similarly, with the stepwise increase of 5% in polymer concentration (from PS 10% w/w), the solution conductivity decreases from 1.19µS/cm to 0.57µS/cm at 20%w/w conc. and 0.63µS/cm at 25% concentration. The overall decreasing trend in conductivity with increasing PS concetration can be ascribed to PS high electrical insulation properties.

The influence of the above solution properties on the fibre morphology is seen in Figure 4-2 and Table 4-1, where 10% and 15% PS solutions produced beaded fibres. The morphology of the beads transformed from spherical in 10% PS to spindle-like shape in fibres spun from the 15%PS solution. This is a result of increase in polymer chain entanglement with increased polymer concentration, reducing the surface tension effect of the solvent on the polymer jet during electrospinning. Jarusuwannapoom et al, [149] in their study had attributed beads formation to the
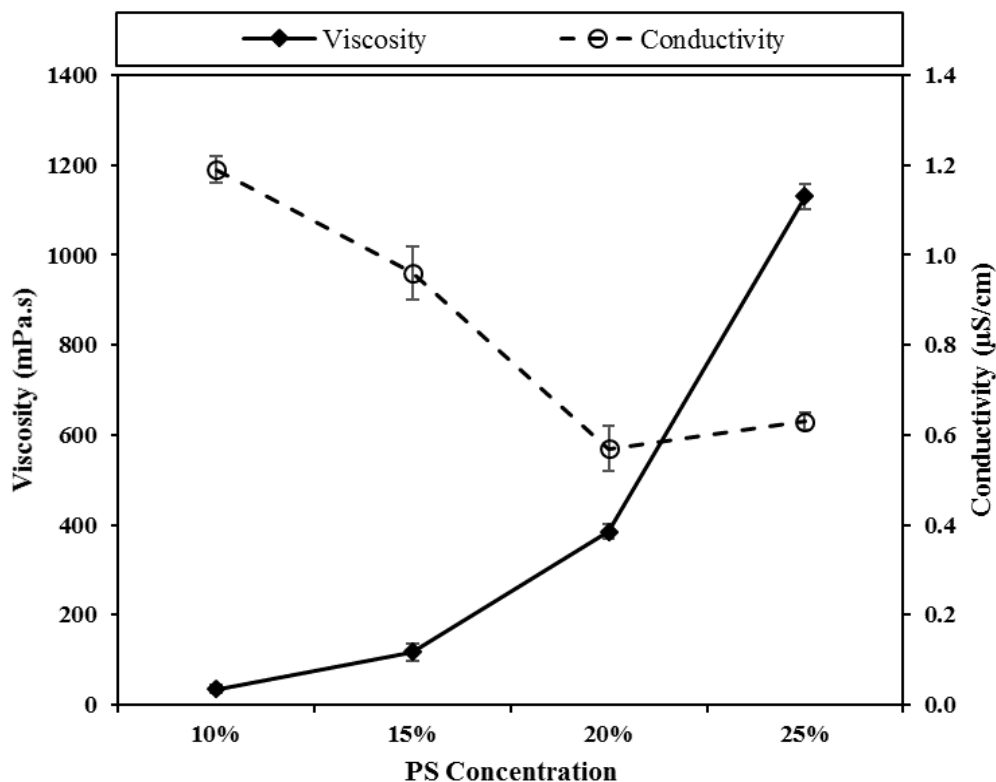
Figure 4-1: Plot shows the effect of increasing PS concentration on the viscosity and conductivity of PS polymer solution dissolved in a solvent mix of DMF:THF (4:1). Error bar represents one standard deviation about the mean (n=5).

surface tension, Coulombic and viscoelastic forces resisting the stretching of the polymer during jet propagation. At 20% PS concentration, uniform and bead free fibres were observed. This could be termed the optimum concentration given the solvent mix of DMF/THF (4:1) used in this set of experiments as other studies have reported beads formation at 20% PS concentration for other solvent or solvent mix [146, 148, 149]. The influence of increasing polymer concentration on mean fibre diameter (MFD) is shown in Table 4-1, using parameters stated in Section 3.2.2.3 (as PS fibres could be produced over a wide range of parameters). The AFD steadily increases from $0.51 \pm 0.18\mu m$ with the 10% PS to $1.92 \pm 0.45\mu m$ in the 20%PS solution. The observed drop in AFD to $1.06 \pm 0.53\mu m$ at the 25% solution is a result of jet instability at a high solution viscosity, leading to a polydispersed fibre deposition as illustrated in Table 4-1 and SEM micrograph in Figure 4-2. The measured average

intra-fibre pore size was also seen to reduce with increasing polymer concentration (Table 4-1).

In view of the above observation, subsequent electrospinning experiments in this thesis were performed at 20% PS concentration
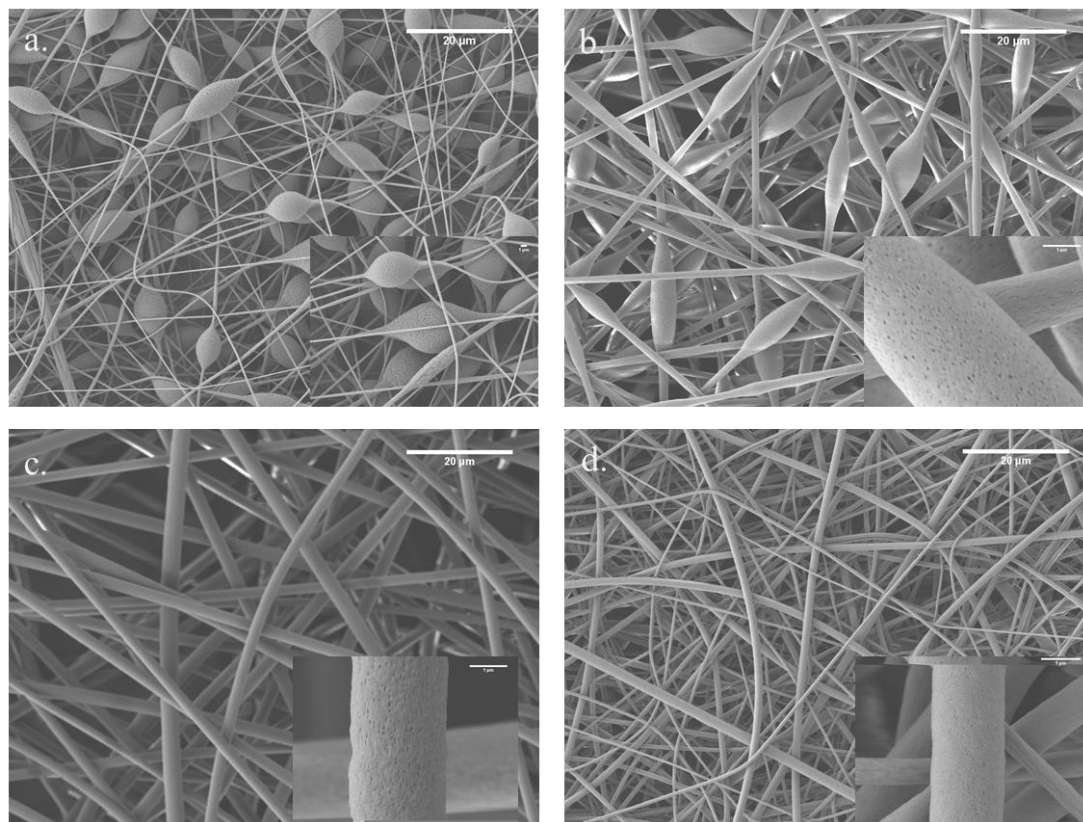
Figure 4-2: SEM micrograph showing the effect of concentration on morphology of electrospun PS fibre; a.) represents 10%w/w; b.)15%w/w; c.)20%w/w and d.)25%w/w PS concentration dissolved in a solvent mix of DMF/THF (4:1).

Table 4-1: Shows the maximum (max.), minimum (min.) and mean fibre diameter of electrospun PS solutions at different polymer concentration (n = 100). Average pore sizes on both fibre and beaded structure is also presented.

Polymer Conc. (%) w/w	Fibre				Beads
	Fibre Diameter (μm)			Pore Diameter (μm)	Pore Diameter (μm)
	Min.	Max.	Mean	Mean	Mean
10	0.15	0.91	0.51 ± 0.18	0.10	0.6
15	0.62	2.01	1.16 ± 0.27	0.10	0.08
20	1.00	3.01	1.92 ± 0.45	0.09	-
25	0.31	2.50	1.06 ± 0.53	0.04	-

4.2.2 Investigating the effect of solvent mix on fibre morphology

The solvent used in an electrospinning experiment often play a key role in the morphology of the resulting fibre. A mixture of solvents to a polymer (solute) could be used in modulating the property of the electrospinning process and the resulting fibre morphology. Figure 4-3 shows the effect of varying solvent mix of DMF and THF on the properties of 20% w/w PS solution. The introduction of THF in the (DMF:THF) 4:1 saw an increase in the viscosity from 376.9 mPa.s in the pure DMF solution to 385.5 mPa.s. Further increase in THF ratio saw a gradual deceasing trend in the viscosity reading. The conductivity on the other hand increases with THF introduction from 0.51µS/cm in the pure DMF and peaks at 1.44µS/cm in (DMF:THF) 2:3 before dropping to zero in the pure THF solution, as THF has previously been reported to be a non-conductive solvent[149].

The influence of the above on the average fibre diameter and intra-fibre pore sizes is presented in Table 4-2, while the morphological structure of each fibre mat is shown in Figure 4-4. Fibres fabricated from 20% (w/w) PS in pure DMF solvent produced an AFD of 2.54 ± 0.59µm, with the presence of macro/meso-pores distributed over a fairly rough fibre surface. The addition of THF into the solution matrix, at a solvent mix ratio of DMF/THF (4:1) saw a drop in the AFD to 1.52 ± 0.31µm, this could be attributed to the sharp increase in viscosity observed in Figure 4-3, while the surface pore size was also seen to drop from 0.09 to 0.03µm. The variation in diameter distribution obtained for the 4:1 solvent mix in this set of experiment (Table 4-2), against those obtained in Table 4-1 can be attributed to difference in the time both experiments were conducted, as slight variation in ambient conditions could have effects on fibre morphology as earlier discussed in Section 2.4.3. A further increase in THF content saw a steady increase in the AFD to 6.76 ± 3.82µm in the pure THF

solvent. The increasing trend in AFD is a result of THF's low dielectric strength and dipole moment of 7.58 and 1.8 respectively [150, 151]. This reduces the solution conductivity thereby reducing the stretching ability of the fibre through a reduction in the jet acceleration during the electrospinning process.
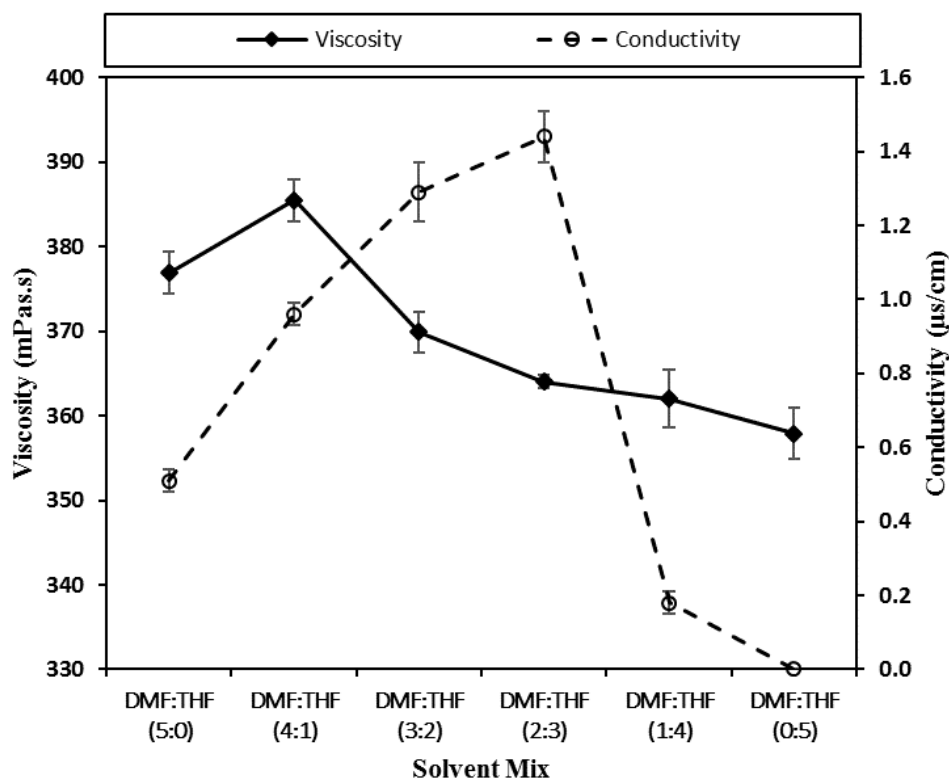
Figure 4-3: Effect of solvent mix of DMF and THF on the viscosity and conductivity of 20% w/w PS concentration. Error bar represents one standard deviation about the mean (n=5

Contrary to previous literature [146], fibres fabricated from pure DMF solvent (5:0) exhibits a bead free structure as shown in Figure 4-4a. It is believed the difference in morphological structure of the fibres could be a combined effect of difference in process and ambient conditions used in both studies. No intra-fibre pores were observed on fibres from ratios 3:2, 2:3 and 1:4 but they exhibit wrinkled, coarse surface morphology, which was found to be consistent with the literature [146]. Fibres from pure THF also exhibits similar structures to earlier reports [59, 78] with fibres having a ribbon-like shape, with densely packed meso- and macro-porous structure. This according to Carper et al [59] can be ascribed to the both vapour induced (VIPS)
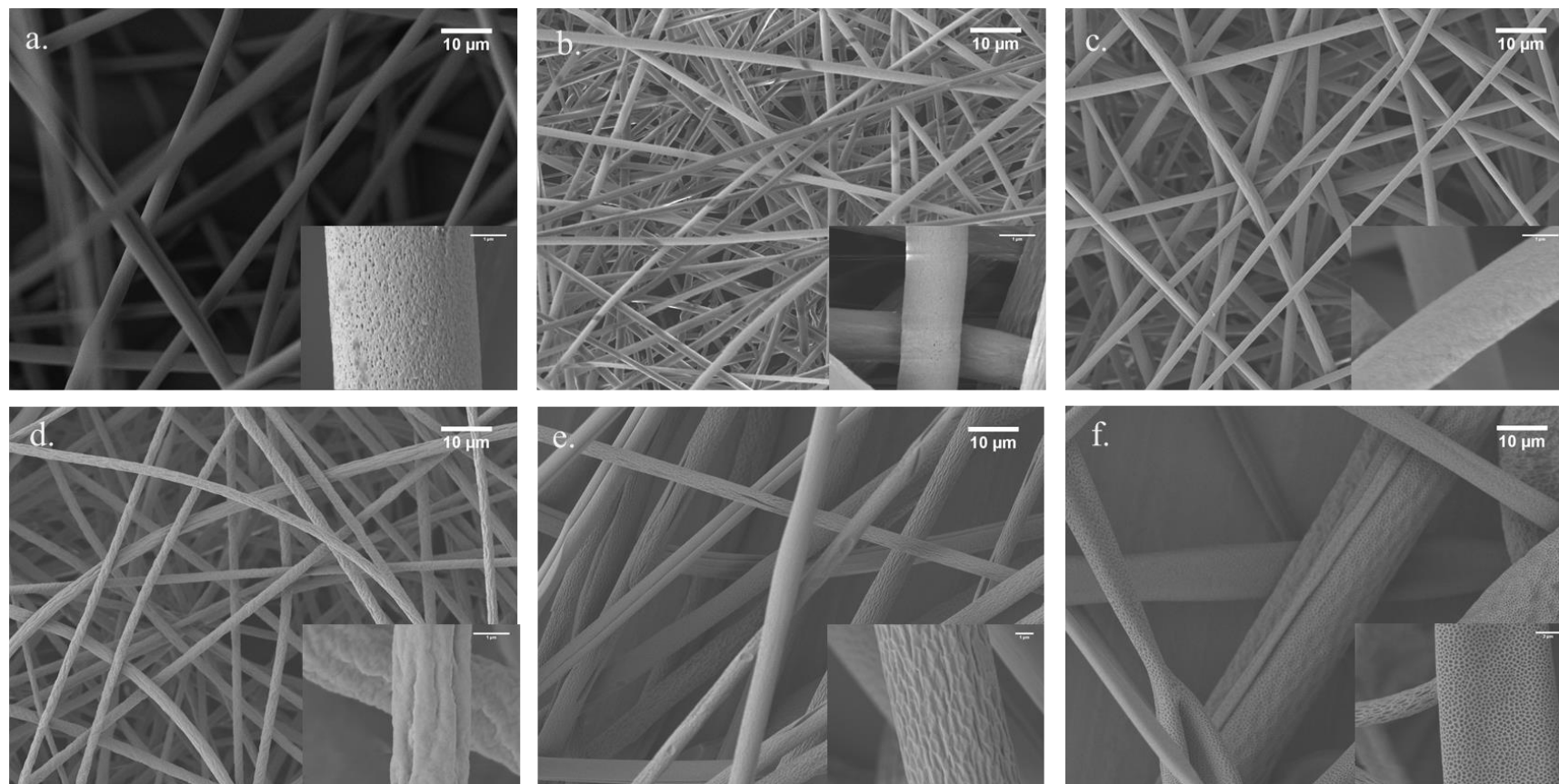
Figure 4-4: Shows the effect of varying solvent mix of DMF and THF on the morphology of electrospun 20% w/w conc. of PS polymer in; a.) DMF:THF (5:0); b.) DMF:THF (4:1); c.) DMF:THF (3:2); d.) DMF:THF (2:3); e.) DMF:THF (1:4); f.) DMF:THF (0:5).

and thermally induced phase separation (TIPS). Due to the need to have fibres with smooth morphology, as the existence of surface rugosities has been shown to impact the droplet conformation on single fibres[152], electrospun PS solution in DMF:THF (4:1) was used in the drop-on-fibre experiment.

Table 4-2: Shows ave. pore size, max. min. and mean fibre diameter of electrospun 20% w/w concentration PS solution dissolved in different solvent mix ratio of N,N dimethylformamide and Tetrahydrofuran (THF). (n=100)

Solvent Mix (DMF:THF)	Fibre			
	Fibre Diameter (µm)			Pore Diameter (µm)
	Min.	Max.	Mean	Mean
5:0	1.60	4.14	2.54 ± 0.59	0.09
4:1	0.90	2.50	1.52 ± 0.31	0.03
3:2	0.80	3.65	1.96 ± 0.58	0
2:3	0.77	3.58	2.07 ± 0.31	0
1:4	2.25	8.10	5.05 ± 1.09	0
0:5	2.25	18.32	6.76 ± 3.82	0.19

4.2.3 Investigating the effect of flowrate on fibre morphology

Feed rate determines the amount of polymer solution available for jet propagation. The effect of varying the process flow rate on PS fibre morphology is presented in Figure 4-5 and Table 4-3. At the optimised TCD of 15cm in Figures 4-5 a, b and c, the AFD was seen to increase steadily from 1.00 ± 0.28µm at a flow rate of 1ml/hr to 3.30 ± 0.37µm at 6ml/hr. Reducing the TCD down to 5cm at the same flow rate of 6ml/hr in Figure 4-5d saw a further increase in the AFD to 4.67 ± 0.60 µm. This is attributed to the reduced fibre stretching as a result of a reduction in the jet flight time. The fibres also appears fused together at the point of contact due to the presence of residual solvent upon fibre deposition [56, 153].

It is important to note that due to equipment availability different scanning electron microscope (Hitachi S3400) was used for this analysis. The flow rate of 6ml/hr was subsequently used for the drop-on-fibre micro-sorption test.

Table 4-3: Shows the min, max and average fibre diameter of electrospun PS fibre at different process flow rate. (n=100)

Flow rate (ml/hr)	TCD (cm)	Fibre		
		Fibre Diameter (µm)		
		Min	Max	Mean
1	15	0.53	2.12	1.00 ± 0.28
3	15	1.78	3.36	2.58 ± 0.41
6	15	2.75	4.69	3.30 ± 0.37
6	5	2.96	6.20	4.67 ± 0.60
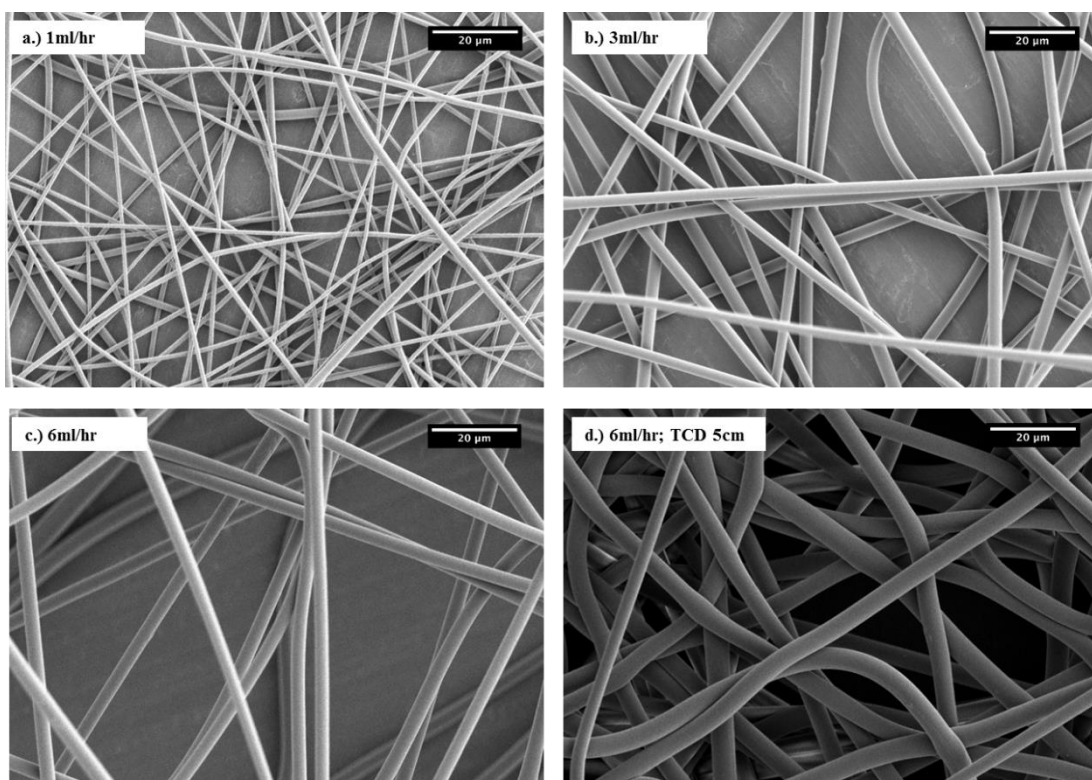
Figure 4-5:SEM micrograph showing the effect of process flow rate on the morphology of electrospun PS fibre; at a.)1ml/hr; b.)3ml/hr; c.)6ml/hr and d.)6ml/hr but at a lower TCD of 5cm, while other were electrospun at 15cm.

4.3 Investigating the affinity and adsorption of electrospun Polystyrene fibre to selected oils

Polypropylene (PP) polymer spun into fibres using melt blown technology has been the material widely available commercially as oil sorbent. Its use as a sorbent has been attributed to its non-polarity, low surface energy and good hydrophobicity, excellent mechanical properties, low density and low cost of the polymer [154]. Despite PP having one of the lowest surface free energy (SFE) among polymer, polystyrene (PS) which has a higher SFE and bears similar elemental properties as PP aside the presence of aromatic phenyl ring in its chemical structure, has been shown to have better oil sorption performance when electrospun [16, 19]. The superior sorption behaviour of electrospun PS fibre has been largely ascribed to its morphological/mat architecture [19]. No study exist in literature that has looked at the microscale interaction of these two fibres with selected oil samples.

The subsequent sections of this thesis chapter, investigates the variation in SFE between of solid and fibrous form of these polymers using the Owens Wendt Rabel Kaeble (OWRK)[125] method. This is followed by a micro scale study of the interaction between single fibre filaments of electrospun PS and melt blown PP with oils of different viscosities.

4.3.1 Morphology of electrospun PS and PP fibre

Prior to investigating the SFE of PS and PP polymers, the morphology of both polymers sorbents were investigated under a scanning electron microscopy (SEM). Figures 4-5a and b shows typical SEM micrograph of electrospun PS and melt blown PP fibre mats respectively. Visual inspection of the two micrographs shows a marked difference in the morphology of the sorbents, with the possibility of making varying

inferences on their ability as oil sorbents. The electrospun PS fibre exhibits uniform

fibre size distribution, with fibre diameter in the range of 1.5µm and 4.2µm, and an

average fibre diameter of 3.02 ± 0.5µm, while a wide variation of sizes in the range of
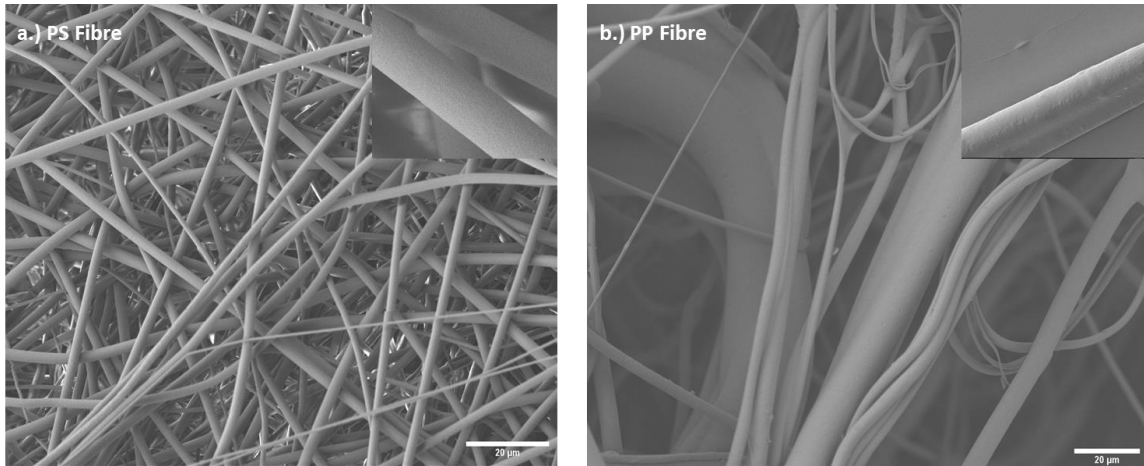
Figure 4-6: a.) and b.) Shows a typical SEM micrograph of electrospun PS and melt blown PP fibre mats respectively. Insert shows a high magnification image of individual fibre filament.

1.1µm and 19.5µm was observed for the melt blown PP fibre. In addition to the large

variation in fibre diameter observed for the PP sorbent, a significant number of the

fibres were observed fused together, unlike in the PS micrograph. This significant

variation in the fibre morphology between the two samples could be the effect of the

difference in processing techniques used in its fabrication. Large numbers of

interconnected, interstitial void spaces were observed between the PS fibre with the

void sizes ranging between 2.1µm and 36.2µm. The PP micrograph on the other hand

had sizes between 3µm and 199.2µm which is over five times greater than values

obtained for the PS sorbent. Gravimetric measurement of the porosity shows PP fibre

mat with a 91.2% porosity in comparison to 99.8% obtained for the PS mat. High

magnification examination of the surface of individual electrospun PS fibre filament

shows the presences of meso- and macro-pores sparsely distributed on its surface,

while PP surface exhibits a smooth morphology.

The high porosity and interconnected pores of the PS mat could imply a good sorption and buoyancy characteristic when used in marine oil spill remediation. The presence of surface pores on the PS fibre surface could enhance good adherence of oil to the fibre filaments, although the presence of surface pores has earlier been reported not to have an influence in sorbent sorption performance[21].

4.3.2 SFE of PP and PS fibre and film: Comparison (WCA)

Sorption behaviour of any porous material (such as polymeric fibrous sorbent) is closely related to its wettability and the capillarity of the material. For a given liquid to get sorbed into the interstitial void between the fibres, there has to be an initial intermolecular interaction between the liquid-fibre interface [118, 155, 156]. Wetting of the fibre surface will only occur if the surface tension of the liquid/ oil medium falls below the SFE of the sorbent[157], therefore an ideal sorbent should have its SFE below the surface tension of water but above that of the oil medium.

Estimation of the SFE of a solid is often done by measuring the contact angle a probe liquid makes on the surface of the substrate. Hedja et al and Owens et al [125, 158] have earlier reported that a pair of polar and non-polar liquid gives a reliable estimation of SFE of a surface using the Owens Wendt Rabel Kaeble (OWRK) fit (see Section 2.10.1). Table 4-3 gives the contact angle measurements obtained for a pair of diiodomethane (DIM) and water on each surface. As seen in the table, there is a difference in water contact angle (WCA) between the film and fibrous sample of both polymers. The higher WCA angle recorded for fibrous samples could be attributed to the cassie-baxter effect[159] (see Section 2.8), as the water droplet seats on trapped air pocket; an effect of the porous nature of the sample. For the non-polar DIM on the other hand, a contact angle of $50.57 \pm 2.8°$ and $35.3 \pm 5.4°$ was recorded on PP and PS

thin films respectively, while for the fibrous sample of both polymers a 0° contact angle was recorded as the DIM was seen to spread and percolate through the fibre pores almost immediately. This indicates complete wetting due to a strong interaction at the interface as well as an effect of the porous nature of the material.

Table 4-4: Water and Diiodomethane (DIM) static contact angle measurenets for electrospun PS and melt blown PP fibre mat and their respective thin films. Reported value represents an average of atleast five measurements at different positions on the samples.

Polymer Sample	Contact Angle (°)	
	Water	DIM
PP Film	116.32 ± 7.2	50.57 ± 2.8
PP Fibre	148.03 ± 7.8	0
PS Film	85.7 ± 2.1	35.3 ± 5.4
PS Fibre	139.8 ± 1.8	0

Table 4-5: Surface free energy (SFE) of electrospun PS and melt blown PP fibre mats with the SFE of the respective polymer thin films obtained using Owens Wendt Rabel Kaebel (OWRK) method

Polymer Fibre Mat	Surface Energy		
	Dispersive Component (mN/m)	Polar Component (mN/m)	Total (mN/m)
PS Fibre Mat	50.88	11.94	62.74
PP Fibre mat	50.80	15.11	65.91
PS Film	41.89	1.56	43.45
PP Film	24.01	0.13	24.14

Table 4-5 and Figure 4-7, illustrates the total SFE obtained for the melt blown PP and electrospun PS fibres alongside the dispersive and polar components using the OWRK fit. The thin film values is also presented for comparison. The SFE value of 43.5mN/m and 25.1mN/m obtained for the PS and PP thin films respective were consistent with previously reported literature values [125, 160]. For the electrospun PS and melt blown PP fibres, the SFE is seen to increase to 62.74mN/m and 65.91mN/m respectively. These surface energy values though high, still falls below those of water;

which is stated to be 72.75mN/m at 20ºC [161]. This indicates the hydrophobic nature

of both fibre surfaces but the higher hydrophobicity of the PS mat in terms of the lower

SFE value recorded could be the effect of the mats surface architecture.
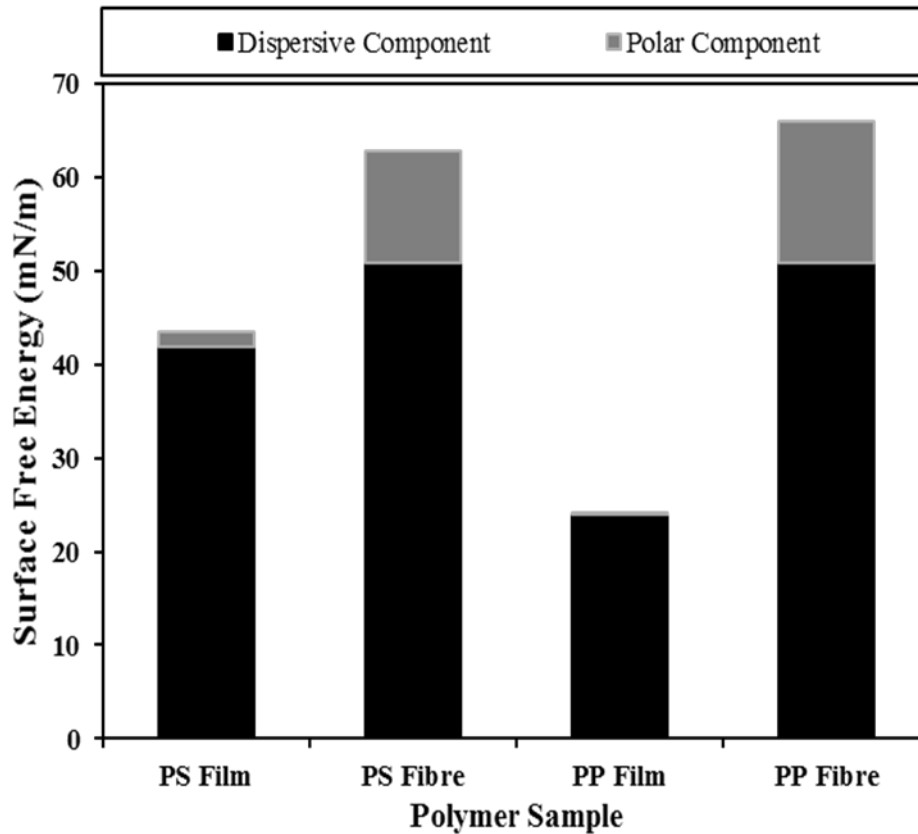
Figure 4-7: Shows a comparison of the surface free energy (SFE) components of electrospun PS and melt blown PP fibres with their respective thin film. SFE values were calculated from contact angle measurement of a pair of polar (water) and non-polar (diiodomethane) probe liquids using Owens Wendt Rabel Kaebel (OWRK) method.

The SFE obtained was further used to construct a wetting envelope as presented in

Figure 4-8. The envelope characterises the wettability of a solid with respect to any

liquid with known dispersive and polar surface energy composition. The figure

illustrates the degree to which different standard alkane oils and water will wet the

surface of the polymer fibre and thin films. As the data point for water falls outside

the wetting envelopes in both figures, this implies that water will not wet the surfaces.

Both fibre and thin films of PS (Figure 4-8b) will completely wet alkane fuels of n-

decane, n-hexadecane, n-dodecane and n-hexane. Figure 4-8a, on the other hand shows that PP fibre will completely wet all the n-alkane fuels in contrast to PP films that will not wet n-hexadecane and n-dodecane. However,it is important to note that the surface tension of oil varies depending on its composition but it is typically believed to be between 20 –30mN/m [142, 162]. Since oils are non-polar in nature it could therefore be said that complete wetting is expected for both PS surfaces, while the wetting of PP will be dependent on the composition of the oil.

To investigate that there was no alteration in the chemical composition of the thin film during sample preparation. ATR-FTIR of the samples were carried out. All peaks observed in the fibre mats could be distinctly identified on the thin film. Figure 4-7, shows that functional groups CH, CH_2 and CH_3, which are known hydrophobic moieties could be seen to be present in all the samples investigated, both fibre and thin film. For the PP, peaks at 2836, 2864, 2919 and 2951cm^{-1} is assigned to the C-H stretching vibration, the distinct peaks at 1457cm^{-1} corresponds to CH_2 bending vibration of PP, while peaks at 1380, 1170cm^{-1} and both 993 and 973cm^{-1} represents the bending vibration, symmetric deformation vibration and rocking vibration respectively of CH_3 [163]. All of these peaks could be seen in both samples, an indication of no oxidation or alteration of the chemical composition of the samples

Solvent	Dispersive Component (mN/m)	Polar Component (mN/m)	Symbol
Water	21.80	51.00	o
N-decane	23.90	0.0	▽
N-hexadecane	27.60	0.0	△
N-dodecane	25.90	0.0	+
N-hexane	18.43	0.0	□
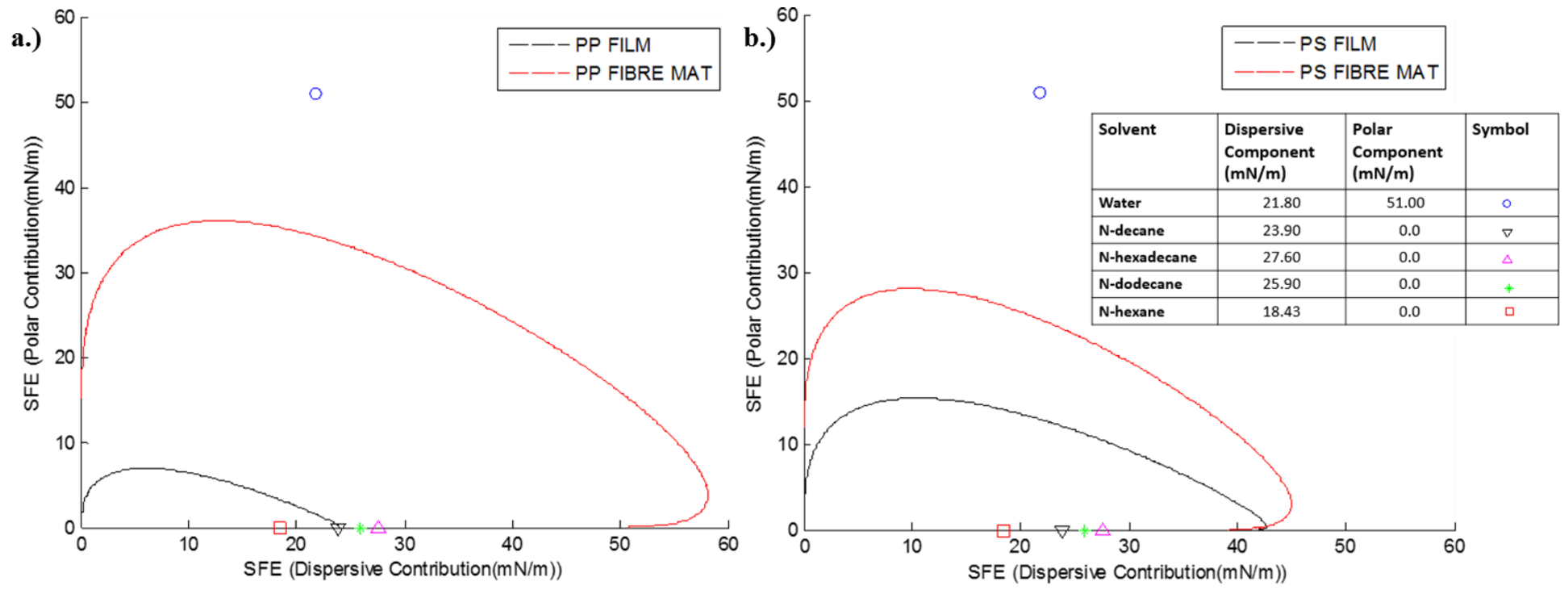
Figure 4-8: Shows a comparison of the wetting envelope of a.)PP fibre mat and PP thin film; while b.) Compares wetting envelope of electrospun PS fibre mat and its thin film. Imbedded on each graph is the coordinate for water and other known hydrocarbon fuels indicating the level of wettability of the polymer surface
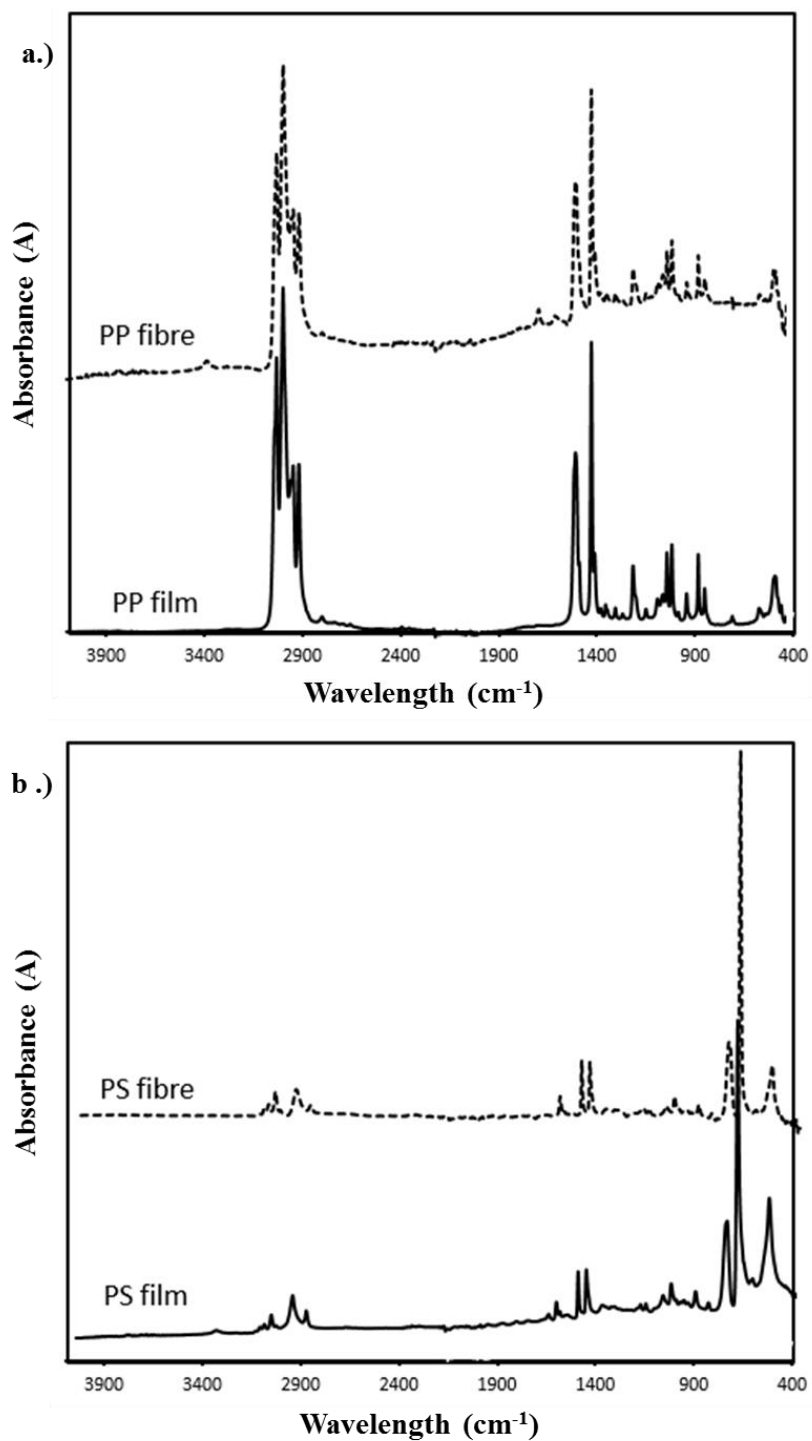
Figure 4-9: Compares the FTIR spectra of a.) Electrospun PS fibre mat and PS thin film, b.) melt blown PP fibre and PP thin film. The solid thin films were prepared as described in section 2.5.

4.3.3   Drop on fibre characterisation

4.3.3.1   Oil droplet morphology on fibres

A liquid drop which completely or partially wets a material having a flat configuration will instil either a barrel shaped (symmetric) or a clamshell (asymmetric) droplet geometry, on a cylindrical filament [129, 164] of the same material. Understanding the droplet morphology could give an insight into the level of affinity between the liquid and the fibre material. Figure 4-10, shows the geometrical structure of different oil types on both electrospun PS and meltblown PP fibres, with all the oils having a barrel-shaped morphology on the fibres. Due to the difficulty in pulling a single filament of the meltblown and electrospun mats, the PP fibre filament used in this analysis was obtained by drawing a fibre strand from a heated PP sorbent at ~200ºC. The PS fibre was obtained by picking a fibre mid-air during electrospinning jet propagation. Sunflower oil was seen to break up into more barrel shaped droplet on both fibres and seemingly exhibits less affinity to the fibres in comparison to motor oil. This is confirmed in Tables 4-6 and 4-7, where a higher average CA was observed for sunflower oil on both fibre type. The tables also shows the theoretical and experimental drop length, the reduced drop volume and adhesive energy, as well as the actual droplet sizes on the fibres.
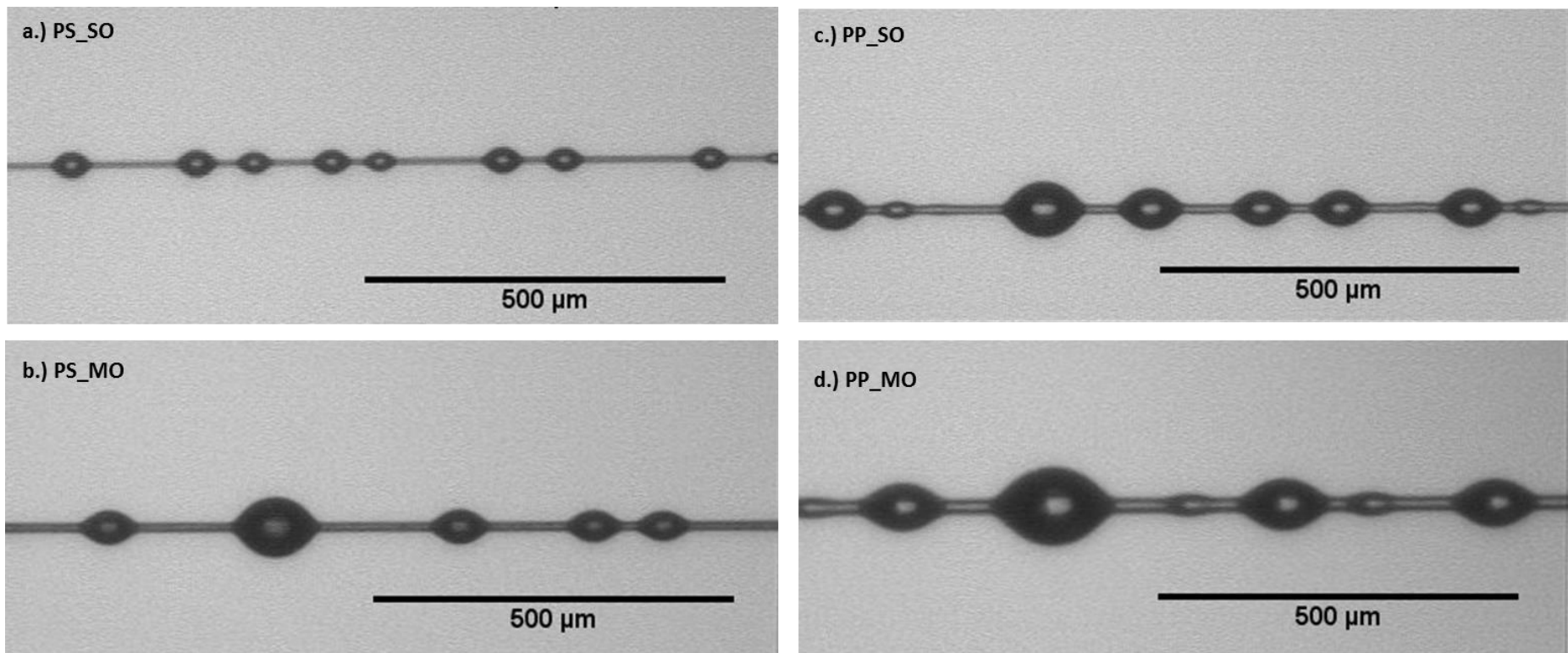
Figure 4-10: Barrel shaped drop-on-fibre system of sunflower and motor oils on electrospun polystyrene and polypropylene fibres; a.) sunflower drop on polystyrene (PS_SO); b.) motor oil on polystyrene (PS_MO); c.)sunflower on polypropylene (PP_SO) and d.) motor oil on polypropylene(PP_MO)

Table 4-6: Shows the contact angle, reduced droplet height (N), theoretical and experimental drop length, actual drop volume and adhesive energy of different oil samples on electrsopun PS fibre filament. Reported values represents a mean of 50 measurements

Oil		θ (°)	N	Drop Length (L)		V	V_{act} (10^{-4} µl)	E	E_{act} (10^{-13} J)
				L_{theo}	L_{exp}				
Sunflower Oil	Mean	37.82	5.14	13.22	13.19	807.59	0.18	12.40	18.00
	SD	3.38	1.38	3.39	3.40	547.80	0.13	6.56	10.23
	Max	44.66	7.74	20.16	20.16	2135.70	0.58	28.36	49.68
	Min	30.70	2.62	6.69	6.69	81.71	0.03	1.97	4.68
Motor Oil	Mean	35.04	5.57	15.95	15.96	1157.79	0.90	15.34	26.18
	SD	4.45	1.62	4.21	4.16	1098.71	0.85	12.15	17.36
	Max	44.83	9.43	26.19	26.07	3793.70	2.88	45.93	71.01
	Min	30.69	2.45	7.25	7.29	67.38	0.05	1.73	7.10

Table 4-7: Shows the contact angle, reduced droplet height (N), theoretical and experimental drop length, actual drop volume and adhesive energy of PP fibre filament. Reported values represents a mean of 50 measurements

Oil		θ (°)	N	Drop Length (L)		V	V_{act} (10^{-4} µl)	E	E_{act} (10^{-13} J)
				L_{theo}	L_{exp}				
Sunflower Oil	Mean	37.38	5.16	14.12	14.08	1324.90	1.99	14.61	5.48
	SD	6.15	1.71	4.14	4.14	2518.06	1.67	9.58	12.20
	Max	49.76	8.95	22.89	22.93	17054	7.31	35.40	35.33
	Min	23.75	1.98	6.51	6.78	52.90	0.10	1.73	-5.36
Motor Oil	Mean	29.84	3.79	11.54	11.54	417.93	5.01	7.53	4.42
	SD	6.29	1.44	3.67	3.67	503.96	5.48	6.08	7.90
	Max	43.19	8.52	22.78	22.72	2815.40	22.00	28.01	31.02
	Min	13.68	1.58	5.06	5.07	18.94	0.20	0.59	-1.72

4.3.3.2 Analysis of theoretical and experimental drop length of droplets on PS and PP fibres

To establish the validity of using B.J Carrol`s theory of drop-on-fibres [128, 130, 142] to quantitatively evaluate the drop volume and adhesive energy between the fibres and the different oil types, a plot of the reduced drop height (N) against the theoretical and experimental reduced drop length was made and presented in Figure 4-10. The figure shows good overlap between the theoretical and experimental drop length and both exhibits a linear correlation with the reduced drop height. A good regression was recorded in all the plots, with motor oil showing a high regression value of 98.4% for both drop lengths on the PS fibre and 97.5% on the PP fibre. Sunflower oil on the other hand had a regression of 91% for both drop lengths (theoretical and experimental) on the PS fibre and about 91% correlation on the PP fibre. The lower regression recorded for the sunflower oil could be the effect of its lower viscosity and the subsequent formation of smaller cluster of barrel shaped droplet on the fibre reducing the accuracy of the measurements.

Based on the strong correlation between the experimental and theoretical drop length distribution with the reduced drop height, this shows that the drop-on-fibre model can be used in analysing drop volume and adhesive energy of the fibres as presented in subsequent section of this chapter.
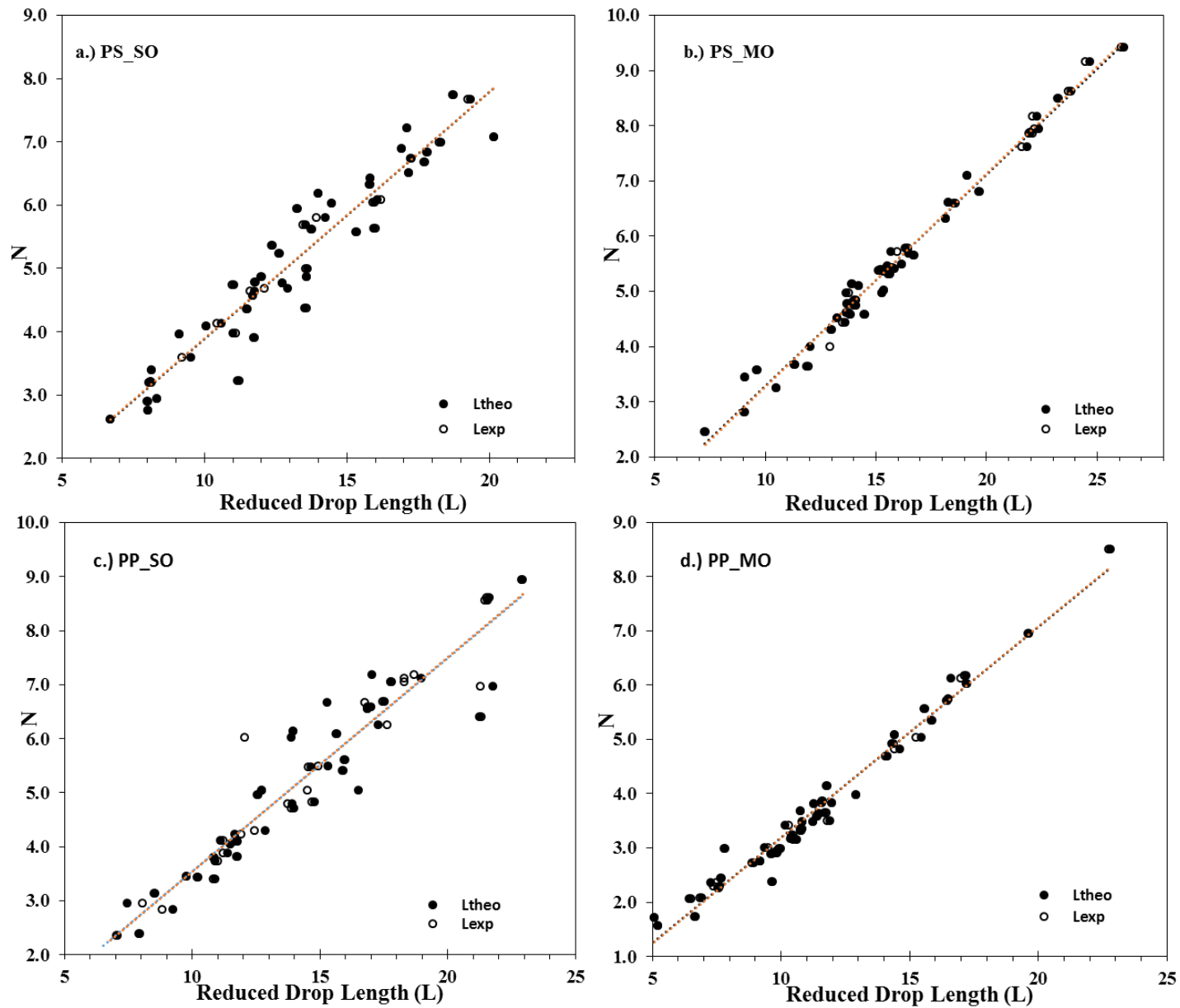
Figure 4-11: Plots of the reduced drop height and both the theoretical (●) and experimental (○) drop length distribution for a.) Sunflower oil on PS fibre (PS_SO); b.) motor oil on PS fibre (PS_MO); c.) sunflower oil on PP fibre (PP_SO); d.) motor oil on PP fibre (PP_MO). Experimental drop length were obtained as described in section 2.6, while the theoretical value was obtained using equation 2-10, section 2.10.2

4.3.3.3 Analysis of volume of oil droplet on fibres

In Tables 4-6 and 4-7, it could be observed that average drop volume recorded for both sunflower and motor oils on the electrospun PS fibre were in the same order of magnitude, but with motor oil having an average volume of 0.9 x 10^{-4}µl. A value 5 times higher than the average volume recorded for sunflower oil on the same PS fibre. Figure 4-12a and b further illustrate the actual drop volume distribution of sunflower and motor oils on the PS fibres. Motor oil could be seen to exhibit a larger drop size range between 0.05 – 2.88 x10^{-4}µl compared to 0.03 – 0.58 x10^{-4}µl recorded for sunflower oil. Though image analysis reveals the average fibre diameter of electrospun PS fibre used for the sunflower oil analysis to be 5.8µm, while those used for the motor oil was 8.5µm. Such difference in fibre size cannot justify the increase in drop volume. It is believed the viscosity of motor oil as seen in Table 4-8 which is almost three times that of sunflower oil will be a major factor in its higher drop volume distribution on both fibres. T. Dong et al [142]reported similar effect of viscosity of motor oil on kapok and polyester fibres.

Drop volume recorded on the PP fibres exhibited similar trend as the PS fibres but with sunflower oil having an average droplet size of 1.99µl, an order of magnitude higher that value recorded for PS fibre. Figures 4-12 c and d illustrates the drop volume distribution for the PP fibres, with sunflower and motor having a range of 0.1 – 7.31 x 10^{-4}µl and 0.2 - 22 x10^{-4}µl respectively.

Table 4-8: Properties of oil used in the drop-on-fibre analysis. Surface tension values were adapted from [142]viscosity values were obtained 25ºC using a Malvern rheometer

Oil Sample	Viscosity (mPa.s)	Density (g/cm^3)	Surface Tension (mN/m)*
Sunflower Oil	37	0.894	33.45
Motor Oil	95	0.812	31.67
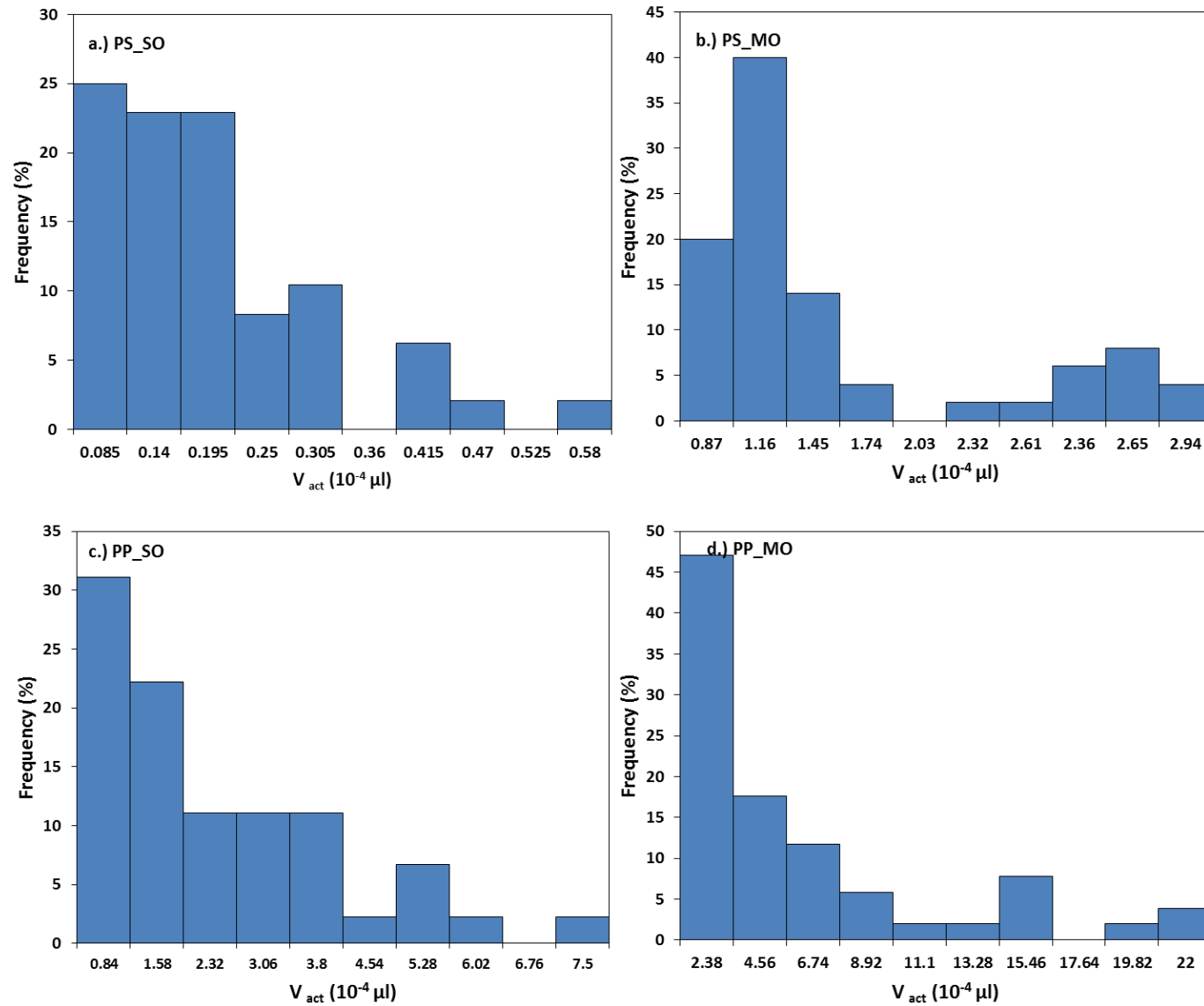
Figure 4-12: Actual drop volume distribution of sunflower and motor oil on electrospun PS and PP fibres; a.) Sunflower oil on PS fibre (PS_SO); b.) motor oil on PS fibre (PS_MO); c.) sunflower oil on PP fibre (PP_SO); d.) motor oil on PP fibre (PP_MO).

4.3.3.4   Analysis of adhesive energy of fibres

Understanding the adhesive energy of electrospun PS and PP fibre will help understand the influence of a fibre inherent ability to adsorb and retain oil as oppose to its mat architecture. Figure 4-13, shows the adhesive energy distribution of sunflower (so) and motor (mo) oil droplets on PS and PP fibres. Despite PS bulk polymer having a higher surface free energy (see Section 4.3.3), electrospun PS fibre exhibits the strongest affinity to the two oil types with an average adhesive energy of 18.00×10^{-13} J and 26.18×10^{-13} J for sunflower and motor oil respectively. For the same oil types, the values recorded on the PP fibre were 5.48×10^{-13} J and 4.42×10^{-13} J. This is contrary to the findings of T. Dong et al, which attributes low adhesive energy of fibres to high surface free energy [142]. Though both bulk PS and PP polymers are known, non-polar hydrocarbons, a plausible explanation for the higher adhesive energy distribution on the PS fibre could be the effect of the presence of aromatic benzene ring in its chemical structure (see Figure 2-9), thereby giving it a higher affinity to the oils. Different oil types often vary in their composition, which invariably could affect their ability to be adsorbed on solids materials. Lubricating oils such as motor oil often comprises mainly of a mixed blend of; paraffinic-naphthenes, naphthenes, aromatic naphthenes, condensed naphthenes, and higher aromatics [165], while sunflower oil comprises primarily fatty acids and esters [166]. Similarities due to the presence of aromatics in the chemical structure of PS and motor oil could have led to a stronger Van der Waals interaction between the motor oil and PS fibre molecules, resulting in the higher adhesive energy distribution observed in Figure 4-13 in comparison to sunflower.
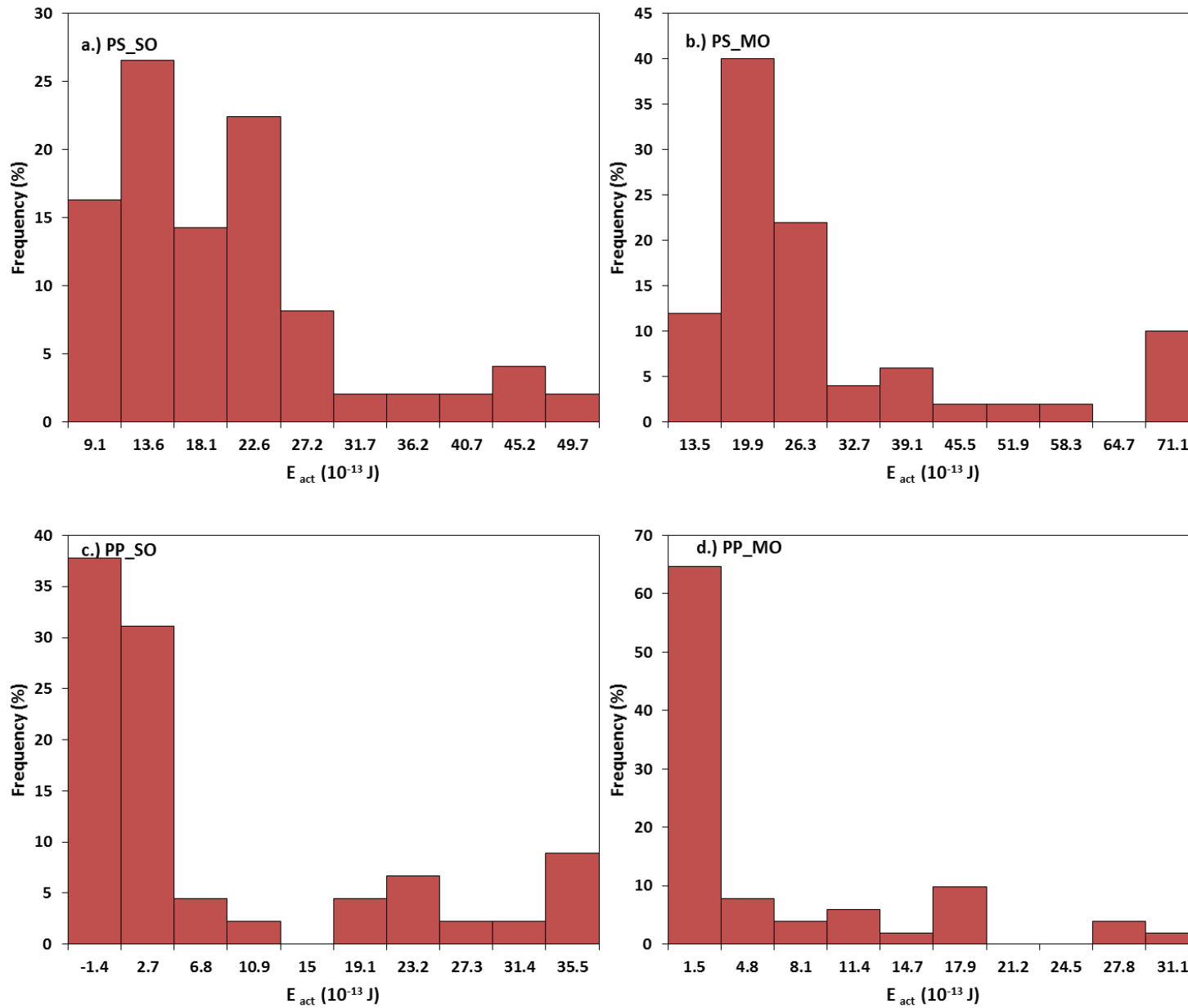
Figure 4-13: Actual adhesive energy distribution of sunflower and motor oils on electrospun PS and PP fibres; a.) Sunflower oil on PS fibre (PS_SO); b.) motor oil on PS fibre (PS_MO); c.) sunflower oil on PP fibre (PP_SO); d.) motor oil on PP fibre (PP_MO).

The high adhesive energy of electrospun PS which falls between 3 – 6 times those of the PP, is an indication of its higher ability to adsorb and retain oils when used as a sorbent.

4.3.3.5 Analysis of the adsorption behaviour of PS and PP fibres to different oil droplet size

The ability of sorbent to completely eradicate oil spill have been widely reported in literature [7, 91] but often with no experimental justification of this fact. In this section we used the principle of same volume earlier reported by T. Dong et al [142] to convert the barrel shaped oil volume to spherical droplet sizes. Table 4-9 and Figure 4-14, shows the mean oil droplet size (µm) and droplet distribution range (µm) of sunflower and motor oil on both el ectrospun PS and meltblown PP fibres. The mean droplet diameter for sunflower and motor oils on the electrospun PS fibres were $2.83 \pm 2.1 \mu m$ and $14.36 \pm 13.7 \mu m$ respectively, this falls in the emulsified oil state of 0.5 – 25 µm droplet sizes. Interestingly for the PS fibre, despite the wide droplet distribution range as seen in the Figure 4-14, the frequency of droplet sizes below the mean value were 60 – 75% of the mean value. The average droplet sizes adsorbed on the PP fibre were $31.67 \pm 26.9 \mu m$ and $79.77 \pm 88.0 \mu m$ for both sunflower and motor oils respectively, with both mean values falling into the dispersed oil state (25 - 100µm).

A combination of the high adhesive energy recorded for PS fibre in Section 4.3.4.4 and its good adsorptivity for oil droplets in the emulsified state, make it an ideal sorbent for use in cleaning up oil sheen (< 1 µm thickness) often impossible to completely eradicate using other physical clean up techniques such as skimmers. In addition to the above, electrospun PS given its oil adherence potential would be suitable for use as membranes in coalescing filtration of oil emulsion [142, 167, 168].

126
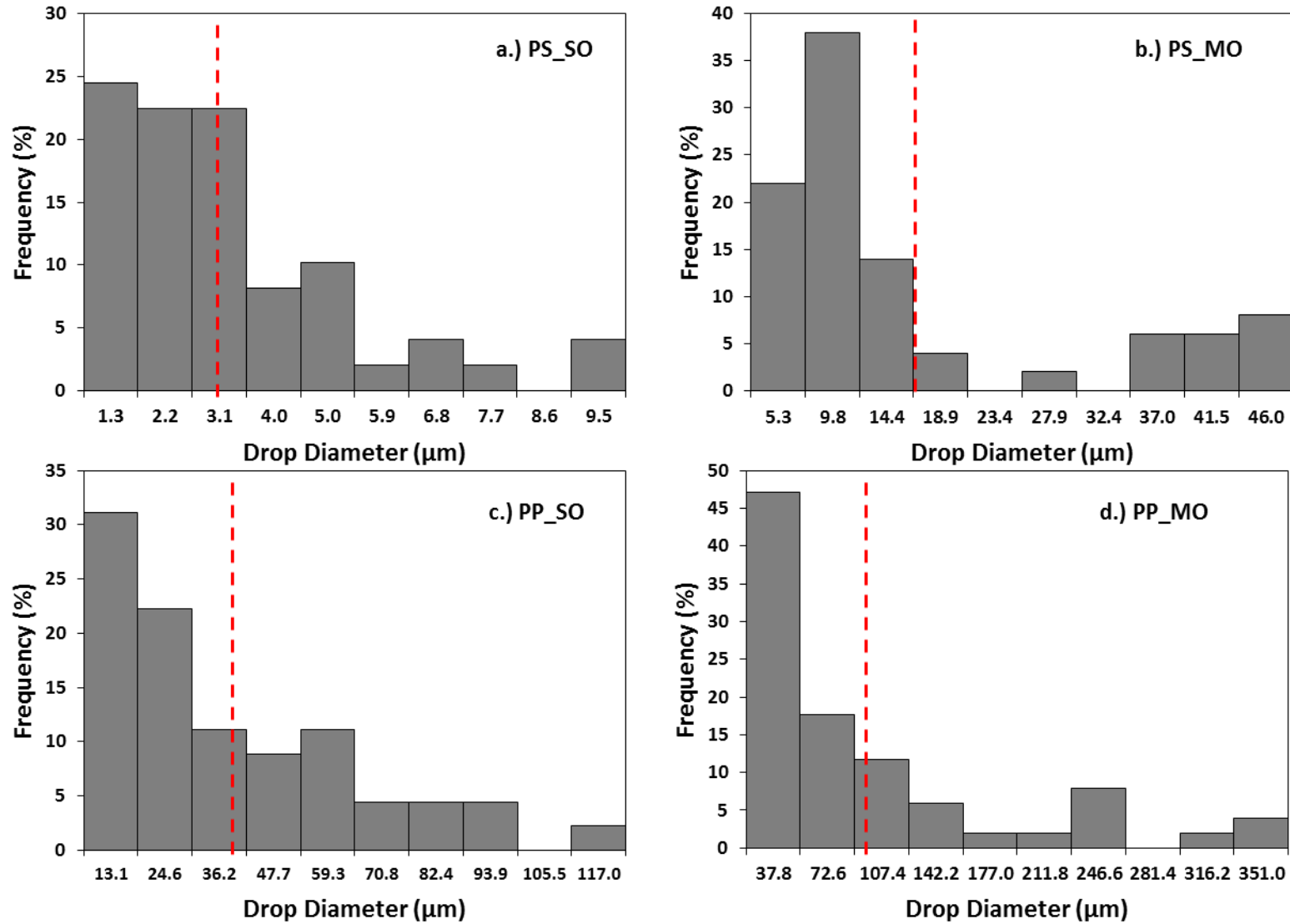
Figure 4-14: A comparison of the distribution of oil droplet sizes adsorbed on each fibre filaments; a.) Sunflower oil on PS fibre (PS_SO); b.) motor oil on PS fibre (PS_MO); c.) sunflower oil on PP fibre (PP_SO); d.) motor oil on PP fibre (PP_MO). Principle of same volume was used in converting the barrel shaped drop volume to spherical diameters.

Table 4-9: Oil droplet size distribution on electrospun PS and Meltblown PP fibres

Oil	PS Fibre		PP Fibre	
	Mean Drop Diameter (µm)	Drop Size Distribution (µm)	Mean Drop Diameter (µm)	Drop Size Distribution (µm)
Sunflower Oil	2.83 ± 2.1	0.47 – 9.30	31.67 ± 26.9	1.56 – 116.31
Motor Oil	14.36 ± 13.7	0.82 – 45.84	79.77 ± 88.0	3.25 – 350.10

4.4 Summary

In this chapter, the effect of polymer concentration (**Section 4.2.1**), solvent mix of DMF and THF (**Section 4.2.2**) and solution flow rate (**Section 4.2.3**) on the morphology of electrospun polystyrene fibre were clearly demonstrated. **Figure 4-2** shows the optimum concentration for the production of uniform bead-free fibres as 20%w/w concentration.

A comparison of the morphology of typical electrospun PS fibre produced in **Section 4.2** and commercial PP sorbent were carried out, with PS fibre seen to exhibit lower fibre diameter and a high level of uniformity in its size distribution. An evaluation of the surface free energy (SFE) of electrospun PS and PP fibre mats with their solid thin film structure were evaluated using OWRK method in **Section 4.3.2**. The SFE recorded for the solid thin films were consistent with literature and the measured values of 43.45 and 24.14mN/m recorded for PS and PP thin film respectively were subsequently used in **Section 4.3.3.4** in calculating the adhesive energy distribution on single fibre filaments using the drop-on-fibre technique. On the drop on fibre experiments, both PS and PP fibres exhibited a barrel shaped conformation as seen in **Figure 4-10**, while **Tables 4-6 and 4-7** shows electrospun PS fibre to exhibit a slightly higher CA in both oils compared to PP fibre. **Figure 4-11**, **Tables 4-6 and 4-7** shows a high level of congruence between the theoretical and experimental drop length, this confirms the suitability of using the theoretical drop-on-fibre model for subsequent

analysis. Despite the low oil drop volume on the PS fibre (**Section 4.3.3.3**; **Figure 4-12**), the fibre exhibited the strongest affinity to both oils (**Section 4.3.3.4**, **Figure 4-13**) with an average adhesive energy of 18.00×10^{-13} J and 26.18×10^{-13} J for sunflower and motor oil respectively, a value 3 – 6 times higher than adhesive energy obtained for PP fibres. This result indicates the ability of electrospun PS fibre having a higher sorption performance to melt blown PP sorbent is more of the polymers inherent ability to adsorb other HCs, rather than the architecture of the sorbent mat.

5 Electrospun PSPU polymer blend

5.1 Introduction

The poor mechanical properties of polystyrene (PS) fibres, particularly after oil sorption has been a major limiting factor facing its application and reusability as sorbents, in oil spill remediation [20, 22]. Previous efforts at improving the mechanical behaviour have explored coaxial and multi-nozzle side-by-side electrospinning of polystyrene (PS) and polyurethane (PU) polymers [21, 22]. These methods, despite its success at improving the mechanical performance of the mats, introduces extra complexities and cost to the fabrication process; requiring intricate nozzle configuration, additional continuous flow pump and voltage source for the fibre production.

As described in Section 2.7.3, polymer blending offers a simple and effective means of modulating and improving the physicochemical, thermal and mechanical properties of polymers [169]. In a binary system, the properties of the blend being a function of the miscibility of the constituent polymers, occasioned by intermolecular interactions such as hydrogen bonding, dipole-dipole forces and ionic bonding [170]. So far, only a limited number of studies have been done creating a composite blend of PS with other polymers for oil spill application [19, 20, 97]. A composite blend of PS and poly acrylonitrile (PAN) previously explored in literature, has the potential of negatively impacting the oil-water selectivity of the polyblend fibre due to the hydrophilic nature of PAN [20].

Consequently, the aim of this chapter is to explore polymer blending as a means of enhancing the mechanical strength of electrospun PS fibre, by blending the polymer in solution with an ether based thermoplastic polyurethane PU. The choice of PU is because of its good abrasion and oil resistance, excellent mechanical strength as well as good elastomeric properties.[151, 171]. This is expected to boost the mechanical performance of the resulting fibre both on a macro and microscale level. Hence, the key objectives of this chapter is:

- To investigate the effect of varying PS and PU ratios on the solution properties, and compare its effect on the morphology of fibres fabricated with a flat (FC) (Section 3.2.2.1) and drum (DC) collector system (Section 3.2.2.2).

- Investigate the effect of solvent type on the morphology of the polymer blend fibres.

- To carry out detailed chemical characterisation of the polymer blend fibres, to demonstrate the formation of a polymer blend mat, down to a micro scale level of individual fibres using EDX and ATR-FTIR spectroscopy.

- To study the effect of blending on the thermal properties of the resulting mat, using TGA and DSC analysis.

- To investigate the influence of blending and fibre collector system on the mechanical properties of the fibre mat by carrying out uniaxial tensile testing of the mat. Also, use AFM testing to explore the mechanical and adhesion properties of a single fibre filament.

- To compare the oil sorption capacity and retention behaviour of the polymer blend mat fabricated using the FC and DC collector systems, and also compare with SC of commercial PP sorbent.

- Lastly, demonstrate the buoyancy, reusability, and oil-water selectivity of the mat.

It is important to state that this is the first time electrospinning polymer blend of PS and PU is being reported, with detailed characterisation.

5.2   Solution Preparation and Electrospinning

Solution properties such as viscosity, surface tension and conductivity play a key role in the morphological structure of electrospun fibres [27, 172, 173]. Solution properties of the pure and polymer blend used in this study are indicated in Table 5.1. The viscosity value of 6.826Pa.s recorded for PU (at 20% wt conc.) solution is seen to be over 18 times higher than those of PS polymer, while the polymer blend shows an increasing viscosity trend from 0.496 - 2.253Pa.s with increasing PU composition in the blend ratios PSPU 9:1 - 6:4. The high viscosity of the PU solution could be a result of a higher polymer molecular chain entanglement at the 20% concentration [151], this effect is transferred to the polyblend solution due to intermolecular interaction of the ternary PS-PU-Solvent system [173]. Similarly, the surface tension of the polymer blend solution increases with increasing PU from 35.7 – 66.2mN/m, with the highly viscous PU solution having the highest recorded surface tension of 164.9mN/m.

Table 5-1: Solution properties of PS, PU and PSPU polymer blends (20% wt conc.) dissolved in a solvent mix of DMF and THF ratio 4:1

Polymer Solution	Viscosity (Pa.s)	Surface Tension (mN/m)
PS	0.366	34.7
PSPU (9:1)	0.496	35.7
PSPU (8:2)	0.772	69.5
PSPU (7:3)	1.074	66.2
PSPU (6:4)	2.253	66.7
PU	6.826	164.9

5.3 Physicochemical Characterisation

5.3.1 Morphology of electrospun PSPU polymer blend fibre

In this section, morphological characterisation of fibres fabricated under 2 different collector system; vertical flat collector (FC) and rotating drum collector (DC) system are investigated. The solvent mix of DMF/THF (4:1) and solution concentration of 20% (w/w) obtained in the previous chapter was maintained in all the PS, PU and PSPU polymer blend solutions. An applied voltage of 15kV and tip to collector distance of 15cm was used for all the electrospinning process, while a feed rate of 3ml/hr and 2ml/hr was used for the FC and DC systems respectively, as these set of process parameters were observed to produce a stable jetting in all the polymer blends. Figure 5-1a and b, shows optical images of fibres obtained under the FC and DC systems respectively, while Figure 5-1c is an image of the commercial PP sorbent. The FC system promotes the formation of a 3D-like cotton structure with increased fibre deposition, while the DC system when carried out below the alignment speed produces a mat of randomly oriented fibre mat[27].
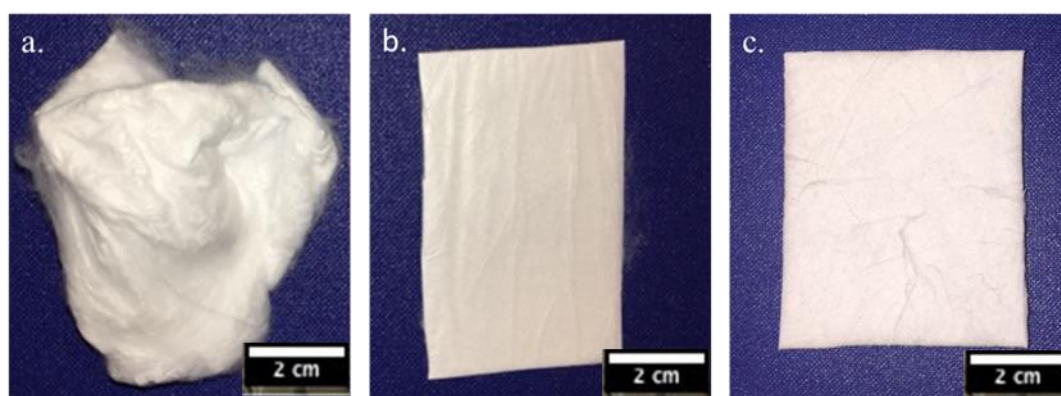
Figure 5-1: Optical image of a.) electrospun PSPU_FC 8:2 fabricated using a flat collector, b.) electrospun PSPU_DC 8:2 produced using a rotating drum system, and c.) commercial PP sorbent

Using methods described in Section 3.3.5, the estimated porosity and theoretical specific surface area (SSA) of the different fabricated sorbent is presented in Table 5-

2. As expected fibres collected using the FC system have a higher porosity values in comparison to those fabricated using the DC system, with the porosity value under each system decreasing with increasing PU ratio. The difference in porosity value between the two systems could be ascribed to the speed of rotation of the drum, enhancing the fibre packing density under the DC system, which invariably reduces the inter-fibre void spaces as well as the porosity of the mat. The compositional effect of PU addition on the porosity is its higher bulk density, which also increases the fibre packing density. The PP sorbent despite having a relatively high SSA due to the high variation in fibre size, recorded the lowest porosity value. This is likely to be the effect of the melt blown technology used in its fabrication, creating the observed structural limitations.

Figures 5-2 and 5-3 shows the FESEM micrographs of the nonwoven fibre mat obtained from varying PS/PU polymer blend ratios, indicating the effect of varying the polymer blend ratio on the fibre morphology. Average fibre diameter of the different blend under FC system was between 3-4µm, with the AFD showing a gradual increase with increasing PU concentration from 3.02µm in the pristine PS mat to 3.86µm in PSPU (6:4) fibres, with the exception of PSPU 7:3 which shows a slight deviation from the trend. Similar trend was observed for the DC system (Table 5-2). The increasing fibre size could be attributed to the increased viscosity of the blend, which increases with increase in PU content. It is important to note that PU has a higher base polymer density of $1.2g/cm^3$ [174] as against $1.04g/cm^3$ for PS polymer [175]. This is believed to be a contributory factor in the viscosity level recorded with increased PU addition. The polydispersed nature of the pure PU fibre is a result of the unsteady nature of the jet at the optimised parameters used for the blend.

Macro and mesoporous pore structures could be seen on the surface of the PS fibres and fibres with a high PS ratio. This is believed was a result of the less dense PS polymer enabling the process of vapour induced phase separation (VIPS). During electrospinning process, VIPS occur when low boiling point solvent such as THF evaporates rapidly from the spinning polymer jet leading to a drop in temperature along the surface of the polymer jet [96, 150]. This causes ambient water vapour to condense on the surface of the polymer and subsequently form pores upon evaporation. Such pore structure could enhances the specific surface area of the fibre. An increase of the higher density PU in the blend as seen in ratio (6:4), slows down the rate of solvent evaporation leading to a reduction in pore formation as well as the appearance of inter-fibre bonding. This is more evident in pure PU fibre mat and mats with a higher PU concentration (PSPU 4:6 and PSPU 2:8) shown in figure 5-
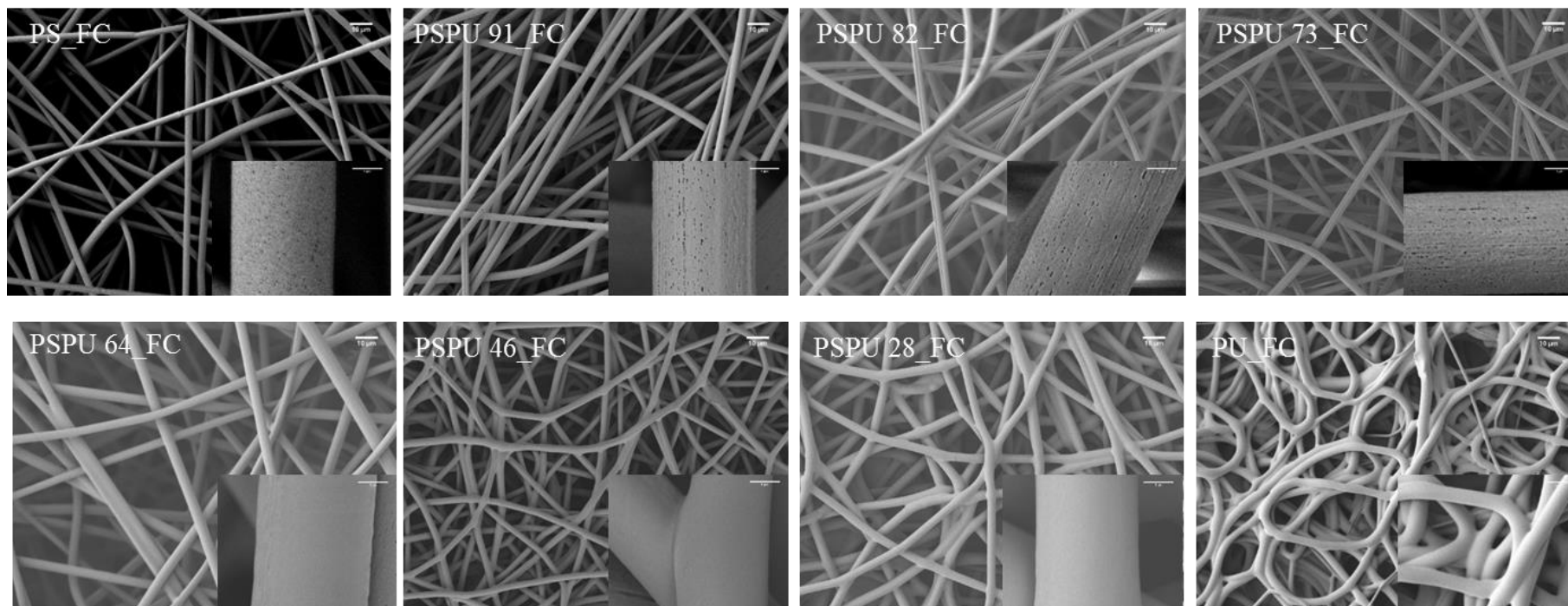
Figure 5-2: SEM micrograph of electrospun PS, PU and PSPU polymer blend mats fabricated using the flat collector (FC) system. Insert is a high manification image of the fibres

Figure 5-3: SEM micrograph of electrospun PS, PU and PSPU polymer blend mats produced using the rotating drum collector (DC) system. Insert is a high magnification image of the fibres

Table 5-2: SSA, Average/Mean fibre diameter and Porosity of electrospun polymer mat fabricated under both FC and DC system

Fibre Sample	SSA	Porosity (%)	Fibre Diameter (μm)
PS_FC	1.24	99.8 ± 0.05	3.06 ± 0.4
PSPU 9:1_FC	1.15	99.7 ± 0.08	3.26 ± 0.5
PSPU 8:2_FC	1.04	99.6 ± 0.05	3.56 ± 0.3
PSPU 7:3_FC	1.05	99.6 ± 0.05	3.47 ± 0.4
PSPU 6:4_FC	0.93	99.0 ± 0.08	3.85 ± 0.9
PS_DC	1.81	97.5 ± 0.81	2.10 ± 0.3
PSPU 9:1_DC	1.26	96.9 ± 0.08	2.99 ± 0.4
PSPU 8:2_DC	1.14	95.9 ± 0.25	3.24 ± 0.4
PSPU 7:3_DC	0,76	95.1 ± 0.16	4.80 ± 0.6
PSPU 6:4_DC	1.13	94.4 ± 0.16	3.19 ± 0.3
PP	1.10	91.2 ± 0.82	3.03 ± 3.9

5.3.2 Effect of solvent composition on polymer blend fibre

To study the effect of solvent composition on the polymer blend, PSPU (8:2) was dissolved in 100% THF and 100% DMF respectively, using the optimised parameter described in Section 3.2.2.3. In 100% DMF, multi-jetting and rapid jet instability was observed during the electrospinning process at an applied voltage of 15kV, while a reduction in the applied voltage to 10kV results in single and stable jet propagation. The high dielectric strength, dipole to dipole moment and surface tension of DMF, increases the solution conductivity[149, 150], hence the instability observed in the 100% DMF solution at 15kV, which had to be modulated by reducing the applied voltage. Figure 5-4a shows the SEM micrograph of a uniformly distributed fibre mat obtained at 10kV with an AFD of 3.17μm, while Figure 5-4b is a more polydispersed fibre mat at 15kV with an AFD of 2.60μm. On the other hand, electrospinning the polyblend in a 100% THF solvent was characterised with stable jetting over a wide

range of applied voltages (10-15kV studied), while the polymer was observed to dry

up rapidly at the tip of the needle due to rapid THF evaporation. Similar effect has

been reported in literature [146, 150], which can be attributed to low boiling point and
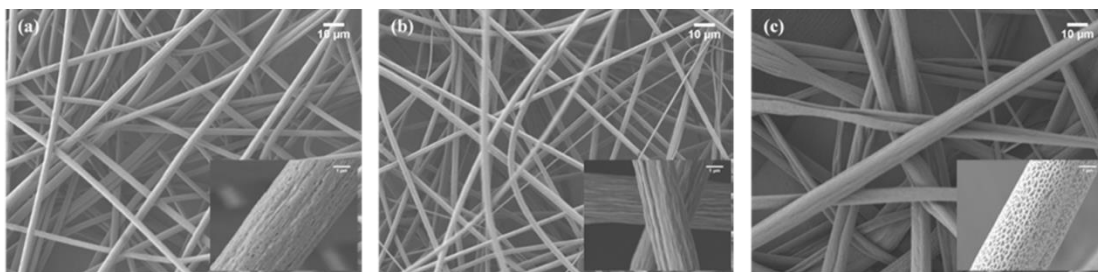
Figure 5-4: SEM micrograph of electrospun PSPU_FC 8:2 a.) produced from a DMF only solvent with an applied voltage of 10kV, b.) fabricated from DMF only solvent, produced with an applied voltage of 15kV; c.) produced from THF only solvent

surface tension of THF. As seen in Figure 5-4c, fibre were similar to those produced

from pure PS polymer dissolve in THF reported earlier in Section 4.2.2.

5.3.3 ATR-FTIR spectroscopy of the fibre mat

Understanding the chemical composition of the polyblend fibres will gives an insight

into its hydrophobicity and a proof of the formation of a bi-component polymer

structure. Figure 5-5 displays the ATR-FTIR spectra of electrospun PS, PU and PSPU

blend mat fabricated using the FC system. The spectra for the pristine PS mat clearly

shows the characteristic absorbance peaks of the aromatic C-C bond stretching at 1493

and 1452cm^{-1}, benzene ring vibration at 1074cm^{-1}; C-H out of plane bending vibration

at 756cm^{-1} while the prominent band at 697 cm^{-1} can be attributed to CH_2 rocking

mode[176, 177]. The CH and CH_2 stretching vibration of the main PS chain was

observed at 2849 cm^{-1} and 2922 cm^{-1} respectively. On the other hand, the crowded

spectra observed for pure PU fibre in the short wavelength band is due to the complex

molecular structure of the polymer [178]. In the pure PU mat spectra, the distinctive

peaks for the stretching vibration of N-H group was observed at 3325cm^{-1}, the

symmetric and asymmetric stretching of methylene groups (CH_2 and CH_3) at 2939 and
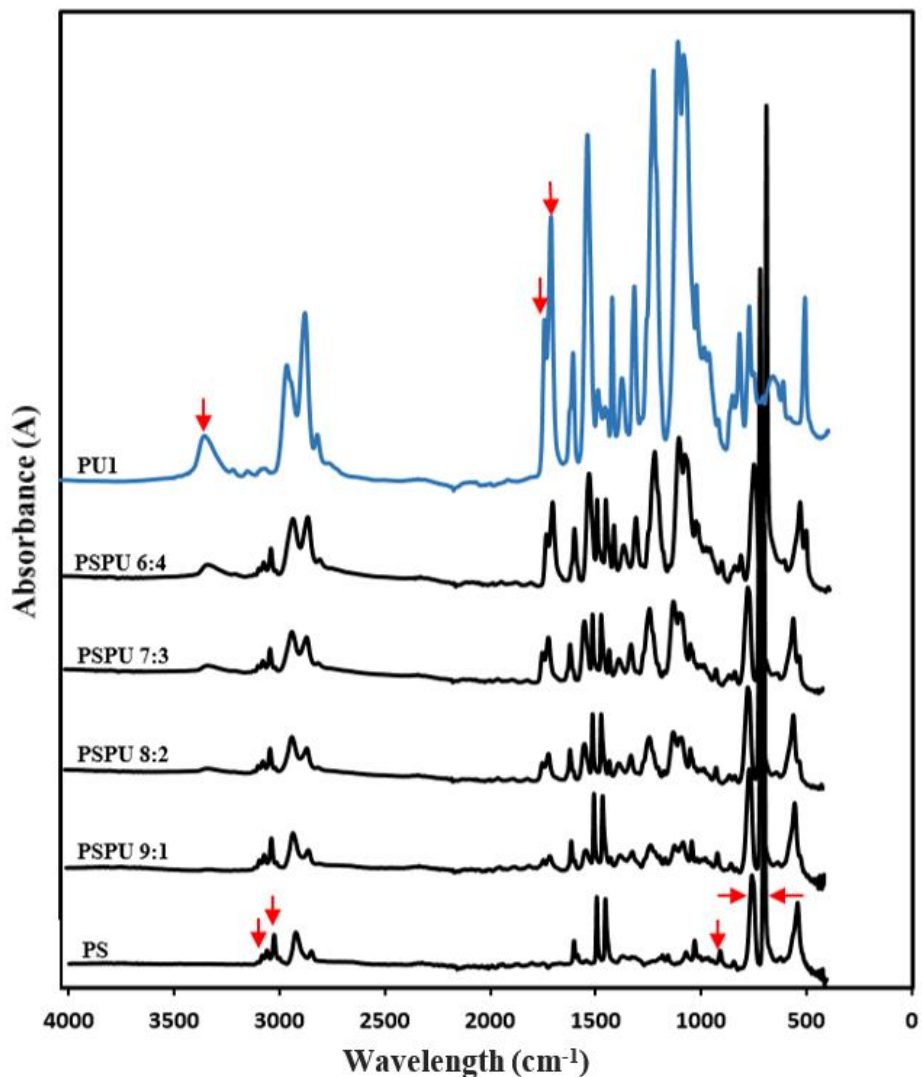
Figure 5-5: ATR-FTIR spectra of neat PS, PU and PSPU polymer mats fabricated using the flat collector system

$2854cm^{-1}$, while the peaks at 1731 and $1700cm^{-1}$ can be ascribed to the stretching vibration of the non-bonded and bonded carbonyl (C=O) group [178, 179].

In the spectra for the different polyblend mats, the presence of absorbance peaks that can be ascribed to the neat PS and PU fibre mat as indicated with red and blue arrows respectively (Figure 5-5), confirms the formation of bi-component mat structure of both polymers in the blend. CH_2 and CH_3 are functional group that are associated with hydrophobicity and can be seen in all the polymer fibre mat [180].

5.3.4 **EDX analysis of single fibre filament**

In a polymer blend fibre, the structural arrangement of the constituent polymers in the filament will depend on the intrinsic properties of the pristine polymers, its molecular weight, surface tension of the blend solution and the relative weight ratio of the constituent polymers [169]. Electrospinning a polymer blend could instil either of the following morphologies; separately spun fibres, filaments with intermittent lump of the constituent polymers or a homogeneously dispersed polymer mix where the polymers in the fibre matrix is separated in scale smaller than the fibre diameter[181]. Here the elemental analysis of the PS, PU and the different PSPU polymer blend fibre is investigated using energy dispersive x-ray spectroscopy. Secondary electron (SE) and backscattered electron (BSE) images are shown in Figure 5-6(a-c) and (a`-c`) respectively of the pure PS, pure PU and the PSPU (8:2) polymer blend mat. The polymer blend shows no sign of segregation of the different polymers. This could be deemed a confirmation of an intra-fibre blended structure, as BSE imaging has the ability to detect elemental difference at a sub-surface level of a sample.

Elemental point analysis was conducted at three different regions along the length of a single fibre filament to ascertain any elemental changes. As the chemical structure of polystyrene (see Section 2.7.1) comprises solely of carbon (C) and hydrogen (H), the spectra of PS fibre in Figure 5-6 a" is seen to show just the presences of C-atom in addition to Al-atom from the Aluminium collector (N.B EDX can only identify elements heavier than beryllium, hence H is not detected). Spectra of pure PU fibre in Figure 5-6c" shows an O- atom peak in addition to C-atom, while spectra from the polymer blend fibres was observed to contain traces of O-atom. The spectra and atomic weight of the O-atom in the blended fibres, was observed to increase with increasing ratio of the PU in the different polymer blend studied.
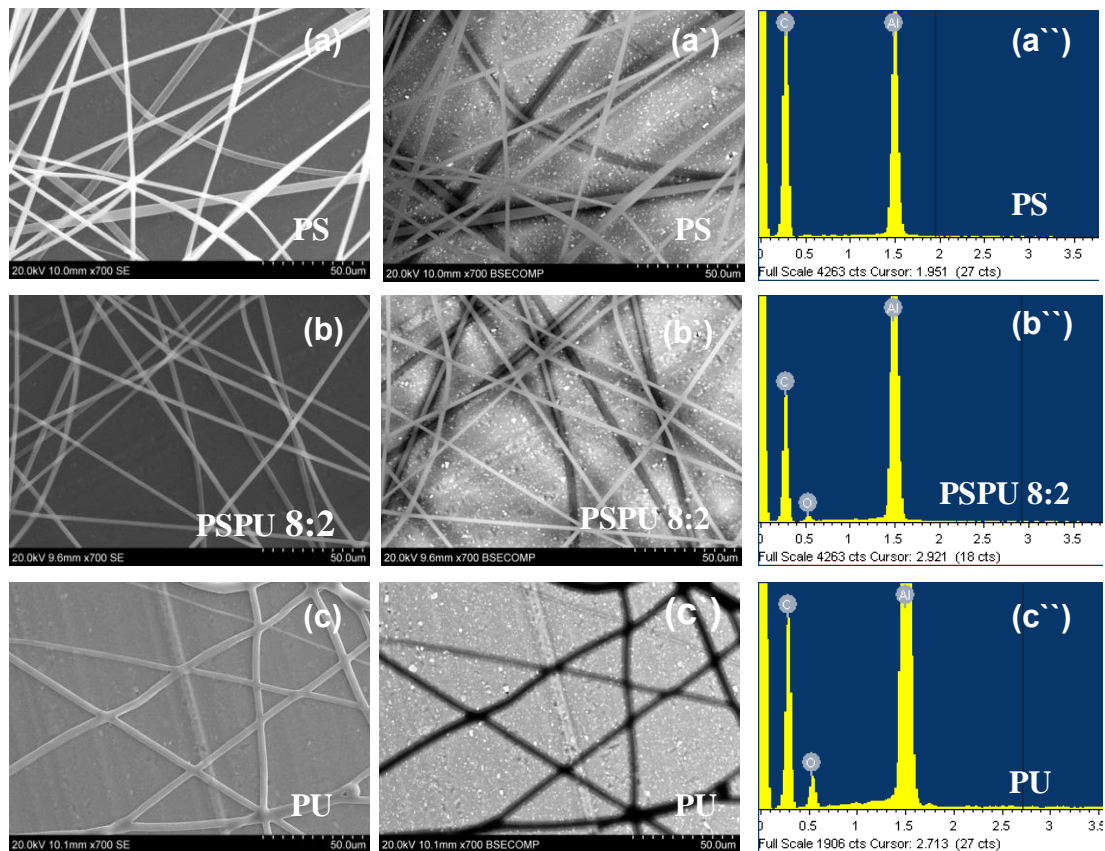
Figure 5-6: Shows a, b and c) secondary electron (SE) image, a', b' and c') back scattered electron (BSE)image and a'', b'' and c'') XRD spectra of electrospun PS, PU and PSPU 8:2 polymer blend mat as indicated on the images. All fibres were produced using the FC system

Creating a polyblend fibre mat via co-spinning polymers from a single nozzle other than side-by-side or multi-nozzle (side-by side) electrospinning, ensures the molecular interaction of the polymers at a nano-scale level and the formation of intermolecular interaction between the constituent polymers[169]. Such nano scale interactions will help in the production of fibre mat where individual filament will have properties from both polymers and could impact new thermal and mechanical properties in the fibres.

5.3.5   XRD analysis of the fibre mat

The X-ray diffraction pattern of the electrospun pure polymers and polymer blend fibres are shown in Figure 5-7. As expected the PS fibre mat exhibits the characteristic

broad halo amorphous peak of polystyrene at $2\theta = 19.6^o$ [182]. The additional peak between 9.8^o and 11.2^o have earlier been attributed to the 210 of the monoclinic structure [183]. This peak could also be seen in all the polymer blends as well as the pure PU fibre mat. The additional peaks observed in the PSPU 6:4 and pure PU fibres (at 37.9^o and 44.1^o) could be attributed to peaks of the aluminium crucible used in the experiment, which becomes detectable due to sample size[184]. Normalising these peaks would show that PSPU 6:4 and the pure PU fibre mat exhibits similar XRD spectra as PS fibre and the other PSPU polymer blend mats. This experiments shows that despite PU being regarded as having a semi-crystalline domain of hard segments in literature [110], the XRD pattern investigated in this study shows PU to be amorphous in nature.
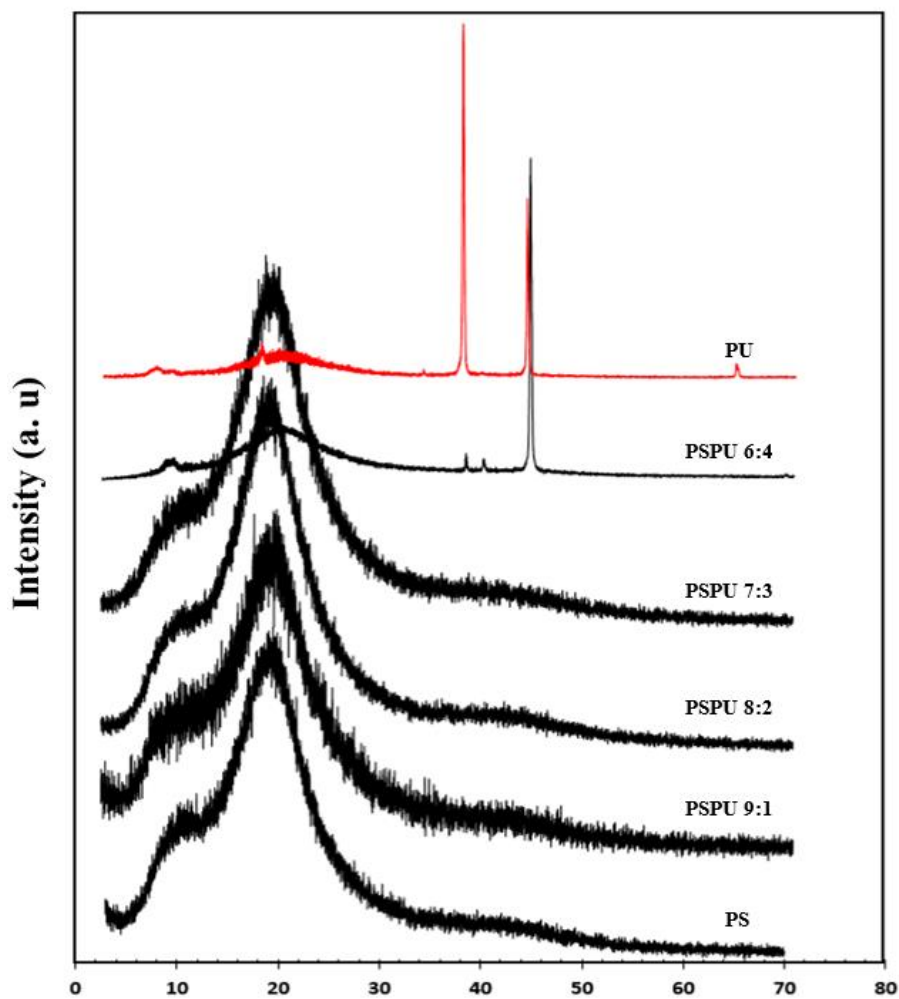
Figure 5-7: XRD spectra of electrospun PS, PU and PSPU polymer blend mat fabricated using the FC system

5.3.6 **Hydrophobicity and Oleophilic Characterisation**

A key desirable property of an oil sorbent is its oil-water selectivity [12, 92]. To evaluate the hydrophobic-oleophilic property of the polyblend mat, 2µl droplet of water and sunflower oil was dropped on a PSPU 82 mat fabricated using the FC system. The oil was seen to spread out and penetrate through the inter fibre void spaces almost immediately, while the water droplet remained on the surface of the mat for the entire period of observation (20 minutes) as seen in Figure 5-8a. This is an indication of the affinity of the polyblend fibre for oil (oleophilicity) as well as a proof of its hydrophobicity.

In Figure 5-8b, different drop sizes of water dyed with red food colouring was placed on a PSPU 82_FC mat, and in all cases the water was seen to remain on the surface of the mat. This shows that irrespective of the droplet size, the polymer blend mat remains hydrophobic. To quantitatively measure the level of hydrophobicity of the different mats, Water Contact Angle (WCA) measurements (Figure 5-9), were carried out as described in Section 3.4.6 The WCA measurement of 123.5° obtained for the pure PS fibre mat is consistent with reported values in literature [96], this value was observed to increase with the polyblend mats to 134°, 134°, and 133.5° for the PSPU 82, 73 and 6:4 respectively. This could be attributed to the effect of a tighter packing of the polymer with increasing PU in the blend.
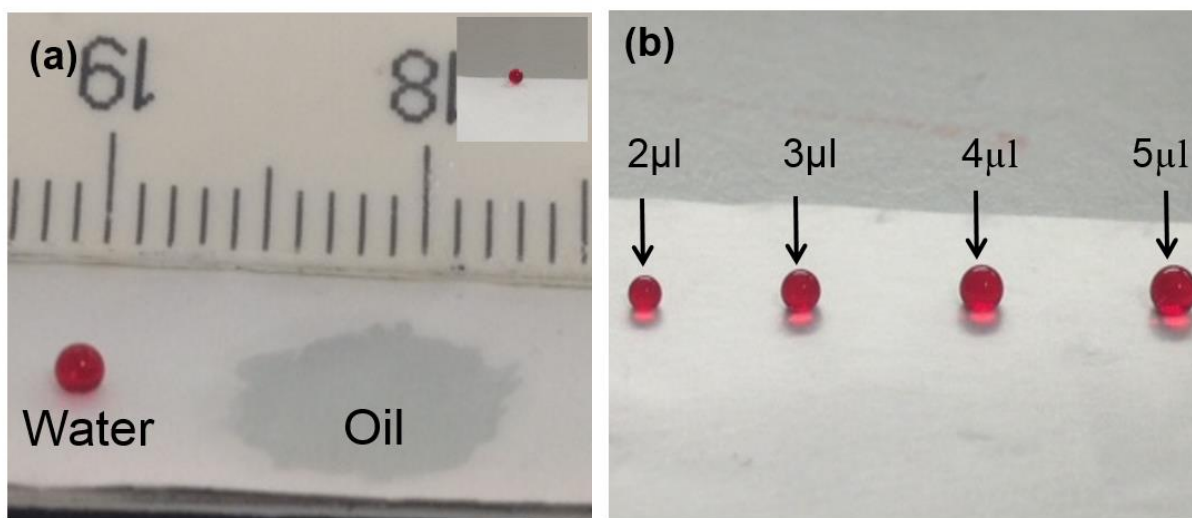
Figure 5-8: Hydrophobic and oleophilic illustration of electrospun PSPU_FC 8:2 fibre mat, a.) Optical image of water dyed with red food colouring and vegetable oil (as indicated), b.) Shows the hydrophobicity of the PSPU_FC 8:2 mat irrespective of the water droplet size.
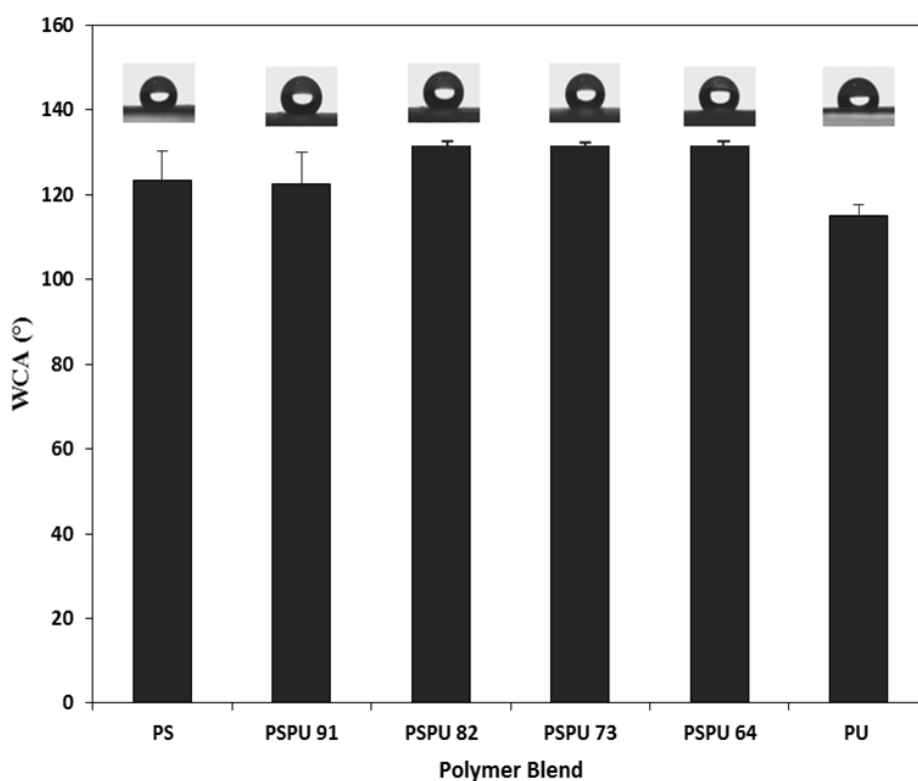
Figure 5-9: WCA of electrospun PS, PU, and PSPU polymer blend fibre mats fabricated with a FC system. Insert images were taken at approximately 4secs upon contact with the fibre mat. Error bars represents one standard deviation about the mean (n≥5)

5.4 Thermal Characterisation

5.4.1 TGA

Thermogravimetric analysis (TGA) is a thermal analysis technique that could be used to determine the maximum temperature the polyblend fibre mats can withstand while in service, before decomposition. The thermal degradation characteristics of the neat PS, PU and PSPU polymer blend fibres is depicted in both the TGA and DTGA thermograph in Figures 5.10 and 5.11. The neat PS fibre mat exhibits a one-step thermal degradation with a single transition temperature, while the neat PU mat shows a two-step decomposition profile (Figure 5.10). The first and second stage degradation of the neat PU fibre can be attributed to the decomposition of the polymer's hard and

146

soft segment respectively [185]. The hard segment degradation peaks at 369.4°C and completely degrades at 397.5°C. This amounts to 45% of the PU composition, while at same temperature (397.5°C), only 7% degradation had occurred in the PS fibre mat despite both pure polymer mats having same weight loss (77%) at 433.3°C.

Based on this and the onset of thermal decomposition of the pure polymer mats (Table 5-3), it can be inferred that the PS mat exhibits a higher thermal stability at the onset of decomposition than the PU fibres. Also, the peak degradation temperature of PU1 which could be ascribed to the soft segment was seen to be 3.1°C higher than the PS fibre counterpart. Similar degradation profile as observed for PU1 has previously been reported in literature for TPUs [186-188], where approximately 3-5% gaseous/residual weight is observed on the thermograph. The thermal degradation mechanism of polyether based TPU such as the one used in this study, has earlier been reported to be an oxidation process, which involves CO_2 production when decomposed under nitrogen atmosphere [187].

All the polymer blend mat were observed to exhibits a two-stage degradation profile which is indicative of the presence of PU in the fibrous mat. Interestingly, the onset of thermal degradation of the blend were much lower than those obtained for the pure polymer fibres, while the peak degradation temperature with the exception of PSPU 6:4 were formed between those of the neat polymer mat. This could be an indication of the existence of interaction between the two polymers in the blend. Similar effect was reported for PLA/PS polymer blend [37].

5.4.2 DSC

The nature of the glass transition (T_g) temperature in a binary polymer blend relative to the T_g of the pure polymer is often used to determine the level of miscibility of the
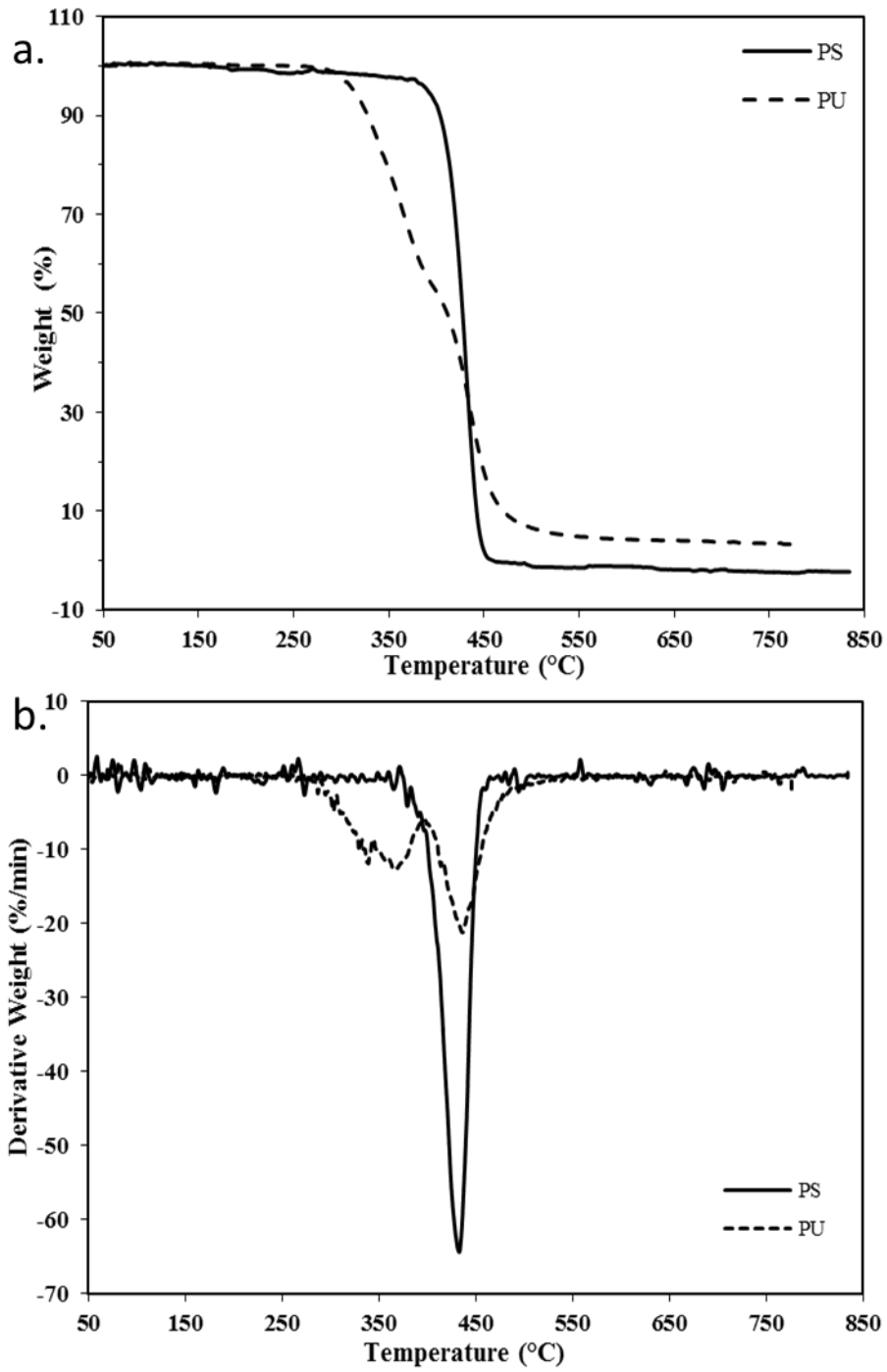
Figure 5-10: Shows a.) TGA and b.) DTGA thermograph of electrospun PS and PU fibre mats fabricated using the FC system. Experiments were persormed as indicated in section 3.4.2.1

Figure 5-11*:* Shows a.) TGA and b.) DTGA thermograph of electrospun PSPU polymer blend fibre mats fabricated using the FC system. Experiments were performed as indicated in section 3.4.2.1

polymers in the blend. As a rule, polymer blends characterised by a single glass transition temperature which falls in between those of the constituent polymers are said to be miscible [115, 116]. A compatible or partially miscible blends has two distinct T_g which are composition dependent, while immiscible blend is characterised by two T_g`s which has the same value as those of the constituent polymer [117]. Figure 5-12 shows the DSC thermograph of electrospun PSPU polyblend fibres.

The glass transition temperature for the neat PU and PS fibre was observed at -40.5°C and 114.7°C respectively, which is consistent with previous work [116]. However, a bimodal endothermic transition was observed for the PS fibre which could be the effect of the high voltage causing some structural changes in the PS fibre as same transition was observed in repeated runs of the PS fibre. In all the polymer blend, the thermograph shows a distinctive, single transition temperature which falls between those of the neat PS and PU polymer. We could infer that there is a strong interaction and miscibility between the two polymers, which could help in impacting new properties in the polymer blend fibres [117].

Table 5-3: Glass transition temperature (T_g), temperature at onset of degradation ($T_{d\ onset}$) and peak degradation temperature (T_d) for electrospun PS, PU and PSPU polymer blend fibres

Polymer Fibre	T_g ($^{\circ}$C)	$T_{d\ onset}$ ($^{\circ}$C)	T_d ($^{\circ}$C)
PS	114.7	412.5	433.2
PSPU1 (9:1)	112.5	292.9	435.3
PSPU1 (8:2)	108.2	298.4	436.2
PSPU1 (7:3)	107.1	299.6	436.0
PSPU1 (6:4)	107.7	302.1	438.5
PU1	-40.5	314.9	436.3
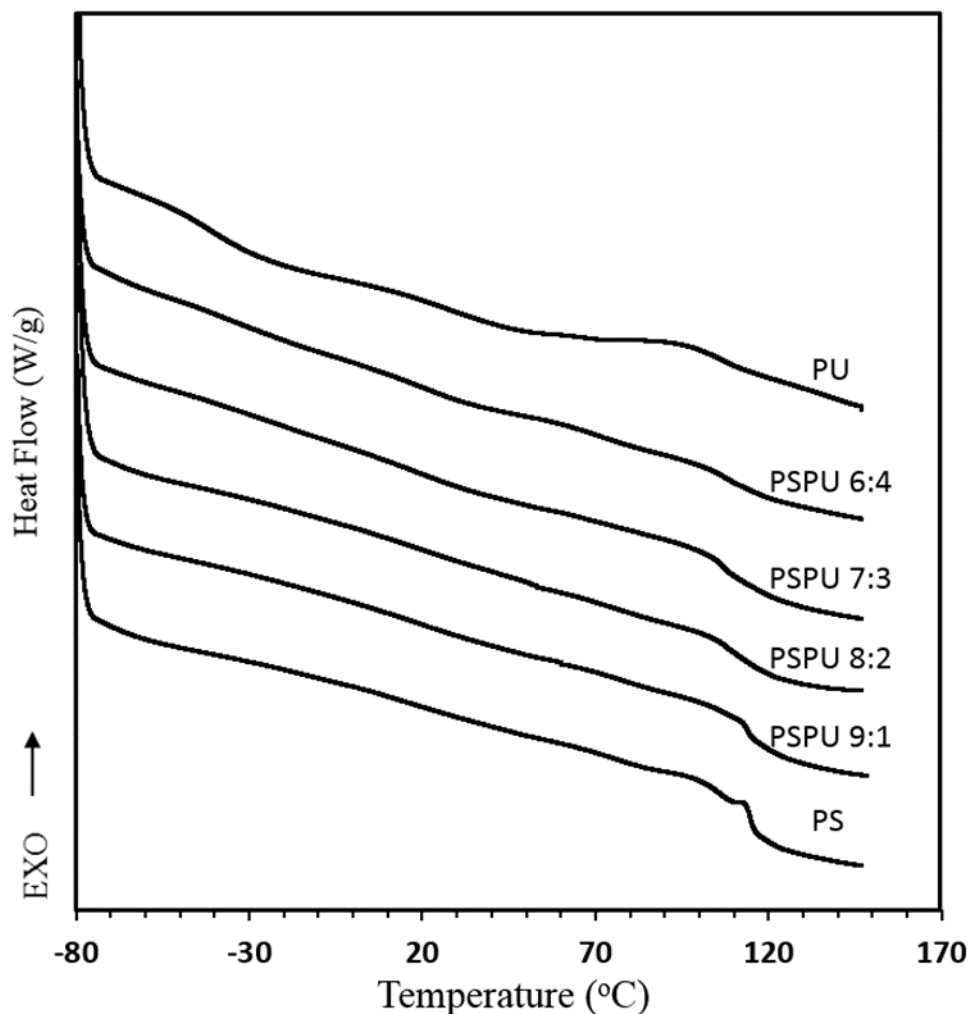
Figure 5-12: DSC thermograph obtained for PS, PU and the different polymer blend fibre mat electrospun using the FC system. Single Tg observed for the polymer blends is an indication of strong miscibility between the PS and PU polymers

5.5   Mechanical properties of the fibre mat

5.5.1   Tensile test characterisation of the polyblend mat

An ideal sorbent particularly for marine oil spill clean-up should have a relatively good mechanical strength and maintain its structural integrity during and after oil sorption [20]. The mechanical properties of electrospun polymer blend is dependent on the intrinsic property of the constituent polymer, the ratio of the polymers and its

interaction in the blend, the structural orientation of the fibres and the existence of inter fibre bonding in the mat[173].

To study the effect of the thermoplastic polyurethane (PU) addition on the mechanical property of the fibres, uniaxial tensile test was carried out on the mats. Figure 5-13a shows the average tensile stress of mats fabricated using both the FC and DC systems. In both systems, the tensile strength of the fibre is seen to increase with increasing PU addition. PSPU_DC 6:4 and PSPU_FC 6:4 experienced approximately 600% and 1000% increase respectively in tensile stress, in comparison to the pristine PS mats fabricated using the respective collector system. For polyblend ratio 8:2, despite the quantitative difference in value of the tensile stress in both systems, both experienced a 200% increase compared to the pristine PS mats. In general, the higher tensile strength value seen for the DC system can be attribute to the higher packing density of fibres fabricated using this system. The increasing trend in mechanical properties seen in both systems could be attributed to the formation of a chemically point bonded structure with PU addition as well as microstructural interaction between molecules of both polymers at a micro/nano scale level. Similar point bonded structure have been reported for PVC/PU polymer blend[173].

A typical stress-strain curve of the polyblend mats fabricated using the DC system is shown in Figure 5-13b, while a quantitative evaluation of the variation in mechanical properties of the polyblend mats is presented in Table 5-4. All the fibres exhibit a linear elastic behaviour with the application of a stress load up to the yield point. Fibre mats with a higher PU ratio from PSPU_DC 8:2 shows a further non-linear elastic behaviour until break point. This could be attributed to the stretching and slippage of the polyblend mat [172] indicating the effect of PU on the mat.
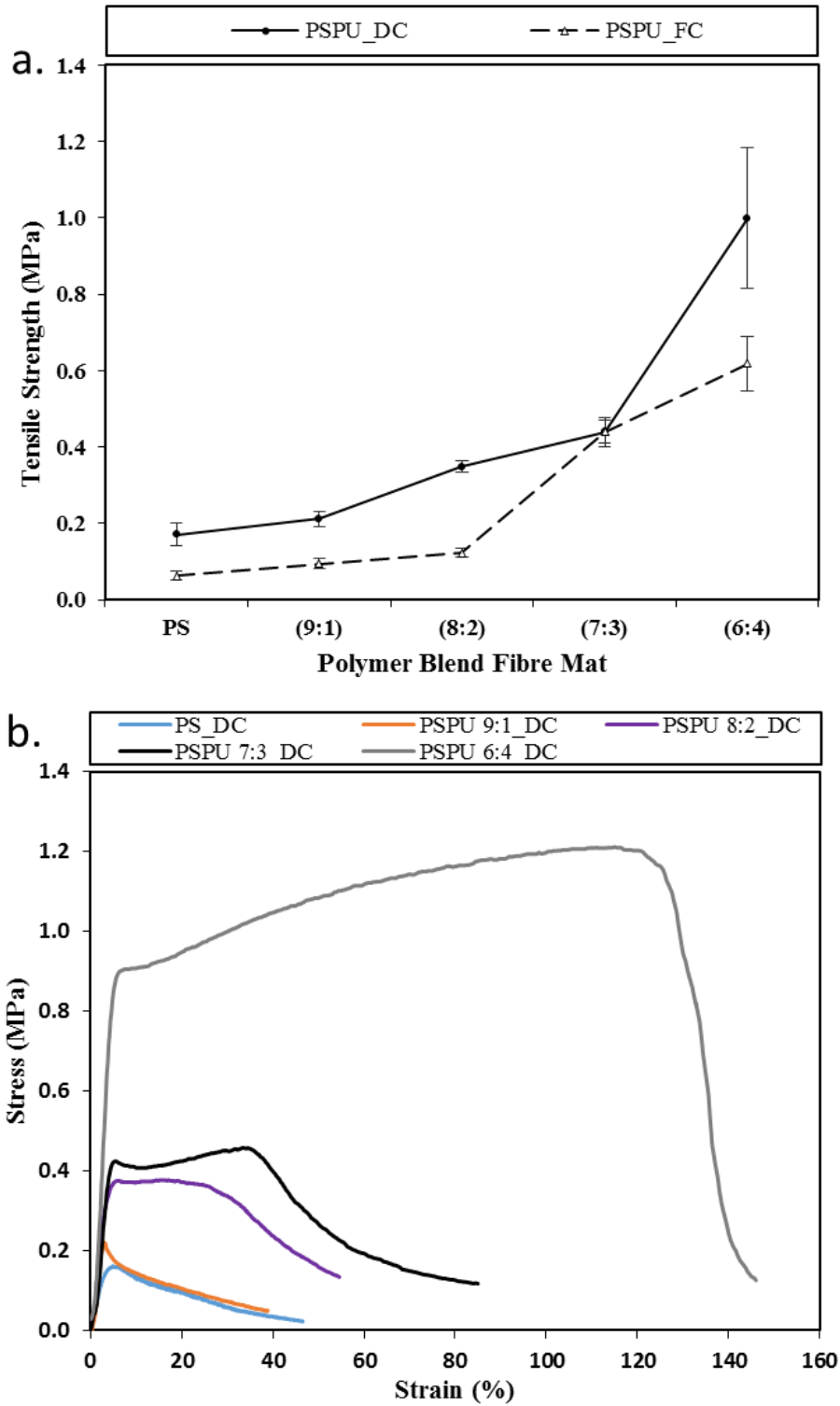
Figure 5-13: Effect of varying the polymer blend ratio on the tensile strength of PSPU polymer blemnd fibre mats. Comparing tensile strength of FC and DC fabricated mats. Error bar represents one standard deviation about the mean (n=5), b.) stress-strain curve of typical PS and PSPU mat fabricated using the DC system.

Table 5-4: Mechanical properties of electrospun PS_DC and PSPU_DC polymer blend mats. Standard deviation about the mean (n=5).

Sample	Modulus (MPa)	Yield Stress (MPa)	Elongation at UTS (%)	Tensile Strength (MPa)
PS_DC	4.92 ± 0.61	0.15 ± 0.03	6.68 ± 1.43	0.17 ± 0.03
PSPU 9:1_DC	9.84 ± 1.35	0.20 ± 0.02	3.23 ± 0.80	0.21 ± 0.02
PSPU 8:2_DC	7.35 ± 2.77	0.29 ± 0.02	21.69 ± 3.21	0.35 ± 0.01
PSPU 7:3_DC	14.55 ± 1.12	0.38 ± 0.02	33.96 ± 2.81	0.44 ± 0.03
PSPU 6:4_DC	19.03 ± 2.46	0.66 ± 0.13	109.16 ± 14.23	1.00 ± 0.18

To further study the effect of PU addition on individual fibre, SEM micrograph of the fractured point on PSPU_FC 6:4 was taken after tensile testing and compared with micrograph of the same mat not tested (Figure 5-14a and b). Figure 5-14b shows plastic deformation of the polyblend fibre after tensile testing, with several localized fractured points observed along the twisted fibre filaments. A reduction in the average fibre diameter of about 50% (3.89µm to 1.96µm) was observed between the two micrographs (Figure 5-14c). This phenomenon further shows that aside the point bonding, the polymer fibre equally plays a role in the enhanced tensile strength, as the fibre filaments had undergone some loading prior to failure. The fractured point could be ascribed to the inability of the fibre filaments to support the applied load following the rearrangement of the fibres during tensile testing [169]
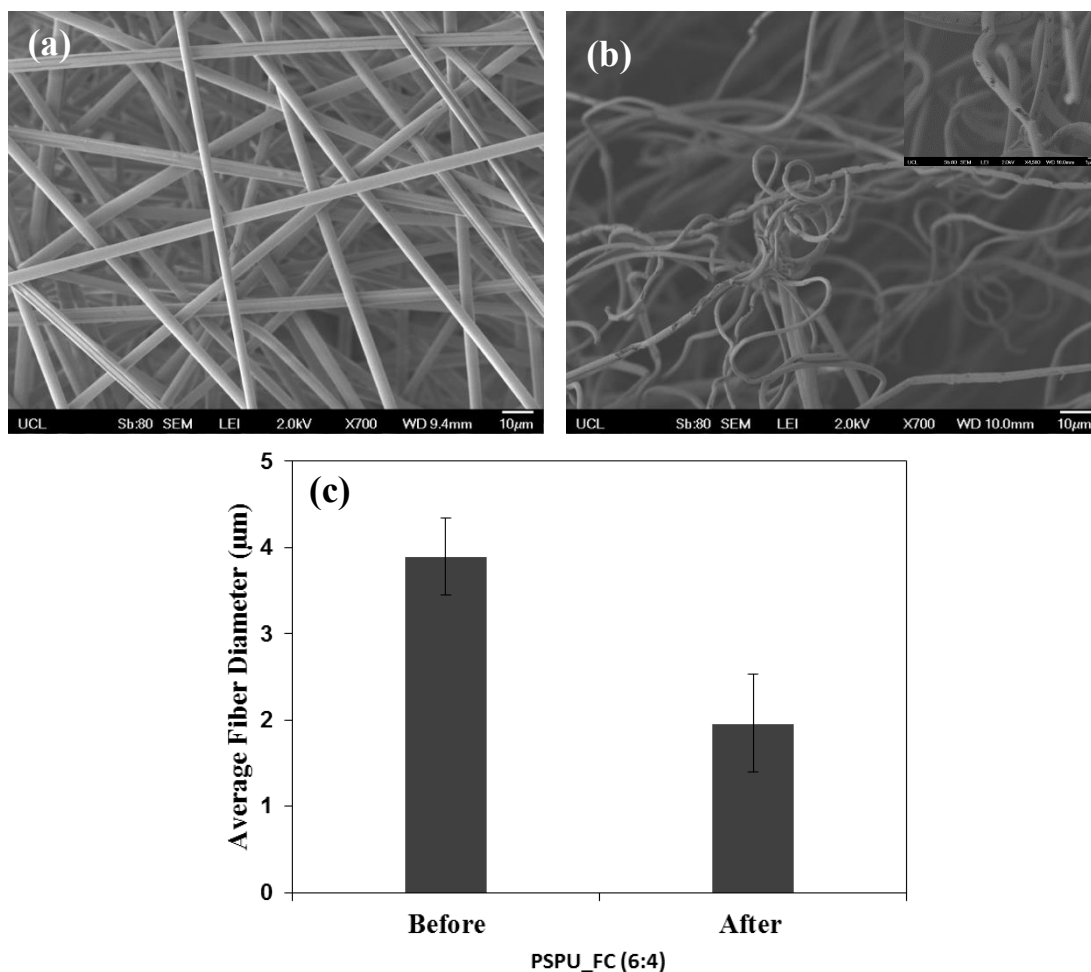
Figure 5-14: Effect of tensile test on electrospun PSPU_FC 6:4 fibre mats. a.) shows the morphology of the fibre mat prior to uniaxial tensile testing, b.) mat morphology at the point of fracture after the test, c.) comparison of the average fibre diameter obtained from both mats. Error bar represents one standard deviation about the mean (n ≥ 100).

5.5.2 **Investigating the mechanical properties of DC fabricated mats along (MD) and across (CD) the axis of rotation of the drum**

Mechanical properties of fibre mat fabricated using the DC system were studied both along the axis of rotation of the drum tagged machine direction (MD) and the drum's axial (Cross) direction (CD). Figure 5-15a and b shows the tensile strength and elongation at UTS respectively of PS, PSPU_DC 8:2 and PSPU_DC 6:4 fibre mat. Though all the fibres fabricated using the DC system exhibits a random orientation, the tensile strength in the CD was consistently higher than in the MD in all the fibre

155

mats. It is believed this could be an effect induced by the transverse movement of the nozzle in the CD of the drum, which may have induced some fibre orientation in that direction, which may not have been easily noticeable on the SEM micrograph.

The strain at UTS shows a reverse trend with both the PS and PSPU_DC 6:2 mat, having a greater elongation of 164% and 152% respectively along the axis of rotation of the drum (MD), while no significant difference was observed for PSPU_DC 8:2.

Table 5-5 shows a detailed quantitative evaluation of the yield stress, modulus, elongation at UTS and tensile strength of the mat. Typical stress strain curve of the data presented in Table 5-5 can be found in the appendix.
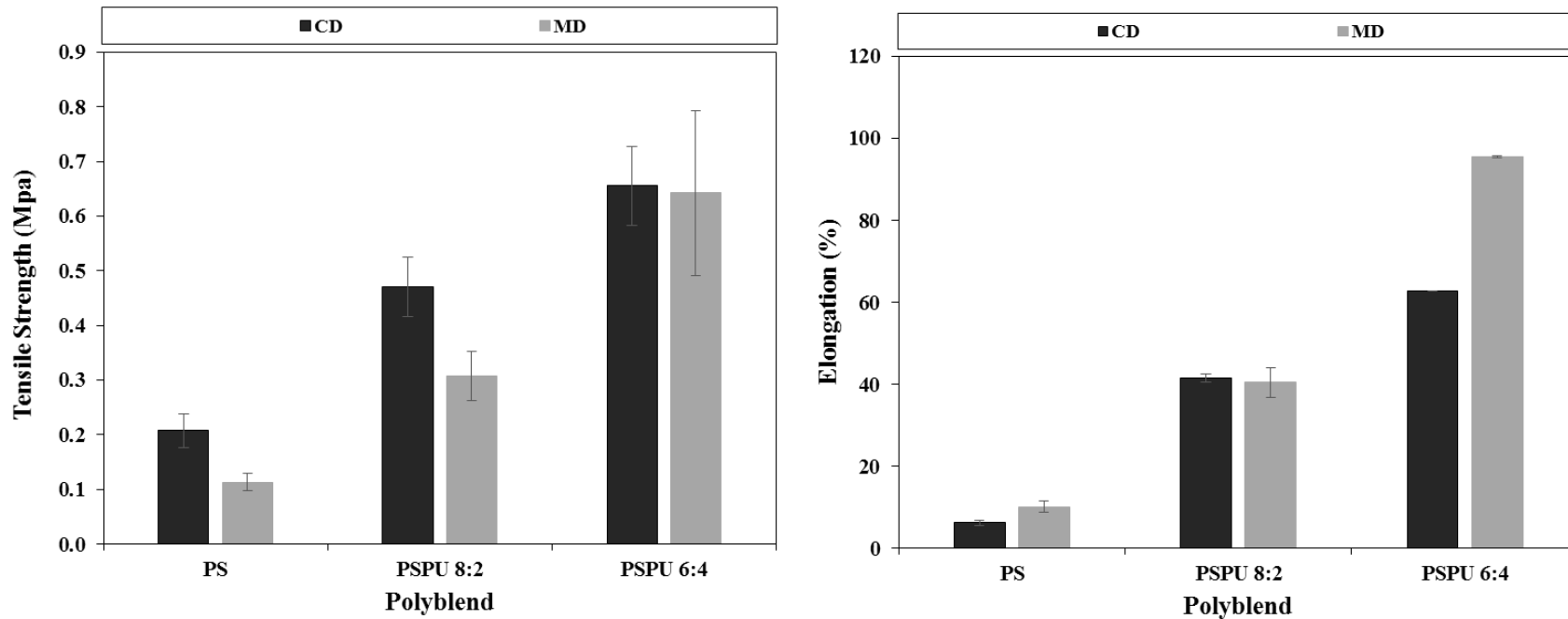
Figure 5-15: Comparison of the mechanical properties in the axial/cross direction of the drum (CD) and rotating direction (MD) of mats fabricated using the DC system, **a.)** Tensile strength and, **b.)** Elongation at UTS of the mats. Error bars represents one standard deviation about the mean (n=5).

Table 5-5: Comparison of the modulus, yield stress, elongation at UTS and tensile stress of DC fabricated mats in the rotating direction (MD) and cross/axial direction (CD) of the mat

Polymer Fibre	Modulus (MPa)		Yield Point (MPa)		Elongation (%)		Tensile Strength (MPa)	
	CD	MD	CD	MD	CD	MD	CD	MD
PS	10.33 ± 1.33	4.11 ± 0.88	0.17 ± 0.05	0.09 ± 0.01	6.20 ± 0.62	10.77 ± 1.33	0.21 ± 0.03	0.11 ± 0.02
PSPU 8:2	8.02 ± 1.67	7.48 ± 0.76	0.17 ± 0.02	0.23 ± 0.03	41.47 ± 1.01	40.44 ± 3.61	0.47 ± 0.05	0.31 ± 0.05
PSPU 6:4	15.40 ± 1.02	10.79 ± 2.59	0.33 ± 0.05	0.31 ± 0.10	62.80 ± 6.62	95.53 ± 10.63	0.66 ± 0.07	0.64 ± 0.15

5.5.3 Effect of crude oil on mechanical properties of electrospun polymer blend fibre mats

The use of sorbents in oil spill remediation often involves leaving the sorbent at the spill site over a considerable period either to attain saturation as a protective barrier[156]. Hence, it is important that a sorbent maintains good mechanical integrity over a substantial period when exposed to the sorbed pollutant. The effect of light crude oil on the mechanical properties of PS_DC, PSPU_DC 8:2 and PSPU_DC 6:4 is presented in Figure 5-16. The tensile strength of the polymer blend mat is seen to reduce over the experimental period of 72 hours (3days), but remains between 150% - 200% higher than the tensile strength of the pristine PS fibre mats, while the % elongation increases with exposure to the light crude oil. The increased elongation could be the result of plasticization effect of the light crude oil on the polymer fibre or an enhanced fibre slippage due to reduced inter-fibre friction during testing. Overall, the polyblend mats shows good mechanical properties than the pure PS mat, indicating its suitability for use as sorbent in shore line protection.
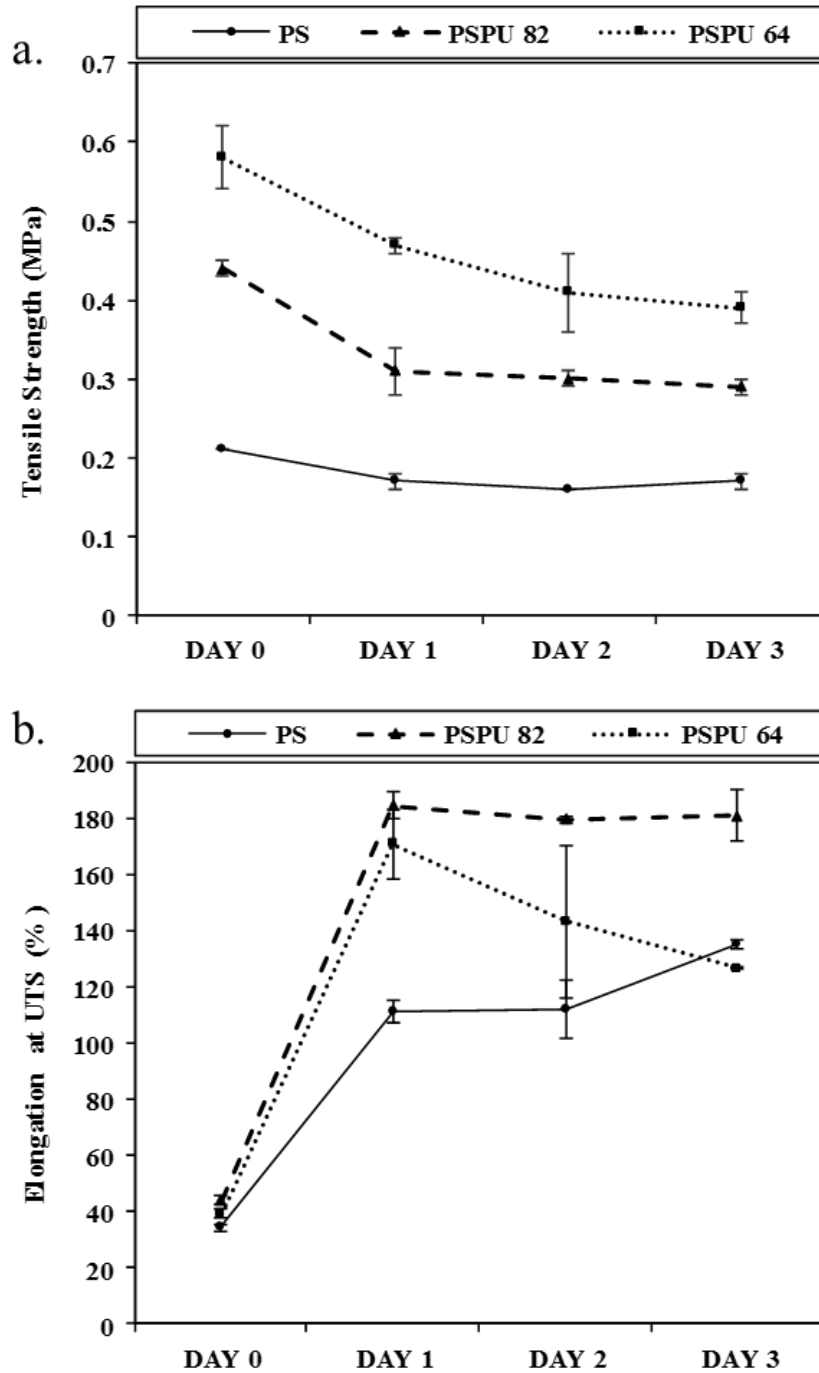
Figure 5-16: Influence of light crude oil on the mechanical properties of electrospun PS and PSPU polymer blend mats fabricated using the DC system. a.) shows the tensile strength and b.) elongation at UTS of mats studied over a period of 3 days. Errors bars represents one standard deviation about the mean (n=3).

5.5.4 AFM Peak Force QNM analysis

Evaluation of the mechanical properties of single fibre filaments fabricated using the

FC system was investigated using the peakforce quantitative nanomechanical mapping

technique described in Section 3.4.8.2. This method enables the simultaneous investigation of the DMT modulus and adhesion properties of a filament down to the nanoscale level, while carrying out a topographic scan of the sample [189]. Figure 5-17 shows the variation in the DMT modulus and adhesion properties with increasing PU content in the fibre filament. The DMT modulus value of 2.9GPa recorded for the pristine PS fibre filament is consistent and within margin of error of literature values[139], which is in the realm of the manufacturer`s reported value. This further validates the QNM approach reported in this thesis.

The decreasing trend in DMT modulus with increasing PU observed in Figure 5-17 may be the effect of the polyurethane soft segment, as the thermogravimetric analysis reported in Section 5.4.1 shows a 55% soft segment composition in the PU used in this study. However, a comparison of the moduli value reported in this section, shows a variation of 2 - 3 orders of magnitude, with values reported earlier in Section 5.5.1. This difference in value with the macro scale tensile testing method can be ascribed to the porosity of the fibre mats as well as the random orientation of the fibres [190, 191].

Figure 5-17 equally shows a decreasing trend between the adhesion behaviour with increasing PU ratio, this indicates a decreasing affinity between the cantilever tip and the sample. The adhesion would have been more meaningful if the cantilever tip is functionalized [189] with a functional group such as the CH_3- group, as this would have indicated the level of hydrophobicity of the surface.
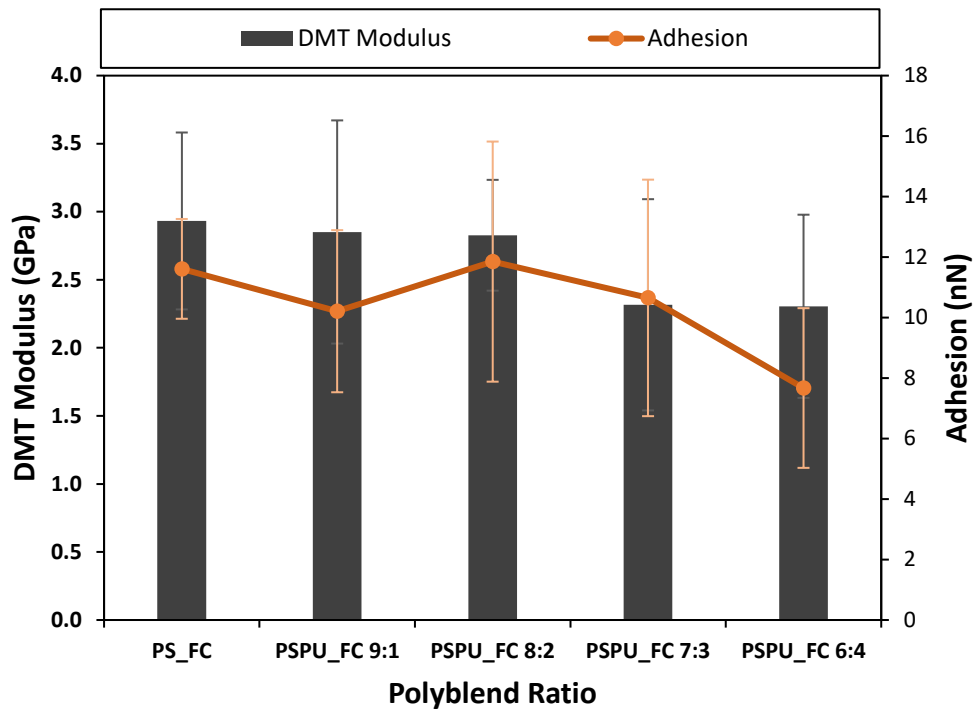
Figure 5-17: DMT Modulus and Adhesion properties of peakforce QNM of 500nm - 1µm scan area on a single fibre filament fabricated using the FC system.

Figure 5-18 shows the 2D and 3D height sensor and the DMT modulus mapping. The contrast in a modulus scan could be an indication of the distribution of the constituent polymers, in the case of polymer blend [189]. Such conclusion cannot be inferred from the below DMT scan, as regions with lower stiffness recorded could be seen on both the pristine PS and polymer blend fibres which could be attributed to height variation on the fibre surface. Such height variation could be advantageous as it could provide more surface area for oil adsorption.
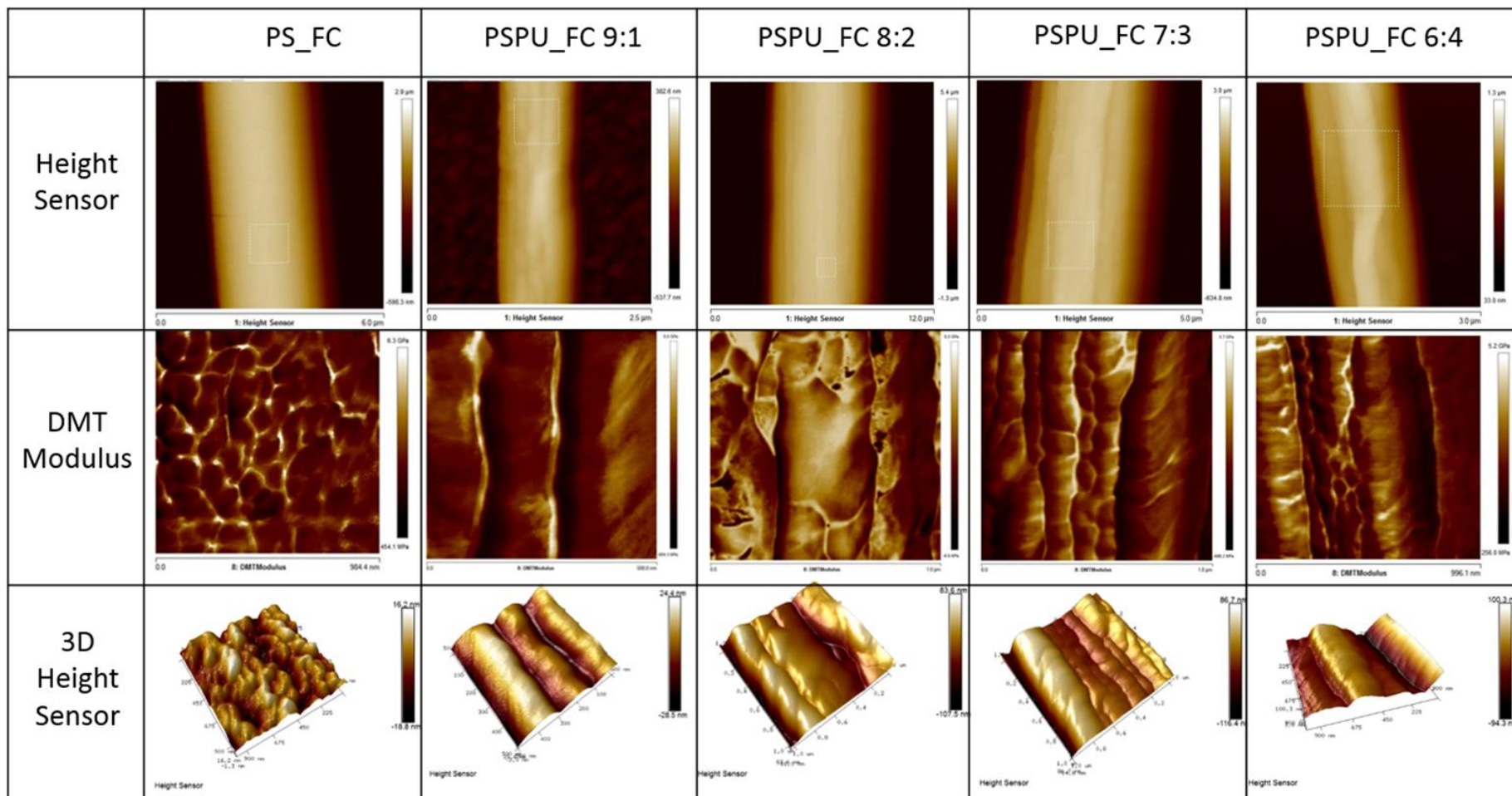
***Figure 5-18*:** Illustration of the 2D and 3D height sensor and the DMT modulus scan of electrospun PS and PSPU_FC fibre mats.

5.6   Oil sorption properties of the polymer blend mats

5.6.1   Evaluation of oil sorption and oil retention capacity of fibre mat (Oil Only System)

To investigate the maximum oil sorption and retention capacity of the polymer blend fibre mats, sorption test were performed as described in Section 3.4.9. Figure 5-19 shows the oil retention behaviour of mats fabricated using both the FC and DC systems. Oil retention behaviour of commercial PP sorbent (mat) was equally studied for comparison with the DC fabricated mats.

The oil retention curve of the different mats was observed to follow a similar trend, with at least 3 distinct zones observed in the desorption process. The first period which occurs within the first minute of drainage, saw rapid release of loosely adsorbed oil from the sorbent. The second period was observed between 5-15mins of desorption in most of the mat and it is the period where the mat experiences a sharp decline in desorption rate. This period could be regarded as the transition period as it occurs before the third stage where the process attains equilibrium in some of the mats. Similar trend has been observed in literature for PP mats [17] and recycled wool sorbent [192]. Although most of the PS and PSPU 9:1 fabricated mats were observed not to have attained steady state within the experimental period of 30mins. It is believed the desorption process will reach a steady state with an increase in observation time.

In Figure 5-19, variation in sorption behaviour was observed in mats fabricated using the different collector systems. FC fabricated sorbent, consistently exhibits a higher initial sorption capacity (at time; $t = 0$) and at the observed period of $t=1$ and $t=30$mins, when compared to DC fabricated mats, as seen in Figure 5-19 and Table 5-6. Sorption

163
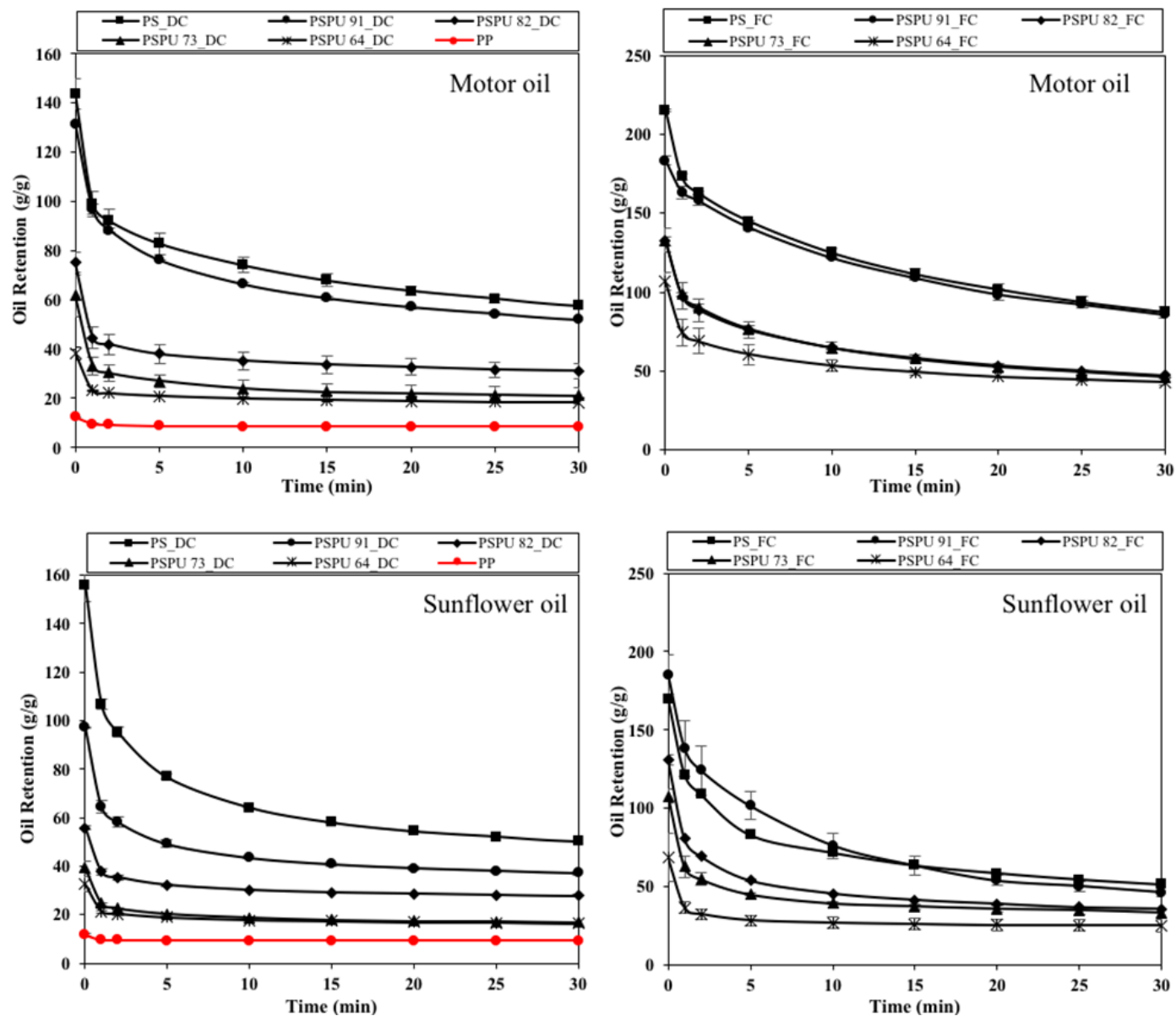
Figure 5-19: Oil retention behaviour of electrospun PS and PSPU polymer blend mats fabricated using both FC and DC systems in sunflower and motor oils. Oil retention curve of the commercial PP sorbent is also tested for comparison. Error bars represents one standard abot the mean (n=3)

capacity of 175g/g recorded for PS_FC at t=1, represents a value 177% higher than DC produced PS mat, while for the polymer blend fibres (PSPU); 9:1, 8:2, 7:3 and 6:4, a higher SC of 168%, 216%, 297% and 322% respectively was recorded for the FC fabricated sorbent over the DC produced sorbents. The higher SC can be attributed to the loose architecture and higher porosity of the FC mats (see Figure 5-1 and Table 5-6). Similar effect of porosity on sorption capacity have been reported in previous studies [134, 193]. A high fibre packing density and low mat porosity could be attributed to the decreasing SC with increasing PU ratio observed in all the different system.

As illustrated in Table 5-6, the higher sorption capacity recorded for motor oil in all the different polymer blend sorbent can be ascribed to its higher viscosity which enhances intermolecular interaction between the oil and the fibre filament. Also, motor oil was observed to experience a lower desorption rate in mats with a high porosity, which is consistent with previous works [134], but as the porosity of the mats drops to 95.9% and below in PSPU_DC 8:2, 7:3 and 6:4, a reversal in trend was observed. The desorption rate for motor oil for these mats can be attributed to a combined effect of both porosity and SSA of the mat, as a dip in SSA was observed in the three sorbents.

The PS and PSPU polymer blend mats were seen to possess higher SC in both oils compared to the commercial PP mat. The poor performance of the PP sorbent could be attributed to a combination of the mat architecture, fibre morphology, material chemistry and the crystalline nature of the polypropylene.

Table 5-6: Relating the fibre mat/sorbent parameters with the oil desorption behaviours of the mats. Sorption capacity and desorption rates at time 0 min, 1 min and 30 mins is represented with t_0, t_1 and t_{30} respectively

Fibre Sample	SSA	Porosity (%)	Motor Oil					Sunflower Oil				
			SC at t_0 (g/g)	SC at t_1 (g/g)	Desorption rate at t_1 (%)	SC at t_{30} (g/g)	Desorption rate at t_{30} (%)	SC at t_0 (g/g)	SC at t_1 (g/g)	Desorption rate at t_1 (%)	SC at t_{30} (g/g)	Desorption rate at t_{30} (%)
PS_FC	1.24	99.8	215	175	19	87	60	170	122	28	47	72
PSPU 9:1_FC	1.15	99.7	183	163	11	86	53	185	138	25	46	75
PSPU 8:2_FC	1.04	99.6	133	97	27	47	65	134	81	39	36	73
PSPU 7:3_FC	1.05	99.6	132	98	26	46	61	108	63	42	37	66
PSPU 6:4_FC	0.93	99.0	107	74	31	43	60	68	37	46	25	63
PS_DC	1.81	97.5	144	99	31	58	60	156	107	31	50	68
PSPU 9:1_DC	1.26	96.9	131	97	26	52	60	97	64	34	37	61
PSPU 8:2_DC	1.14	95.9	75	45	40	31	57	56	38	32	28	50
PSPU 7:3_DC	0.76	95.1	62	33	47	21	66	39	25	36	17	56
PSPU 6:4_DC	1.13	94.4	38	23	40	18	53	32	21	34	16	50
pp	1.10	91.2	12	10	17	9	25	12	10	17	9	25

5.6.2 Investigating buoyancy and oil sorption capacity in oil - water medium

A key desirable property of a sorbent for marine is the ability to maintain buoyancy before and after oil sorption particularly when used in marine oil spill clean-up [3, 19]. Buoyancy tests were performed as described earlier in Section 3.4.4. Figure 5-20, shows oil sorption process PSPU_FC 8:2 and PSPU_DC 8:2 sorbent under static condition. In both cases, the sorbent was seen to remain on the surface of the oil-water medium for the entire duration of the experiment (30 mins), even when completely saturated with oil. The same buoyancy level was experienced under dynamic condition, which demonstrated the suitability of the polyblend sorbent for marine oil spill remediation. Figures 5-20 c and d, shows the surface after the removal of the soaked sorbent. Good buoyancy was observed under dynamic condition for both fibre sorbents in result not shown in this thesis.
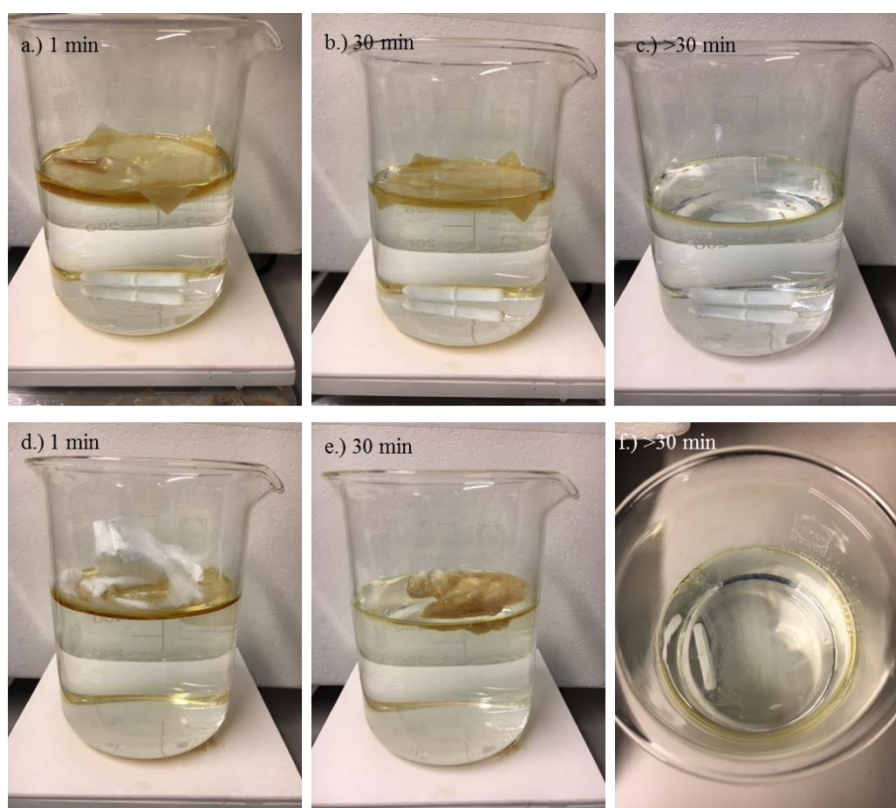
***Figure 5-20*:** Illustration of the buoyancy of PSPU 8:2 mats fabricated using FC and DC system. Test were conducted under static conditions and time indicated on image a.), b.), d.) and e.) represents duration of sorbent exposure to the oil-water medium, while c.) and f.) shows water surface after the fibre mats were removed.

Figure 5.21, shows the average sorption capacity for PSPU_FC polymer blend fibres in an oil-water medium, and a comparison with maximum sorption capacity recorded in literature for coaxial[22] and multi-nozzle[21] electrospun mat of both polymers, described in Section 2.6.3
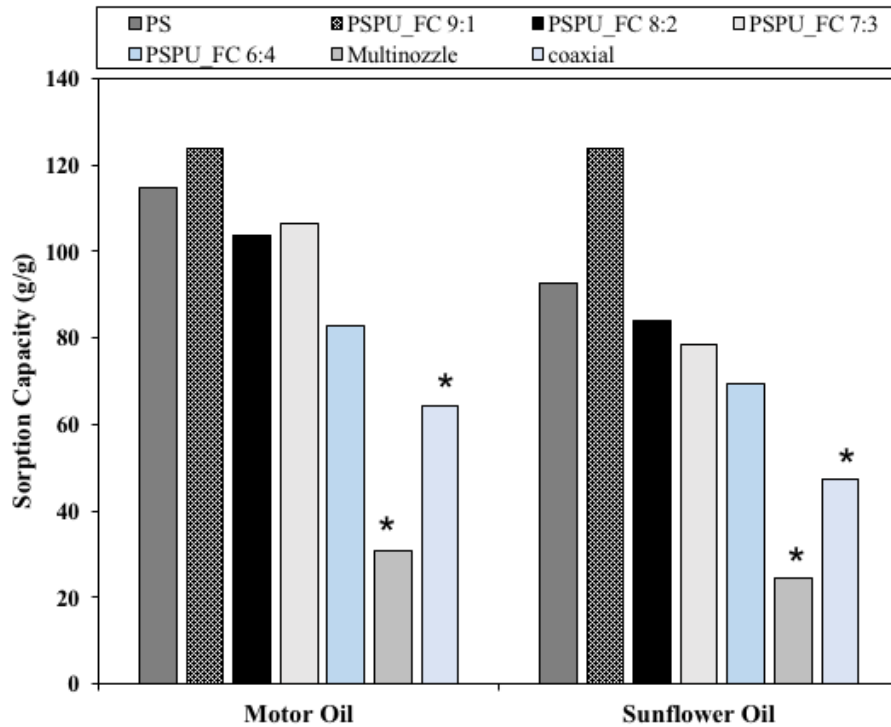
Figure 5-21: Oil sorption capacity in motor and sunflower oils of electrospun PS and PSPU polymer blend mat fabricated using the FC system. Asterixed, are values for multi-nozzle and coaxial electrospun PS and PU mats reported in literature. All testes were carried out in oil-water medium and under static condition

Test were conducted under similar test procedure as the previous literature work and as described in Section 3.4.9. Generally, it can be seen from Figure 5-21, that the PSPU polymer blend mat exhibits a higher sorption capacity of between 2-5 times those obtained in the earlier reported literatures. The higher sorption behaviour in the polyblend mat could be a combination of greater intermolecular interaction between the PS-PU polymers, effect of polymers molecular weight, and the fibre packing density[134]. For the two oil types investigated, PSPU_FC (9:1) recorded the highest SC of 123.88g/g and 123.95g/g in motor oil and sunflower oil respectively. The

enhanced SC at this blend, could be the effect of intermolecular interaction between the polymers with the PS still playing a dominant effect in the blend.

5.6.3 Sorption behaviour under static and dynamic conditions (Oil-Water medium)

The sorption behaviour of PSPU_FC polymer blend mat was investigated in an oil-water system under both static and dynamics conditions as described in Section 3.4.9, using light crude and vegetable oil.

Figure 5-22 shows oil sorption capacity for the PS and PSPU polymer blend mat under static conditions, the SC of the pristine PS fibre mat was 80.49g/g and 42.50g/g for vegetable and crude oil respectively. An addition of 10% PU in the polymer matrix (PSPU_FC 9:1) saw an increase of 16.7% and 5.5% in both vegetable oil and crude oil respectively. Further increase in PU ratio in the blend, saw a gradual decline in the sorption capacity. The initial rise in sorption behaviour as observed for PSPU_FC 9:1 could be the elastomeric PU giving the mat some structural integrity that enhances its oil sorption, this effect was seen to collapses with further increase in the PU ratio in the blend. This could be a result of the high density of PU polymer and the introduction of point bonding between the fibres, thereby reducing void spaces available for sorption. The higher sorption capacity observed for vegetable oil could be attributed to the higher viscosity of the oil, which enhances the molecular interaction between the oil and the fibre filament, hence greater adsorption. Generally, a high viscous oil introduces either an increase adherence to the fibre or a decrease in the ability of the oil to infiltrate the void spaces between the fibre filaments [8, 11]. The same trend in sorption behaviour was observed under dynamic condition as seen in Figure 5-22b at an agitation speed of 250rpm, but with a lower sorption capacity for all the different mats.
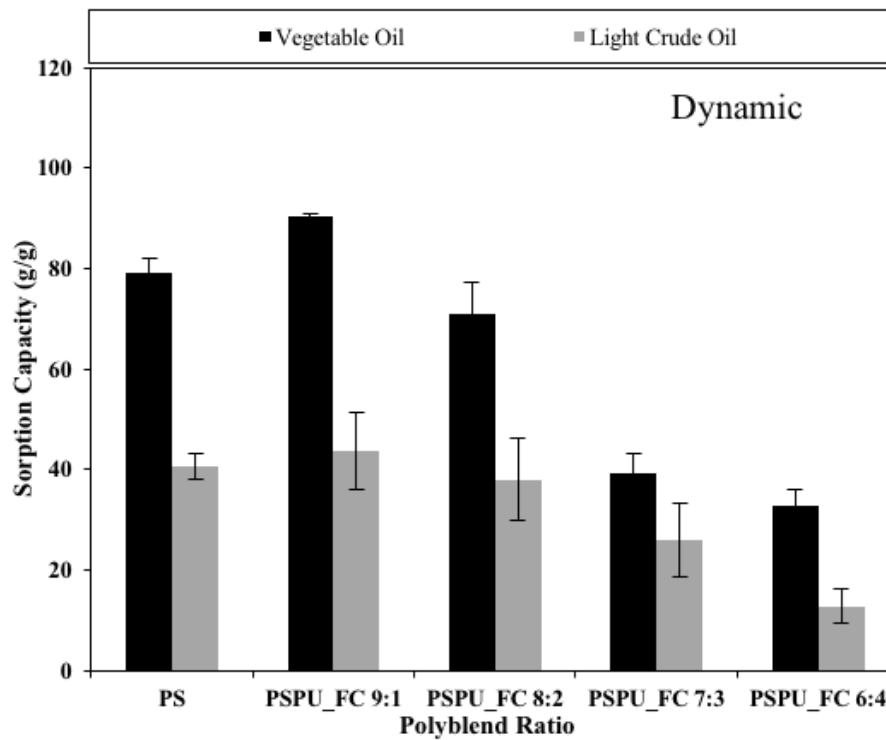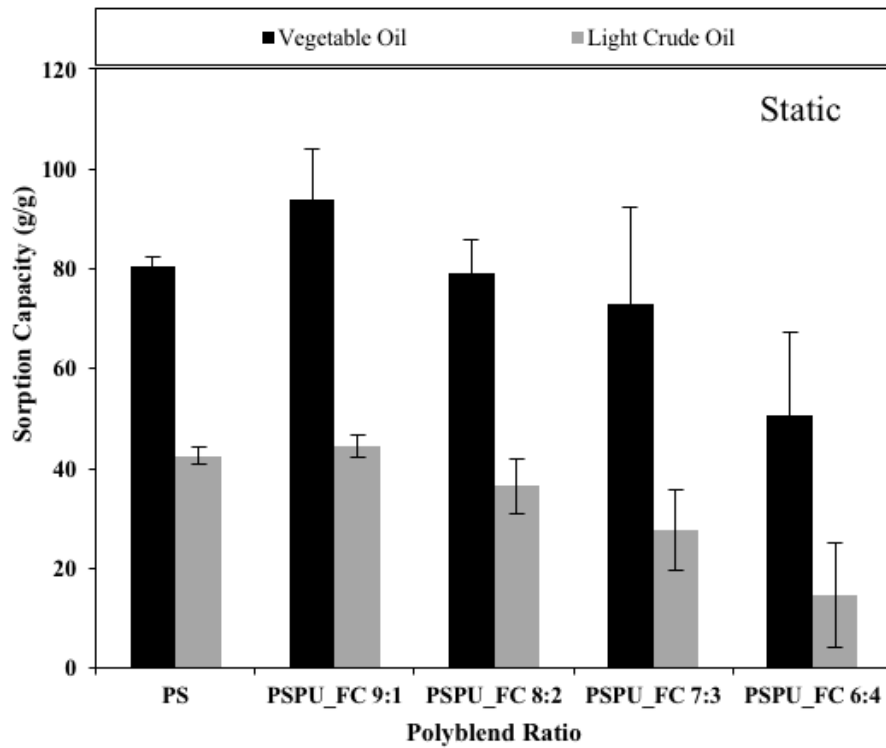
Figure 5-22: Oil sorption capacity under static and dynamic conditions of electrospun fibre mats fabricated using FC system. Error bar represents one standard deviation about the mean (n = 3).

5.6.4 **Reusability and recoverability of the PSPU polymer blend mat**

A key aspect of oil spill clean-up process is the reusability of the sorbent and the ability to recover the sorbed oil [14]. The reusability of the electrospun polymer blend fibre was investigating using PSPU_FC 6:4, given its high mechanical properties as seen in Section 3.5. Figure 5-23 shows the result of five successive sorption cycle of the fibre mat using motor oil as test medium. A sharp decline of approx. 50% in sorption capacity was observed after the first cycle; from 72.7 g/g to 35.0 g/g. The SC was then seen to approach a limiting value afterwards. The sharp drop in SC capacity after the first cycle could be the effect of irrecoverable collapse in the mat porosity due to the manual desorption process used in this study. It is important to note that the sorption capacity of 28.9g/g recorded after 5th cycles, represents approximately 3 times the SC of the conventional PP sorbent (see Section 5.6.3) and about 2 times values recorded for both PP [17] and wool based sorbents [192] in literature.
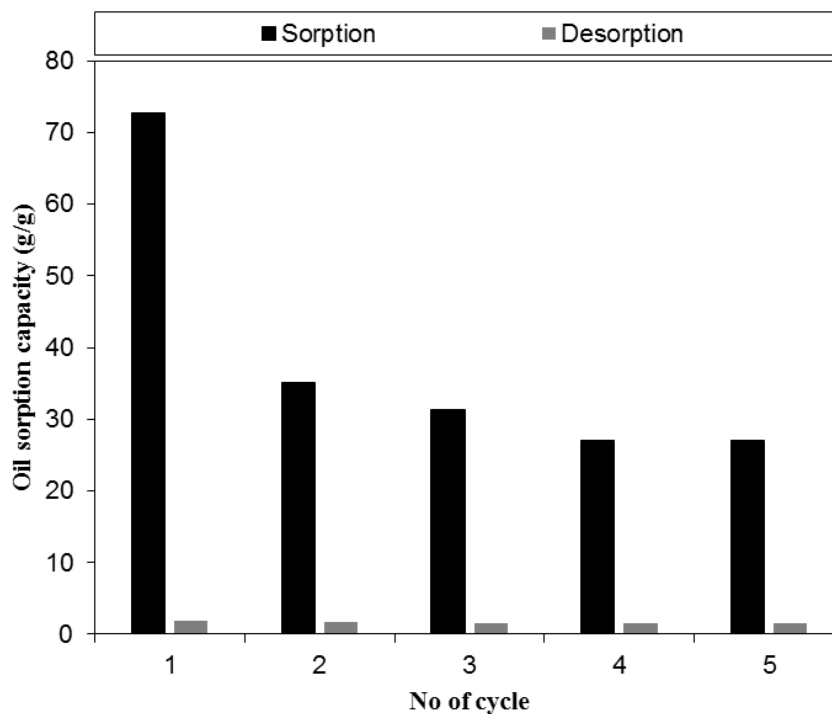
Figure 5-23: Demonstration of reusability of electrospun PSPU_FC 6:4 polymer blend, showing sorption and desorption of the fibre mat.

5.7 Summary

As stated in **Section 4.1**, the aim of this chapter is to explore polymer blending as a means of increasing the mechanical properties of electrospun PS fibre. A blend of PS and thermoplastic polyurethane (PU) were studied and as shown in **Figure 5-13**, this overall objective was achieved.

The morphological structure of the PSPU polymer blend fibres were studied for both flat collector (FC) and rotating drum collector (DC) system (**Figures 5-2 and 5-3**). In both cases, though not a linear effect, the average fibre diameter shows an increasing trend with increasing PU ratio (**Table 5-2**), this was attributed to the observed increase in the viscosity and surface tension of the blend solution with increase PU ratio as illustrated in **Table 5-1**. Also, increasing PU content in the blend results in a higher packing density and the formation of chemically point bonded structures, attributed to the higher density of PU, causes a reduction in rate of solvent evaporation.

The formation of a bi-component PS-PU mat structure is confirmed in **Figure 5-5**, while EDX analysis in **Figure 5-6**, further confirms the creation of a polymer blend down to a single fibre filament. This effect could be attributed to intermolecular interaction between the binary polymer constituent. The formation of a single glass transition temperature in the DSC thermograph (**Figure 5-12 and Table 5-**3), further indicates the existence of a strong miscibility between the polymers.

Oil viscosity, mat/sorbent porosity, polymer blend ratio, and fibre collection system were observed to be key to the oil sorption and retention capacity of the mat as seen in **Table 5-6 and Figure 5-19**. Despite the decreasing trend in oil sorption and retention capacities of the polyblend mats with PU addition, values obtained were between 2 – 9 times those of the commercial PP sorbent (**Table 5-6**).

In the same vein, SC of the polymer blend mat was between 2 - 5 times, those obtained for coaxial and multi-nozzle side-by-side electrospinning of PS and PU polymers reported in literature. Excellent buoyancy under both static and dynamic conditions were observed for the poly blend mats in **Figure 5-22**. Good reusability of the mat was shown with PSPU_FC 6:4 in **Figure 5-23**.

It is believed that despite the contrasting trend in the mechanical and SC behaviour of the polymer blend mat, a compromise can be reached between these 2 key properties, depending on the viscosity of the oil to be sorbed.

6 Post Treatment of PS fibre mat: Heat and Ultrasonic Treatment

6.1   Introduction

One of the major constraint facing the exploitation of electrospun PS as oil sorbent is its poor mechanical strength, due to the lack of bonds between the fibres. In the previous chapter (Chapter 4), polymer blending was used to improve the mechanical properties of electrospun (ES) PS fibre mat. Here, we will explore a two-step processing approach - fibre production and subsequent heat or ultrasonic treatment of the fibre mat. This will provide a basis for comparison between a single processing (polymer blend) and two-step approach (heat and ultrasonic treatment) in improving the mechanical properties of PS fibres.

Heat treatment is an established technique often used in enhancing the mechanical properties of electrospun fibres [194, 195]. Only a limited number of studies on the thermal treatment of electrospun PS have been reported in literature [196, 197]. None of these studies have investigated the impact of thermal treatment on the mechanical or sorption behaviour of the fibres. Ultrasonic energy, a technology commonly used in the textile and apparel industry [198], has reportedly been used to enhance the mechanical strength of fibres. This has been achieved either by passing the fibrous mat through a pair of ultrasonic rollers [199] or exposing the fibres to ultrasonic energy in an ultrasonic bath, containing a liquid medium [200]. Ultrasonic technology is yet to be explored for electrospun fibre bonding.

This chapter therefore aim to explore the feasibility of using thermal and ultrasonic energy treatment to enhance the mechanical strength of electrospun PS mat, while also studying the effect on the physicochemical and sorption behaviour of the mat. Mats fabricated using the rotating drum set up discussed in previous chapter (Chapter5) will be used in this study. The specific objectives of this chapter are as follows;

- To study the effect of heat treatment temperature on the morphology of electrospun PS fibre mats.

- To study the effect of heat treatment on the chemical and thermal property of the fibre mat.

- To evaluate the effect of thermal treatment temperature on the mechanical and sorption behaviour of the fibre mat.

- To evaluate the effect of thermal treatment time on both the mechanical and sorption behaviour of the mat.

- To study the effect of ultrasonic exposure on fibre morphology, sorption and mechanical properties of PS fibre mat.

6.2 Heat treatment

Previous literature studies on the thermal treatment of electrospun fibres, have shown that heat treatment could induce dimensional shrinkage of the mat. This has been attributed to molecular chain relaxation of the polymer`s amorphous region [173, 201]. To mitigate this, tension/restrained thermal treatment is employed in this chapter, as this has previously been demonstrated as a method that does not impact on the polymer mat`s dimension during heat treatment [202]. The effect of heat treatment on the

morphological, chemical, mechanical and sorption behaviour of the mat is described in subsequent subsection.

6.2.1 Physicochemical properties of heat treated PS fibre mat

6.2.1.1 Effect of heat treatment on fibre morphology

The heat treatment process explored to enhance the mechanical properties of electrospun PS fibre mats were carried out using the thermal treatment process described in Section 3.7. The strengthening of the mechanical behaviour of electrospun polymer fibre mat after heat treatment had previously been associated to the formation of inter-fibre bonds between adjacent fibre at the point of contact[203], which could occur either below [204] or above [196, 197] the glass transition temperature of the polymer. Thermal analysis of electrospun PS fibre mat carried out earlier in Section 5.4 had shown the glass transition temperature (T_g) of the mat to be 114.7^{o}C, hence the thermal treatment was conducted between 90°C and 130°C at an incremental temperature of 10°C.

Figure 6-1, shows the SEM micrograph of untreated and heat treated PS fibre mats. No inter-fibre bonds was observed in both the untreated and heat treated mats at 90°C and 100°C as seen in Figure 6-1b and c, but with an increase in treatment temperature close to the T_g at 110°C (figure 6-1d,) the formation of inter-fibre bonds were observed. Further increase in the treated temperature above the T_g (Figure 6-1e and f) saw an in increase in the number of point bonding of adjacent fibres. The increased bonding could be attributed to the ability of the molecular chains to glide past one other at temperature above the glass transition temperature, thereby enhancing inter-fibre bonds upon cooling.

176
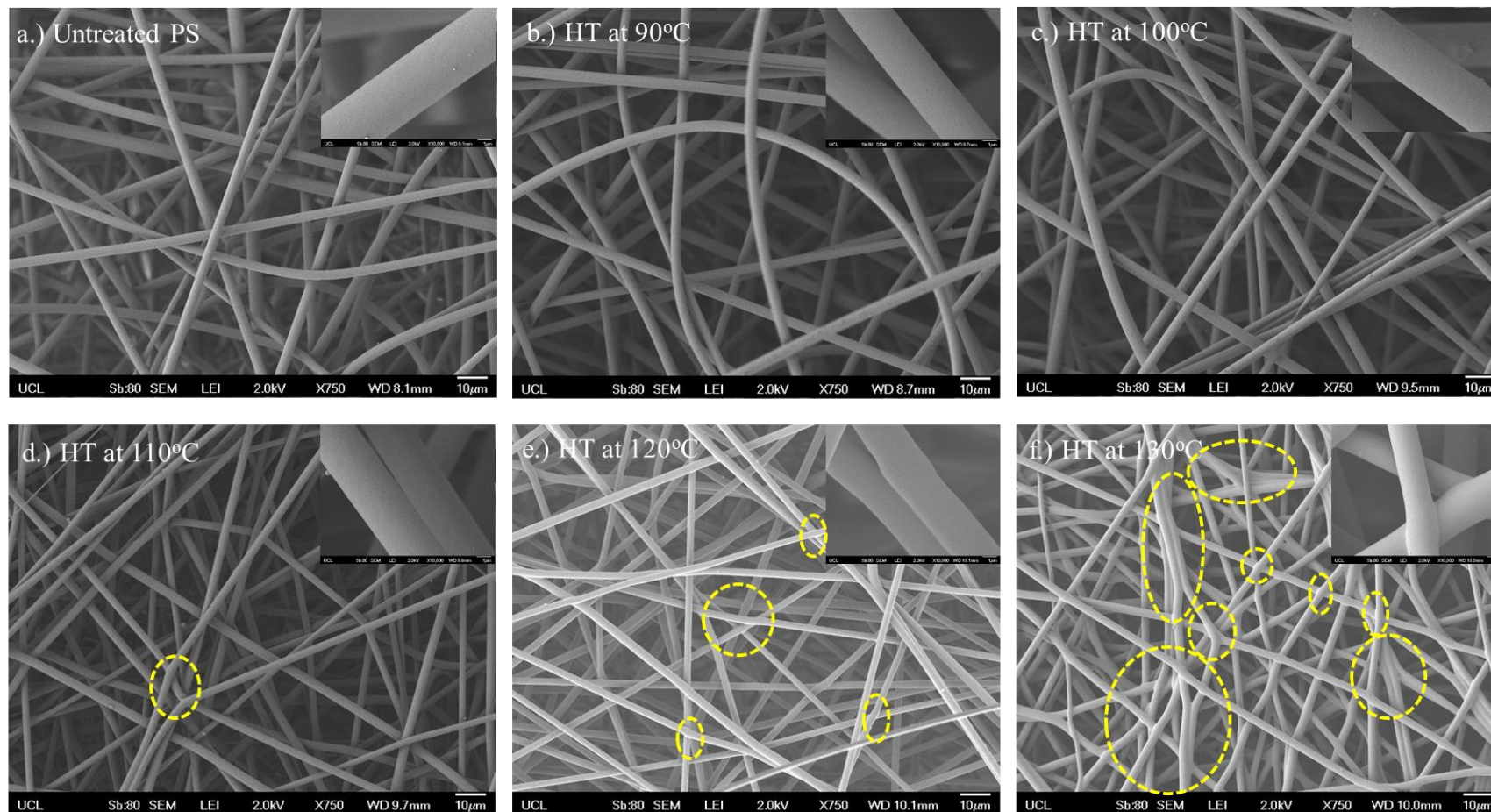
Figure 6-1: SEM micrograph showing the effect of heat treatment on electrospun PS mat at different treatment temperature; a.) Untreated PS mat and heatreated at b.) 90ºC; c.)100ºC; d.) 110ºC; e.) 120ºC and f.) 130ºC

Analysis of the SEM micrograph to evaluate the effect of HT on the fibre diameter (Table 6-1 and Figure 6-2), reveals that despite no change in the morphology of HT fibre at 90°C and 100°C a steady increase in the average fibre diameter (AFD) was observed. The AFD increased from 3.13µm in the untreated mat to 3.33µm when HT at 100°C. Similar effect was earlier reported by Shirazi et al [196]. Further increase in HT temperature above the T_g saw a gradual decline in AFD to 2.20µm at a HT temperature of 130 °C. The thinning of the fibre diameter is a combined effect of the tension heat treatment mode employed in this study and a rearrangement of the fibre`s molecular chain as the applied heat exceeds a certain activation energy, in this instance the polymers T_g.

For a restrained heating mode, heating the fibre mat above T_g causes polymer chains to arrange along the axis of the applied external force leading to a reduction in the fibre diameter[202]. Also, HT above 100°C causes loose fibres on the polymer mat structure to relax, causing a reduction in mat thickness and subsequent reduction in the porosity of the mat as seen in Table 6-1. The gentle drop in the porosity level observed in Table 6-1 is a result of the gravimetric method employed in the porosity measurements, as the sample size of 3cm x 3cm used for this study had fairly the same mass. The only difference between the samples was the thickness as a result of fibre compacting upon increasing treatment temperatures.

The surface hydrophobicity of the mats before and after heat treatments was evaluated using water contact angle (WCA) measurements. As shown in Figure 6-3, the untreated PS fibre exhibits the least hydrophobicity with an average WCA of 126.1°. It also recorded the largest variation in measured CA (112.6 – 136.6°) as illustrated in the standard deviation. This could be the effect of the loose nature of the sample surface. Heat treating the mat above 100°C saw a rise in the measured WCA with a

Table 6-1: Fibre diameter, mat thickness and porosity of electrospun PS mat before and after thermal treatment

		Before Heat Treatment	Heat treatment Temp				
			90ºC	100ºC	110ºC	120ºC	130ºC
Fibre Diameter (µm)	Mean	3.13	3.25	3.33	2.70	2.35	2.20
	SD	0.50	0.41	0.52	0.37	0.40	0.31
	Max	4.49	4.42	5.90	3.88	3.61	3.48
	Min	1.83	2.21	2.25	1.58	0.88	1.38
Mat Properties	Mat Thickness (µm)	1200	1200	700	410	220	200
	Mat Porosity (%)	99.7 ± 0.16	99.7 ± 0.08	99.5 ± 0.00	99.05 ± 0.24	98.5 ± 0.08	98.4 ± 0.00
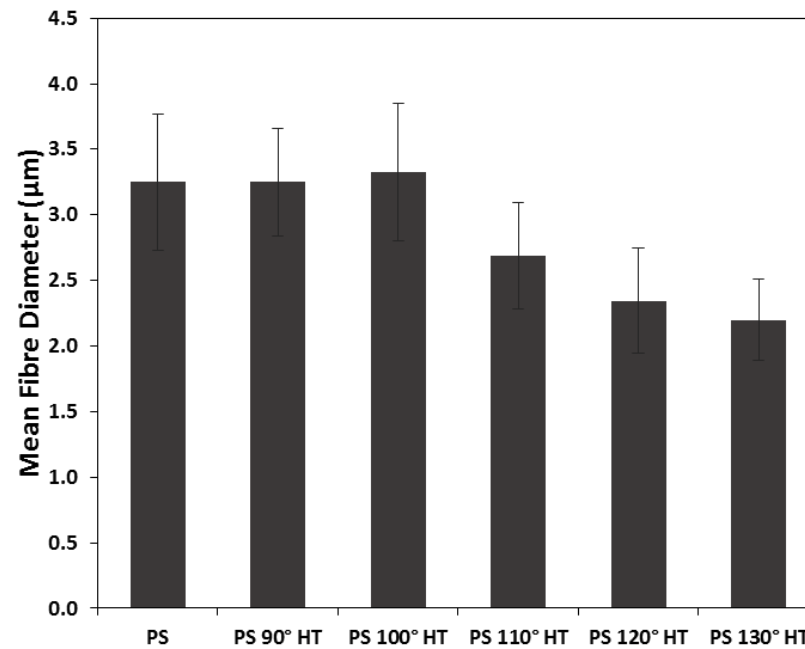
Figure 6-2: Average fibre diameter (AFD) distribution of electrospun PS fibre mat at different heat treatment temperatures. Error bars represents one standard deviation about the mean (n≥200).

Table 6-2: WCA for untreated and heat treated PS mat

	WCA (^{o})
PS Untreated	126.1 ± 9.21
PS 90° HT	130.1 ± 4.72
PS 100° HT	139.5 ± 3.48
PS 110° HT	141.0 ± 5.25
PS 120° HT	141.6 ± 5.03
PS 130° HT	136.1 ± 1.54
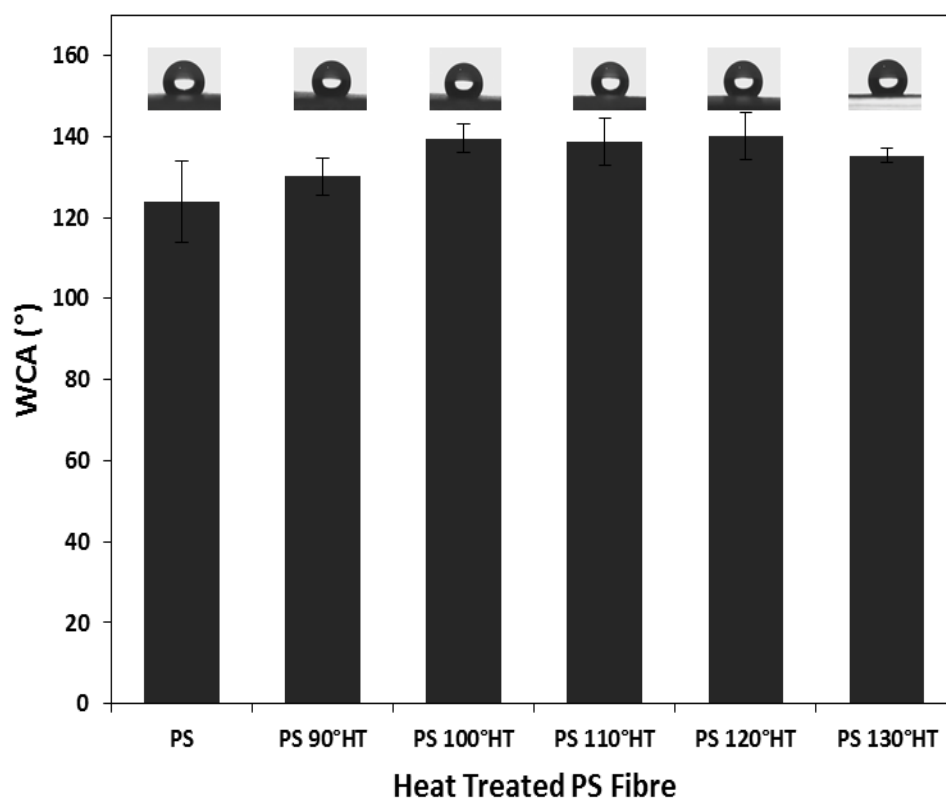
Figure 6-3: Water contact angle (WCA) distribution of 4µl of water on the surface of untreated and different heat treated PS mat. Inserted images were taken at approximately 4sec upon contact with the fibre mat. Error bars represent one standard deviation about the mean (n = 7)

peak value of 141.6º at a HT temperature of 120ºC. The mat surface also appears smoother with thermal treatment, due to an increased compactness and reduction in loose fibres on the mat surface. This result is contrary to the Wenzel theory[119] discussed in Section 2.8. The increase in WCA of heat treated mat has earlier been attributed to a combined effect of capillary action and the Cassie-Baxter effect by Shirazi et al [197]. In the case of heat treated mat, Cassie-Baxter effect [159] being more dominant due to a reduction in mat pore sizes and surface roughness.

6.2.1.2   Effect of heat treatment on PS chemical composition

The effect of thermal treatment on the chemical composition of electrospun PS mat was investigated by carrying out FTIR analysis on the fibre mats. Figure 6-4 illustrates that no changes occurred in all the heat treated mats. Similar results reported earlier in literature [196] was attributed to the use of vacuum oven in the thermal treatment process. This result indicates that similar effect can be obtained using an air assisted oven and also illustrates the inherent ability of the mats to adsorbed oils due to its chemical structure remain unchanged, even after thermal treatment. Any changes in the oil sorption behaviour of the mats after thermal treatment will be a function of changes in the mat architecture such as porosity and its 3D structure.

Despite the fact that heat treatment had no effect on the chemical composition of the thermally treated PS mat, DSC analysis of the mat reveal some microstructural movement of the polymer molecules before and after heat treatment. As seen in Figure 6-5, untreated PS mat and mats heat treated at 90 and 100ºC exhibits similar exothermic peak earlier reported in Section 4.4, which was attributed to molecular orientation of the PS molecules during the electrospinning process. Heat treating the mat at temperatures from 110ºC and above saw a disappearance of this exothermic
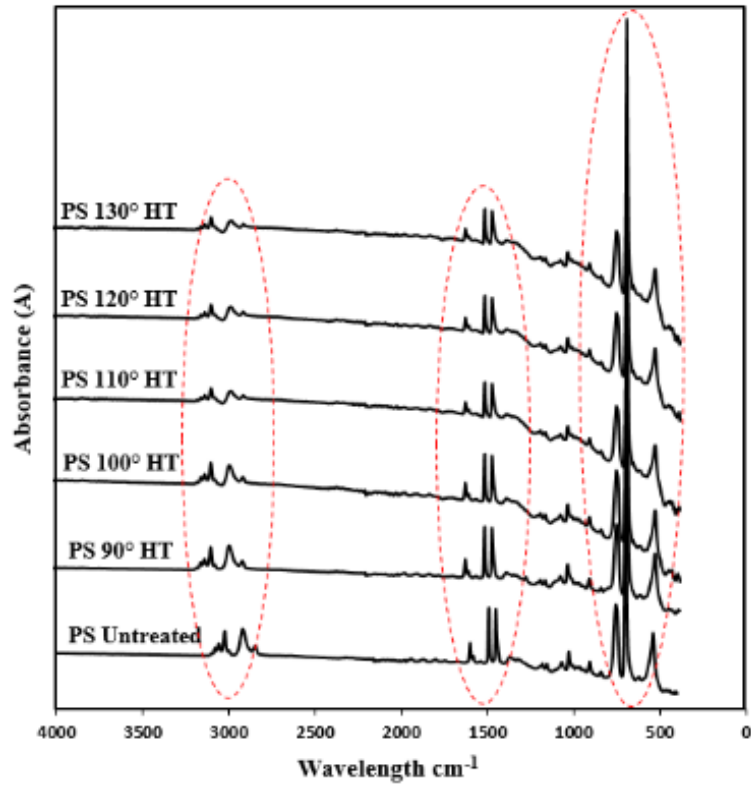
Figure 6-4: ATR-FTIR spectra of untreated and heat treated electrospun PS fibre showing no changes in the chemical structure of the different functional group after heat treatment
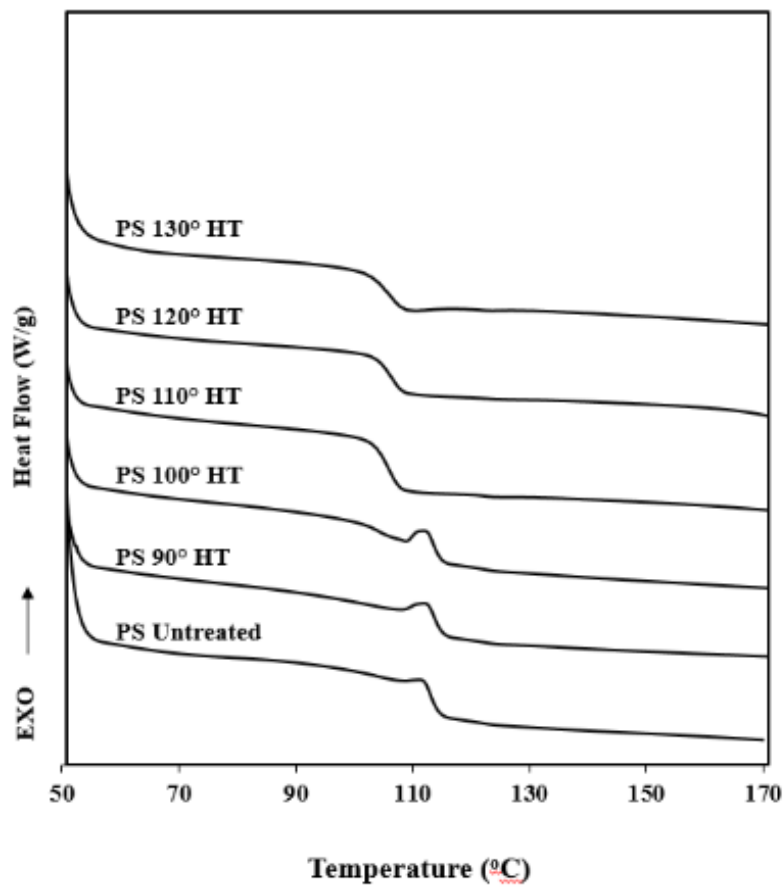
Figure 6-5: DSC thermograph of untreated and heat treated PS mat at different heat treatment temperature

peak and a drop in the measured T_g. An explanation to this will be heat treating the PS mat at temperature around the polymer glass transition temperature saw the PS molecules getting activated and able to flow, hence assumes their inherent randomized amorphous structure upon cooling. This also explains the SEM micrograph in Figure 6-1, where inter-fibre bonds were observed on heat treated at 110 ºC and above.

6.2.2 Investigating the effect of heat treatment on mechanical properties

The effect of thermal treatment on the mechanical properties of PS fibre mat at different treatment temperature is shown in Table 6-3 and Figures 6-6. The results indicates that at treatment temperature of 90ºC (for 5 min), no change was recorded in the ultimate tensile strength (UTS), which was maintained at 0.15 ± 0.02 MPa, same as the untreated mat. The enhanced modulus and reduced elongation at UTS observed at this treatment temperature, indicates an increase in the PS mat stiffness, despite the UTS being unaffected. Further increase in treatment temperature led to a steady increase in UTS and the modulus, with the highest value of 123.77 ± 15.68 and 2.76 ± 0.58 MPa obtained at treatment temperature of 130ºC for both the Modulus and UTS respectively. The sharp increase in both parameters observed at heating temperature of 110ºC and above, could be ascribed to a combined effect of inter-fibre bonds, as observed in Figure 6-1 and the mat`s compactness or reduced porosity as seen in Table 6-1. The effect of fibre compactness and porosity on electrospun fibre mat has been demonstrated in previous studies [205, 206]. It was reported that low porosity results in fibre densification, which inhibits fibre movement during tensile testing, resulting in higher UTS value[206]. A high porosity mat on the other hand will allow fibre movement and slippage, hence a lower strength material is created. The stress-strain curve in Figure 6-7, confirms the above statement as both untreated PS mat and mat heat treated at 90ºC, which earlier in Section 6.2.1.1 was shown to have a high porosity
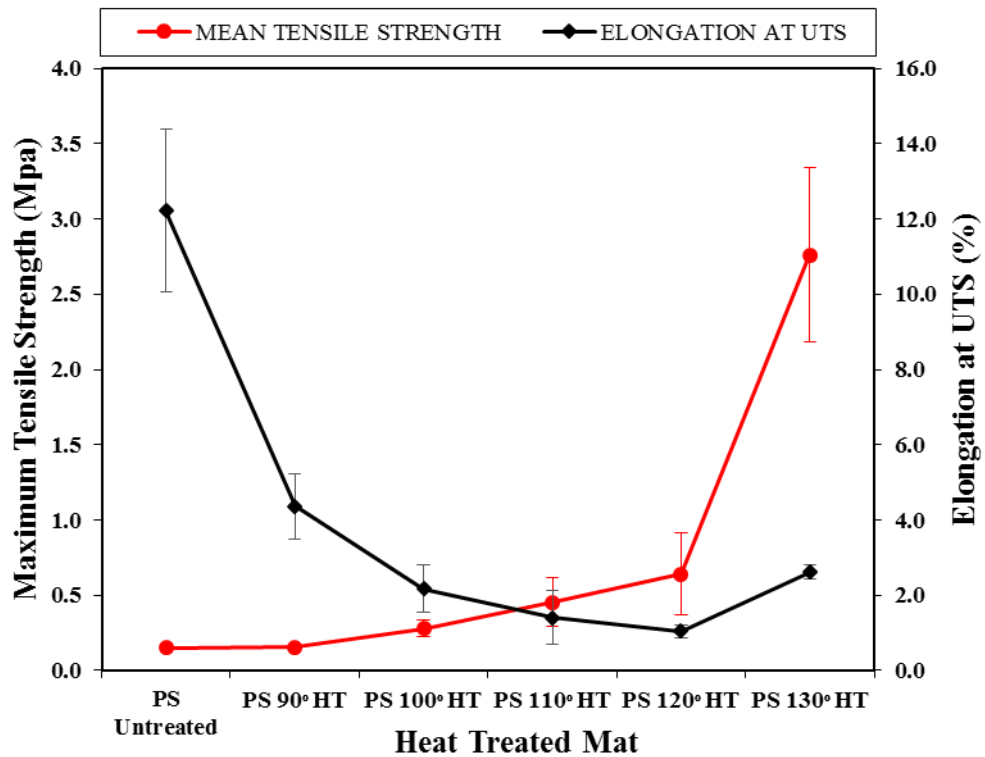
Figure 6-6: A comparison of the maximum tensile strength and elongation at UTS of the different heat treated fibre mats. Tensile test were performed with test method described in section 3.4.3.1. Error bar represent one standard deviation about the mean (n = 5)
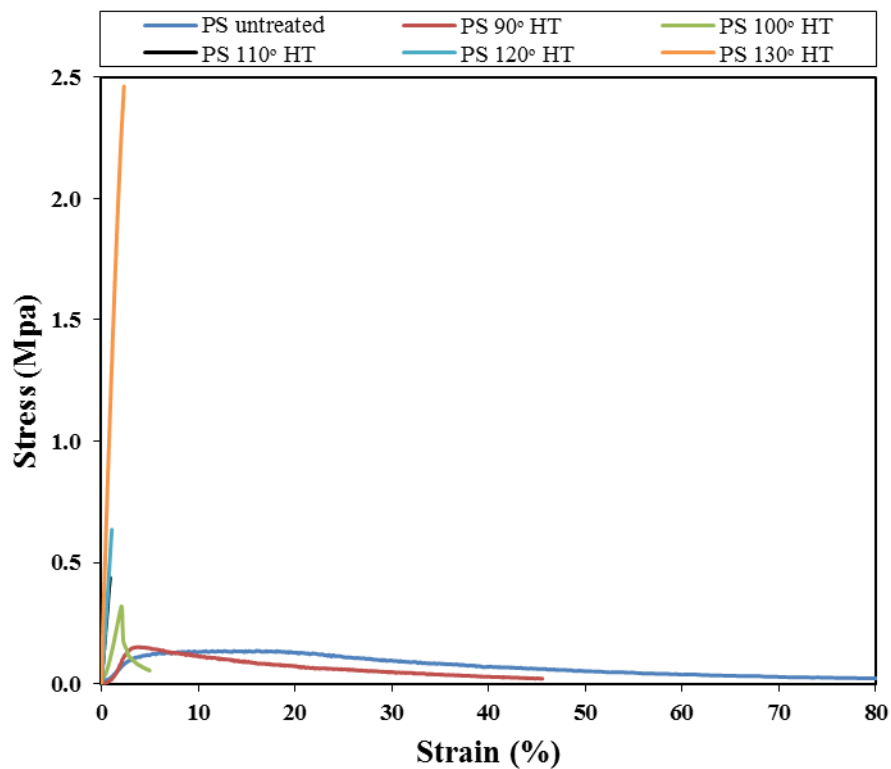
Figure 6-7: Stress - strain curve showing a typical untreated and heat treated PS fibre mat.

level, both exhibit a high fibre slippage and low tensile strength. The steep elastic deformation demonstrated by mats heat treated above the Tg, implies a rigid material which could impacts on the mats oil sorption behaviour.

This results indicates that heat treatment at temperature around the Tg will induce inter-fibre bonds, fibre compacting and reduced porosity which enhances the mechanical properties of the mat.

Table 6-3: Mechanical properties of untreated and heat treated PS mat after 5mins at different heat treatment temperatures. Standard deviation represents n =5

	Modulus (MPa)	Ultimate Tensile Strength (MPa)	Elongation at UTS (%)
PS Untreated	3.84 ± 0.26	0.15 ± 0.02	12.23 ± 2.18
PS 90ºC HT	6.29 ± 1.55	0.15 ± 0.02	4.36 ± 0.86
PS 100ºC HT	12.24 ± 2.53	0.28 ± 0.05	2.17 ± 0.63
PS 110ºC HT	40.39 ± 9.55	0.45 ± 0.16	1.40 ± 0.72
PS 120ºC HT	70.66 ± 14.31	0.64 ± 0.27	1.04 ± 0.18
PS 130ºC HT	123.77 ± 15.68	2.76 ± 0.58	2.62 ± 0.19

6.2.3 Effect of heat treatment on oil sorption behaviour

The effect of different heat treatment temperature on the oil sorption capacity of electrospun PS mat is presented in Figure 6-8. Oil sorption test was conducted in an oil-water system using a test method previously described in Section 3.4.4, as WCA test presented earlier in Figure 6-3 indicates strong hydrophobicity of all the different heat treated mats. The result in Figure 6-8 shows a declining trend in sorption capacity (SC) of both motor oil and sunflower oil with increasing treatment temperature. At 90ºC heat treatment, despite no apparent changes in mat porosity or fibre densification, a drop in SC of 33.49% was observed for motor oil from 116.08g/g in the untreated mat to 78.21g/g. Similarly for the same heat treated mat, a drop 24.21% was recorded for sunflower oil. This could be the effect of the slight increase in AFD recorded at this treatment temperature, probably due to polymer chain relaxation. Further increase in heating temperature led to a sharp drop in SC, resulting from reduced porosity and fibre densification. Jiang et al [97] has previously attributed high SC to high porosity fibre mats. It is important to note that the SC of the heat treated mat up to 110ºC remain higher than those of commercial PP fibres recorded in literature [17] and in section 4.6.

Heat treatment temperature of 90ºC was chosen for further analysis to investigate the effect of heating time on both mechanical and sorption capacity of the fibre mat, as mat heat treated at this temperature for 5mins exhibits the highest sorption behaviour of the thermally treat mats.
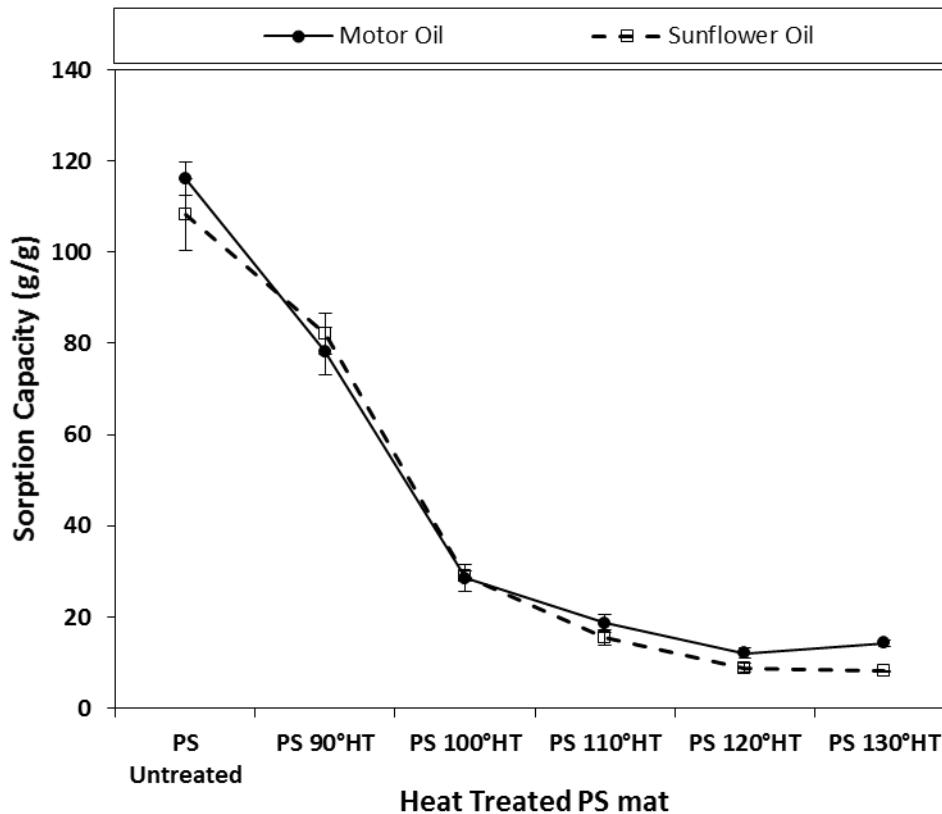
Figure 6-8: Effect of heat treatment on sorption capacity of untreated and heat treated PS mat. Error bars represent one standard deviation about the mean (n=3)

6.2.4 Evaluating the effect of heat treatment time on oil sorption and mechanical behaviour of PS mat

The results presented in Section 6.2.3 shows that heat treatment of the PS mat at 90℃ for the 5mins heating duration had no effect on the tensile strength of the mat. We hypothesis that this could be a result of inadequate heating time or heat exposure of the mat. An incremental heating duration of 5mins (to 10 and 15 mins) was explored at same heating temperature of 90℃. Table 6-4 and Figure 6-9, shows the effect of increase in heating time on the mechanical properties of the mat, where an increase in treatment time to 10mins led to an 86.7% increase in UTS and over 100% increase in modulus. Further increase in heating duration to 15 mins, caused a drop in both UTS and modulus. Similarly, the elongation at UTS was seen to decrease steadily with increasing treatment time. Based on this, it could be inferred that the optimum heating

time at a heating temperature of 90ºC is 10 mins, as further increase in heat treatment duration weakens the interaction force between the polymer molecules, thereby reducing the mechanical properties of the mat. Zhang et al[202], reported a similar results for electrospun polysulfone (PSU), but in that case the optimum heating time was obtained after heat treatment for 3hrs. The impact of heat treatment duration on the mechanical properties of polymers can be better explained by the time-temperature equivalent principle[207].

Figure 6-10 depicts a typical stress- strain curve for the different heat treatment periods, the steep elastic region for the 5 and 10mins treatment duration indicates a higher modulus, hence a stiffer material. It is important to note that for sorbent it is desirable to have a material with less stiffness as fibre movement could enhance sorption performance of the mat.

The effect of increasing the treatment duration on the oil sorption capacity is presented in Figure 6-11. This figure compares the sorption behaviour with the mean tensile strength. Due to a reduction in mat porosity and enhanced fibre densification the sorption capacity of both sunflower and motor oil decreases with increasing treatment duration.
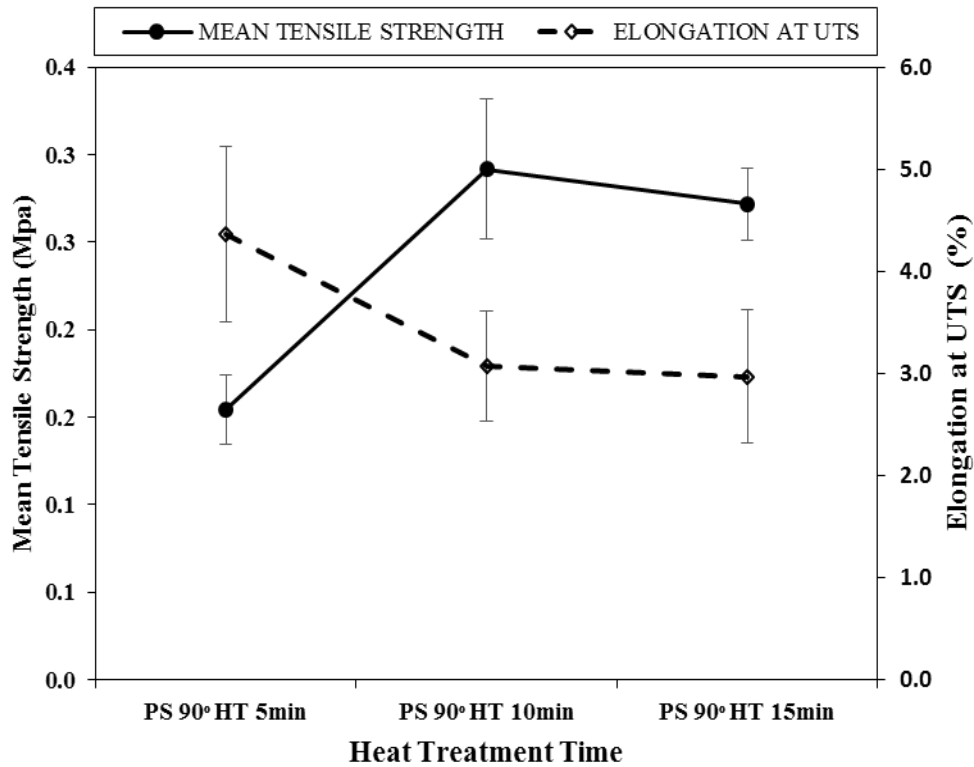
Figure 6-9: Effect of heat treatment time on the maximum tensile strength and elongation at UTS of of electrospun PS mat heat treated at 90℃. Error bars represents one standard deviation about the mean (n=5)
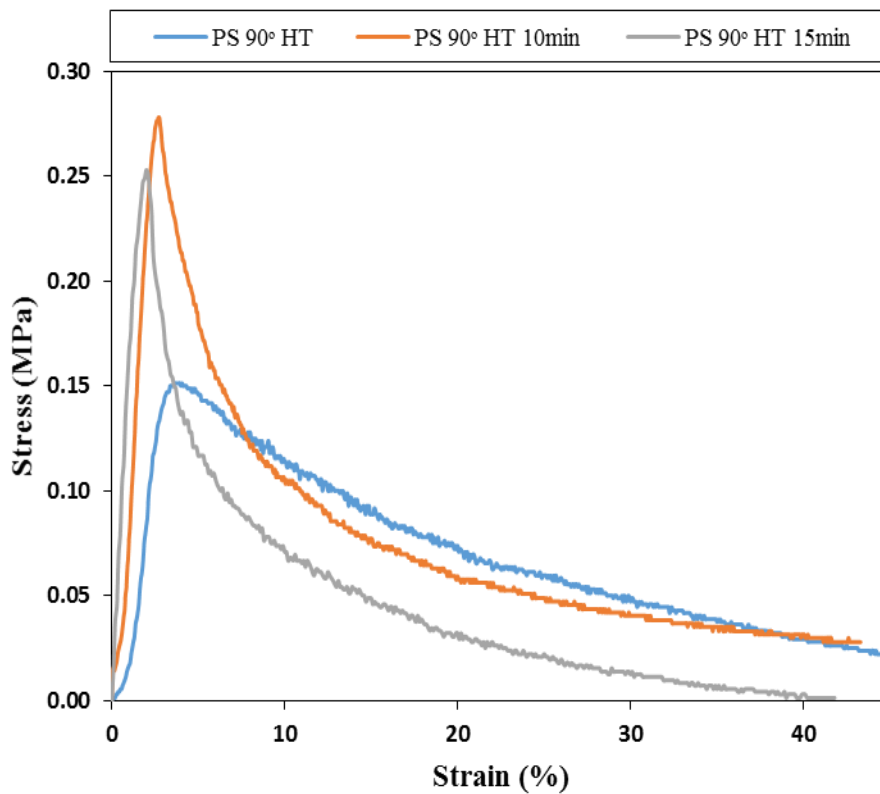
Figure 6-10: Stress strain curve of a typical heat treated PS mat heat treated at 90℃ at different heat treatment durations.

Table 6-4: Mechanical property of electrospun PS mat heat treated at 90ºC at different heat treatment duration. Standard deviation represents n =5

	Modulus (MPa)	Ultimate Tensile Stress (MPa)	Elongation at UTS (%)
PS 90ºC HT 5min	6.29 ± 1.55	0.15 ± 0.02	4.36 ± 0.86
PS 90ºC HT 10min	13.66 ± 2.83	0.28 ± 0.05	3.07 ± 0.55
PS 90ºC HT 15min	12.91 ± 1.32	0.27 ± 0.05	2.97 ± 0.65
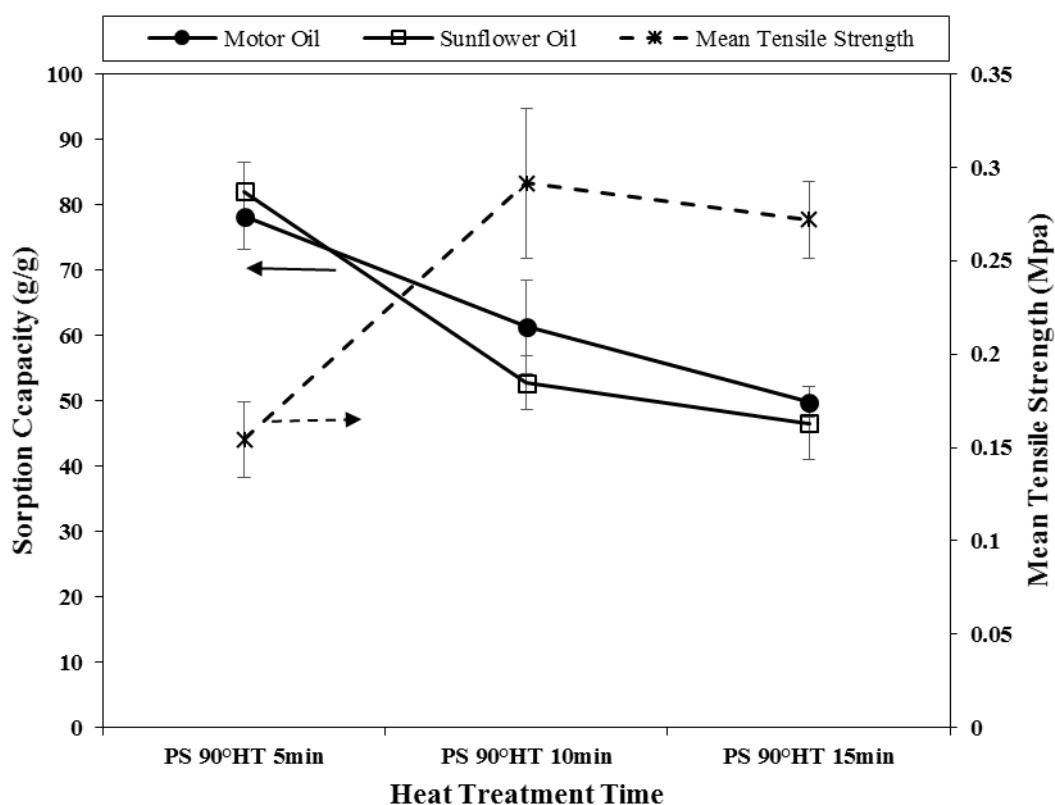
Figure 6-11: Comparison of both oil sorption capacity and mean tensile strength of PS mat heat treated for 5,10 and 15 mins. Error bars represent one standard deviation about the mean (n=5)

6.3 Ultrasonic Bonding

Ultrasonic energy in the form of ultrasonic sewing is often used in bonding nonwoven fibres [198, 199, 208]. The process involves the use of high frequency vibration which generates heat, that melts the thermoplastic polymers and bonds are formed between the fibres upon cooling. The melting of the fibres, and application of pressure on the

material under ultrasonic sewing compromises the porosity of the mat, which is a property desirable of sorbents. In this section we explore the use of an ultrasonic bath, by immersing the fibre mat into a liquid that is non-solvent to PS polymer and exposing it to ultrasonic frequency of 42,000Hz. This is to mitigate the effect of direct contacting of ultrasonic sewing. Kocak et al,[200] had applied a similar method to Luffa fibre and reported an increase in the mechanical properties of the ultrasonically treated fibres than the conventionally treated fibres. The effect of this treatment on the morphology and sorption behaviour of the mat is reported in the subsection below;

6.3.1 Effect of ultrasound on fibre morphology

To investigate the effect of ultrasonic energy on polystyrene fibre mat, the mats were immersed in a 50% ethanol (EtOH) solution, as both ethanol and water are known non solvent to polystyrene[209, 210]. Details of the experimental procedure is given in Section 3.8. SEM micrograph in Figure 6-12, indicates that for the two treatment time scale of 5 and 10 mins investigated, no obvious changes in morphology of the mat was observed in comparison to the two controls (PS untreated and 50% EtOH with no ultrasonic treatment - UT). Since no inter fibre bonds were observed, this implies that previous inter-fibre bonds reported for ultrasonic sewing were a result of the melting and pressure exerted by ultrasonic rollers[200]. Analysis of the SEM micrographs in Figure 6-13, reveals a slight drop in the AFD from 3.37µm in the untreated PS mat to 3.20µm and 3.12µm after 5 mins and 10 mins treatment durations respectively. It is believed the EtOH could have caused a slight shrinkage in the fibre diameter but this cannot be conclusively ascertained as error bars falls within the range of the AFD for the control samples.
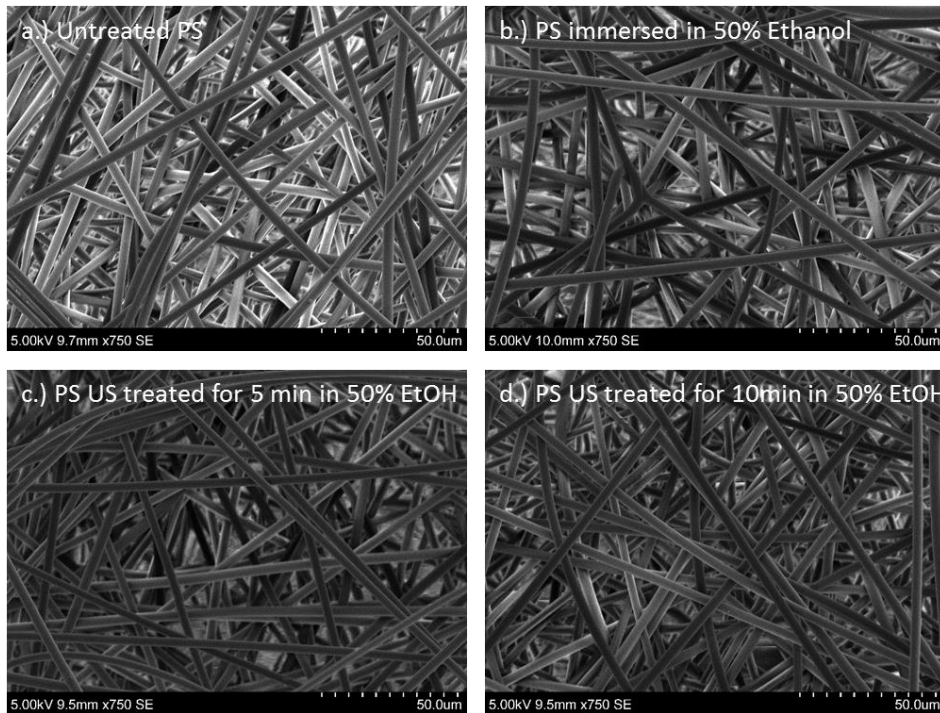
Figure 6-12: SEM micrograph of a.) Untreated PS fibre mat; b.) PS mat immersed in EtOH with no ultrasonic treatment; c.) PS mat immersed in 50% EtOH and ultrasonically treated for 5mins; d.) PS mat immersed in 50% EtOH and ultrasonically treated for 10mins
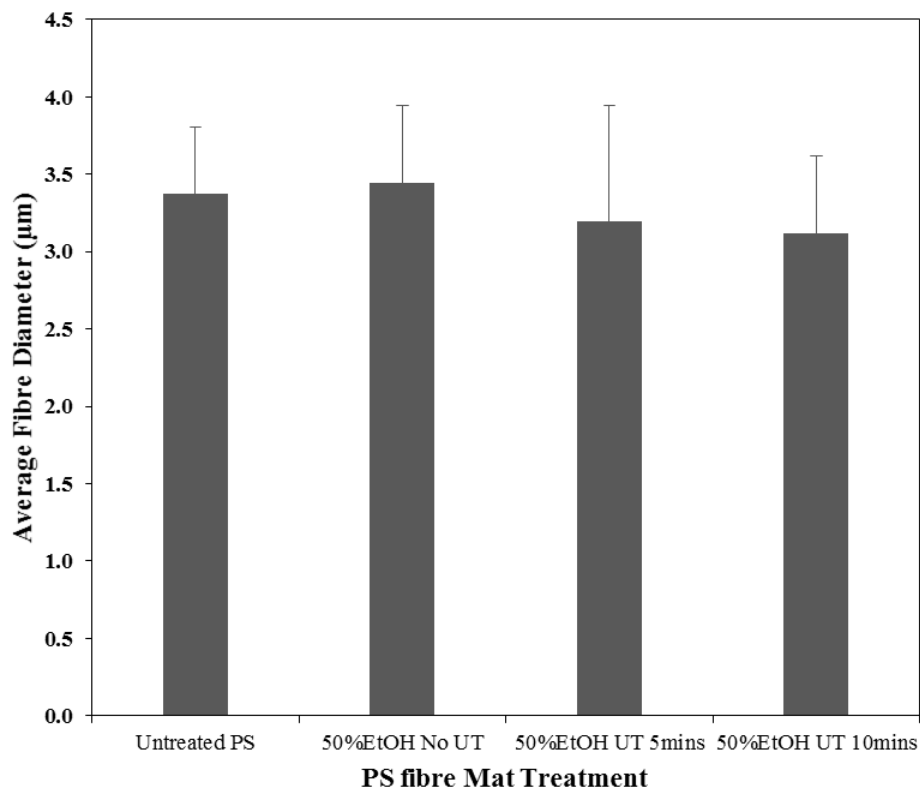
Figure 6-13: Average fibre diameter (AFD) of PS fibre mat comparing the untreated mat, control and mats ultrasonically treated for 5 and 10 mins. Error bars represents one standard deviation about the mean (n=100)

6.3.2 Evaluating the effect of ultrasound on mechanical and sorption properties of ES PS mat

The effect of exposing PS fibre mat to ultrasonic energy and ethanol solution is presented in Figure 6-14. Immersing the fibre mat in ethanol solution for 5mins with no ultrasonic exposure, saw a drop in sorption capacity from 84.81g/g to 62.90g/g. Similarly, the mean tensile strength of the mat was also seen to drop from 0.12MPa to 0.1MPa. This represent a 25.8% and 12% drop for the SC and mean tensile strength respectively. The drop in both parameters could be ascribed to the densification of the fibre mat following the immersion in 50% EtOH solution, as a fall of 9% in mat thickness was recorded after the immersion (see Appendix). Further treatment of the mat ultrasonically for 5min and 10 mins saw no appreciable difference in the sorption performance of the mats. The densification of the mat upon immersion in EtOH solution, unlike under thermal treatment, resulted in a drop in tensile strength of the mat. Ultrasonic treatment of the mats then saw a slight, steady rise in tensile strength, though the value after 10mins exposure still falls below the tensile value for untreated mat. It could be inferred that though EtOH is a non-solvent to PS, its exposure to PS causes a drop in mechanical properties probably due to increase lubricity between the fibres. Sorption capacity on the other hand remains fairly constant after the immersion which could be the effect of the mat thickness remaining constant in all the treatment conditions. This indicates a strong relationship between mat thickness/porosity and sorption capacity.
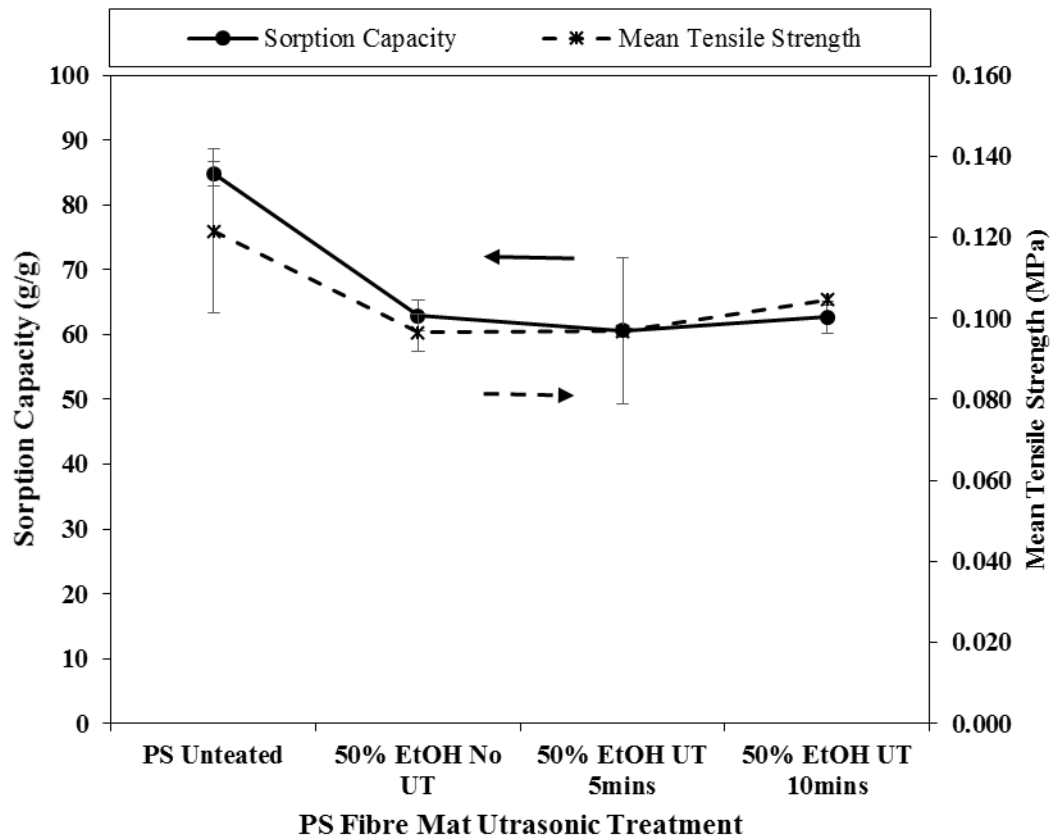
Figure 6-14: Comparison of Sorption capacity and mean tensile strength of electrospun PS fibre mat under different ultrasonic treatment duration when immersed in 50% EtOH with mats with no ultrasonic treatments as control. Error bars for represent one standard deviation about the mean (n=5)

6.4 Summary

The aim of this chapter as stated in **Section 6.1** is to explore the feasibility of enhancing the mechanical strength of electrospun PS fibre mats using thermal treatment (**Section 6.2**) and ultrasonic energy (**Section 6.3**), while also studying the effect on the physicochemical and sorption properties of the mat.

Figure 6-1, shows that thermal treatment of PS fibre mat at temperatures from 110ºC and above induces inter-fibre bonds in the mat structure, while at temperatures below this no bonding was observed. Analysis of the SEM micrograph (**Figure 6-2 and**

Table 6-1) reveals that despite no changes at heat treatment temperatures below 110ºC, the average fibre diameter increases progressively at 90 and 100ºC, but starts to decline steadily at heat treatment temperatures above 110ºC. The effect of this on the mechanical property is illustrated in **Figure 6-6 and Table 6-3**, where the mechanical strength is seen to increase almost rapidly with increasing heat treatment temperature from 110ºC. This could be attributed to the decreasing porosity of the mat as the mat thickness decreases and become more compacted.

Despite the increase in mechanical strength, thermal treatment was seen to have a negative impact of the sorption performance (**Figure 6-8**), as the sorption capacity was seen to decrease with increasing heat treatment temperature. Investigating the effect of heat treatment time on both sorption capacity and mechanical strength (**Figure 6-11**), shows an increase in tensile strength when treatment time is increased to 10 mins at 90ºC HT temperature. Further increase in treatment duration causes a slight drop in strength. The increased strength could be attributed to the principle of time-temperature equivalence. Conversely, the sorption capacity was seen to decreases with increasing treatment duration. On the chemical composition of the mats, HT with an air oven as used in this study was seen not to have no effect on the chemical composition/structure of the mat (**Figure 6-5**), while all mats surface was seen to remain hydrophobic (**Figure 6-3**).

Ultrasonic treatment on the other hand, shows no effect on the sorption capacity with a slight increase in tensile strength observed with increasing UT time (**Figure 6-14**), though at the UT durations studied the tensile strength still falls below those of the pristine PS fibre mat.

7 Conclusion and Future Work

7.1 Summary and overall conclusion

The overall aim of this thesis as highlighted in Section 1.2 is in two parts, first is to comprehensively investigate the contribution of individual filaments of electrospun PS and melt blown polypropylene fibres to the oil sorption behaviour of the macroscale mat. This was successfully achieved in Chapter 4. The second aim of this project is to explore ways to address the poor mechanical strength of electrospun PS fibre [20]. This was achieved using a one-step improvement technique of electrospinning a polymer blend in Chapter 5 and a two-step approach of post treating the PS fibre mat using heat or ultrasonic energy treatment in Chapter 6.

Specific objectives to achieve the above aims were highlighted in Sections 4.1, 5.1 and 6.1. Details of some of the key findings and their effect on the physicochemical, mechanical and sorption behaviour of Polystyrene (PS) fibre mat as well as the microscale evaluation of the oil sorption of single filament of the sorbent are presented below;

In Chapter 4, the optimisation process for electrospinning polystyrene was established. This was to ensure that fibres of the best morphological structure was produced for the drop-on-fibre micro sorption experiment. For the production of uniform, bead-free and smooth morphology fibres (**Tables 4-1 and 4-2**) and (**Figures 4-2 and 4-4**), an optimum concentration of 20%w/w polystyrene and solvent mix of DMF/THF ratio 4:1 was established. The study also demonstrates the effect of varying concentration and solvent mix of DMF/THF on solution properties i.e. viscosity and conductivity

(**Figure 4-1 and 4-3**) and how this impacts the morphology of the fibres. Increased viscosity was attributed to the creation of smooth morphology fibres due to enhanced polymer chain entanglement, while both high viscosity and low conductivity was seen to cause an increase in average fibre diameter (AFD).

Based on previous literature [16, 19], the higher oil sorption performance of electrospun polystyrene (PS)/PS-based fibre has been identified but the underlining factor behind the superior behaviour remain yet to be clearly understood. The establishment of a better understanding at the microscale level of the oil sorption behaviour of individual fibres will benefit the design and fabrication of future electrospun oil sorbent and also improve the chances of its future commercialisation. In an effort to achieve this, electrospun PS and melt blown PP mats were first characterised based on diameter and porosity. Electrospun PS mat showed uniform fibre distribution (1.5 to 4.2µm diameter) while melt blown PP exhibited polydispersed distribution (1.1 and 19.5µm diameters). With respect to porosity, the former exhibited high porosity of 99.8% while the latter showed low porosity 91.2% (**Section 4.3.1**). Inter-fibre void spaces for PP mat was also seen to be over 5 times higher than the PS mat. Previous study [19], has attributed these characteristics of electrospun PS mats to contribute majorly to the superior oil sorption behaviour.

Considering the literature finding above [19], this thesis carries the study further by conducting a microscale evaluation of the oil adherence of filaments of both sorbents. Findings include a barrel-shaped oil droplet morphology on the fibres for both sunflower and motor oil (**Figure 4-10**), while a high level of congruence between the theoretical and experimental drop length was established (**Figure 4-11, Tables 4-7 and 4-8**). This finding confirms the suitability of using the theoretical drop-on-fibre model for this study. Single filament of electrospun PS exhibits the strongest affinity

to both oils, with a mean adhesive energy of 18.0 x 10^{-13} and 26.2 x 10^{-13} J for sunflower and motor oil respectively (**Figure 4-13, Tables 4-7 and 4-8**). These values are 3-6 times higher than the mean adhesive energy obtained for melt blown PP fibres. These findings indicate that contrary to earlier literature which attributes the superior oil sorption performance of electrospun PS/PS based fibres to the mat architecture[16, 19], the inherent properties of PS polymer (i.e. the presence of aromatic phenyl ring) plays a dominant role in its sorption behaviour.

Chapter 5 studied polymer blending as a single step approach to enhance the mechanical properties of electrospun PS fibre. This was achieved by incorporating a thermoplastic polyurethane (PU) into the polymer solution matrix. Two fibre collector systems - a flat collector (FC) and rotating drum collector (DC) system (**Figures 5-2 and 5-3**) were studied. Results presented in **Figure 5-13** shows the attainment of the overall objective of the chapter with the mechanical strength of fibres from both systems increasing with increased PU addition. Samples of PSPU ratio 6:4 fabricated using a DC system (PSPU_DC 6:4) and those fabricated using the FC system (PSPU_FC 6:4) recorded a 600% and 1000% increase in tensile strength respectively, in comparison to the pure PS mat. However, oil sorption capacity shows a decreasing trend with increasing PU addition (**Figure 5-19**) due to an increase in fibre packing and reduced mat porosity (**Table 5-6**). Despite the reducing trend, the sorption capacity (SC) values recorded for the polymer blend still remain 2 – 9 times higher than the value recorded for the commercial PP sorbent (**Figure 5-19 and Table 5-6**). More so, 2 - 5 times higher sorption capacity values was seen when compared to literature values obtained for coaxial and multi-nozzle electrospinning of both polymers [21, 22].

Polymer blend presented in this thesis offers a simple and effective approach of enhancing the mechanical properties of electrospun PS-based sorbent. This is also an improvement to previous work where a blend of PS with hydrophilic polyacrylonitrile (PAN) was reported [20], as PAN has the ability of negatively impacting the oil - water selectivity of the mat.

Chapter 6 of this thesis explored heat (HT) and ultrasonic treatment (UT) as post treatment strategies to enhance the mechanical properties of electrospun PS mat. Heat treatment around the polymer glass transition temperature (110ºC) was seen to induce inter-fibre bonds with the amount of bonds proportional to treatment temperature (**Figure 6-1**). However, in the ultrasonic treated mat, no inter-fibre bonds was observed in the SEM micrograph for the treatment conditions utilized (**Figure 6-12**). The tensile strength and sorption capacity of UT mat experienced a drop of 12% and 25.8% respectively (**Figure 6-14**). HT mat on the other hand, recorded an increase in tensile strength from heat treatment temperature around T_g of a 110ºC (**Figure 6-6 and Table 6-3**), while a decline in SC was recorded with increasing treatment temperature (**Figure 6-8**). At 110ºC, over 80% was lost in SC, this value remain higher than those of commercial polypropylene (PP) sorbent.

In terms of the wider application of the findings in this thesis, the establishment of a strong link between the chemical structures of the bulk polymer with the oil affinity of the fibres implies that it is a key factor to consider in future design of electrospun oil sorbent. This will influence the choice of polymer considered for this application. Comparing the approach explored in Chapters 5 and 6, the polymer blend offers a better prospect due to the gentle drop in SC recorded with increasing PU content and the lack of additional post treatment cost in comparison to UT and HT methods. A

compromise can always be reached between the level of mechanical strength and the sorption capacity desired when using polymer blend approach.

7.2   Future work

Section 7.1 highlighted some of the key findings of this study. This section will present suggestions for future work aimed at complementing and creating a better understanding of the findings of this thesis. These future studies are expected to facilitate the eventual commercialisation of electrospun sorbents as improved alternative to commercial PP sorbent.

- As indicated in Section 4.3.3.1, due to the difficulty in picking out a single filament from the fibre mat, electrospun PS fibre was picked in-flight with a tweezer, leading to a bit of variability in the fibre sizes used in the drop-on-fibre analysis. Future studies should investigate if there is any effect of fibre diameter (fibre size) on the oil adsorptivity of these fibres.

- Polymer blends of other polyether-based thermoplastic polyurethane with different ratios of hard and soft segment should be explored with polystyrene. This should be aimed at enhancing the mechanical properties of the resulting fibre as well as positively impacting on the sorption performance. Microscale evaluation of the oil affinity of the resulting polymer bend fibres should also be explored.

- Since the ability of electrospun polymer blend in enhancing the mechanical properties of fibre mat has been established, multi-nozzle electrospinning of the PSPU polymer blend reported in this study should be explored for higher production.

- Electrospun PS/PS based fibre should be explored for use as an oil sorbent as well as a bio-carrier of hydrocarbon degrading bacteria; this will serve dual purpose of sorbing and degrading of oil spills.

References

1. BP. *Energy consumption in the UK and the world.* 2017 [cited 2017 04/09/2017]; Available from: http://www.bp.com/en/global/corporate/energy-economics/statistical-review-of-world-energy/oil/oil-and-oil-product-consumption.html.

2. Adebajo, M.O., et al., *Porous materials for oil spill cleanup: A review of synthesis and absorbing properties.* Journal of Porous Materials, 2003. **10**(3): p. 159-170.

3. Annunciado, T.R., et al., *Experimental investigation of various vegetable fibers as sorbent materials for oil spills.* Marine Pollution Bulletin, 2005. **50**(11): p. 1340-1346.

4. Husseien, M., et al., *Availability of barley straw application on oil spill clean up.* International Journal of Environmental Science and Technology, 2009. **6**(1): p. 123-130.

5. Wahi, R., et al., *Oil removal from aqueous state by natural fibrous sorbent: An overview.* Separation and Purification Technology, 2013. **113**: p. 51-63.

6. Dong, T., et al., *Theoretical and experimental study on the oil sorption behavior of kapok assemblies.* Industrial Crops and Products, 2014. **61**: p. 325-330.

7. Al-Majed, A.A., et al., *A sustainable approach to controlling oil spills.* Journal of Environmental Management, 2012. **113**: p. 213-227.

8. Teas, C., et al., *Investigation of the effectiveness of absorbent materials in oil spills clean up.* Desalination, 2001. **140**(3): p. 259-264.

9. Wu, Z.Y., et al., *Carbon nanofiber aerogels for emergent cleanup of oil spillage and chemical leakage under harsh conditions.* Scientific Reports, 2014. **4**.

10. Bayat, A., et al., *Oil spill cleanup from sea water by sorbent materials.* Chemical Engineering & Technology, 2005. **28**(12): p. 1525-1528.

11. Castro, A., et al., *Floating boom performance under waves and currents.* Journal of Hazardous Materials, 2010. **174**(1-3): p. 226-235.

12. Choi, H.M. et al., *Natural sorbents in oil-spill cleanup.* Environmental Science & Technology, 1992. **26**(4): p. 772-776.

13. Rajakovic, V., et al., *Efficiency of oil removal from real wastewater with different sorbent materials.* Journal of Hazardous Materials, 2007. **143**(1-2): p. 494-499.

14. Ceylan, D., et al., *Evaluation of butyl rubber as sorbent material for the removal of oil and polycyclic aromatic hydrocarbons from seawater.* Environmental Science & Technology, 2009. **43**(10): p. 3846-3852.

15. Mesquita, S.R., et al., *Toxic assessment of urban atmospheric particle-bound PAHs: relevance of composition and particle size in Barcelona (Spain).* Environ Pollut, 2014. **184**: p. 555-62.

16. Lin, J.Y., et al., *Nanoporous polystyrene fibers for oil spill cleanup.* Marine Pollution Bulletin, 2012. **64**(2): p. 347-352.

17. Wei, Q.F., et al., *Evaluation of nonwoven polypropylene oil sorbents in marine oil-spill recovery.* Marine Pollution Bulletin, 2003. **46**(6): p. 780-783.

18.   Choi, H.M., et al., *Oil sorption behavior of various sorbents studied by sorption capacity measurement and environmental scanning electron-microscopy.* Microscopy Research and Technique, 1993. **25**(5-6): p. 447-455.

19.   Zhu, H.T., et al., *Evaluation of electrospun polyvinyl chloride/polystyrene fibers as sorbent materials for oil spill cleanup.* Environmental Science & Technology, 2011. **45**(10): p. 4527-4531.

20.   Li, P., et al., *Electrospun PS/PAN fibers with improved mechanical property for removal of oil from water.* Marine Pollution Bulletin, 2015. **93**(1-2): p. 75-80.

21.   Lin, J.Y., et al., *Facile control of intra-fiber porosity and inter-fiber voids in electrospun fibers for selective adsorption.* Nanoscale, 2012. **4**(17): p. 5316-5320.

22.   Lin, J.Y., et al., *Co-axial electrospun polystyrene/polyurethane fibres for oil collection from water surface.* Nanoscale, 2013. **5**(7): p. 2745-2755.

23.   Toncheva, A., et al., *Dual vs. single spinneret electrospinning for the preparation of dual drug containing non-woven fibrous materials.* Colloids and Surfaces a-Physicochemical and Engineering Aspects, 2013. **439**: p. 176-183.

24.   Greiner, A., et al., *Electrospinning: A fascinating method for the preparation of ultrathin fibres.* Angewandte Chemie-International Edition, 2007. **46**(30): p. 5670-5703.

25.   Agarwal, S., et al., *Electrospinning of manmade and biopolymer nanofibers-progress in techniques, materials, and applications.* Advanced Functional Materials, 2009. **19**(18): p. 2863-2879.

26.   Huang, Z.M., et al., *A review on polymer nanofibers by electrospinning and their applications in nanocomposites.* Composites Science and Technology, 2003. **63**(15): p. 2223-2253.

27.   Ramakrishna, S.F., et al., *An introduction to electrospinning and nanofibres.* 2005.

28.   Nayak, R., et al., *Recent advances in nanofibre fabrication techniques.* Textile Research Journal, 2012. **82**(2): p. 129-147.

29.   Bhardwaj, N., et al., *Electrospinning: A fascinating fiber fabrication technique.* Biotechnology Advances, 2010. **28**(3): p. 325-347.

30.   Ramakrishna, S., et al., *Electrospun nanofibers: solving global issues.* Materials Today, 2006. **9**(3): p. 40-50.

31.   Reneker, D.H., et al., *Bending instability of electrically charged liquid jets of polymer solutions in electrospinning.* Journal of Applied Physics, 2000. **87**(9): p. 4531-4547.

32.   Larmor, J., *Note on the complete scheme of electrodynamic equations of a moving material medium, and on electrostriction.* 1898: Harrison and Sons.

33.   Cooley, J.F., *Apparatus for electrically dispersing fluids.* 1902, Google Patents.

34.   Morton, W.J., *Method of dispersing fluids.* 1902, Google Patents.

35.   Andrady, A.L., *Science and technology of polymer nanofibers.* 2008: John Wiley & Sons, Inc. 403.

36.   Anton, F., *Process and apparatus for preparing artificial threads.* 1934, Google Patents.

37.   Anton, F., *Artificial fiber construction.* 1938, Google Patents.

38.   Anton, F., *Method of producing artificial fibers.* 1939, Google Patents.

39. Anton, F., *Artificial thread and method of producing same*. 1940, Google Patents.

40. Taylor, G., *Electrically driven jets.* Proceedings of the Royal Society of London Series a-Mathematical and Physical Sciences, 1969. **313**(1515): p. 453-&.

41. Taylor, G., *Disintegration of water drops in electric field.* Proceedings of the Royal Society of London Series a-Mathematical and Physical Sciences, 1964. **280**(1380): p. 383-+.

42. Baumgarten, P.K., *Electrostatic spinning of acrylic microfibers.* Journal of Colloid and Interface Science, 1971. **36**(1): p. 71-+.

43. Reneker, D.H. et al., *Electrospinning jets and polymer nanofibers.* Polymer, 2008. **49**(10): p. 2387-2425.

44. Garg, K., et al., *Electrospinning jets and nanofibrous structures.* Biomicrofluidics, 2011. **5**(1).

45. Wang, X.W., et al., *Jet shaping nanofibers and the collection of nanofiber mats in electrospinning.* Journal of Materials Science & Technology, 2006. **22**(4): p. 536-540.

46. Morad, M.R., et al., *A very stable high throughput taylor cone-jet in electrohydrodynamics.* Scientific Reports, 2016. **6**.

47. Larrondo, L., et al., *Electrostatic fiber spinning from polymer melts .1. experimental-observations on fiber formation and properties.* Journal of Polymer Science Part B-Polymer Physics, 1981. **19**(6): p. 909-920.

48. Yarin, A.L., et al., *Taylor cone and jetting from liquid droplets in electrospinning of nanofibers.* Journal of Applied Physics, 2001. **90**(9): p. 4836-4846.

49. Deitzel, J.M., et al., *Key parameters influencing the onset and maintenance of the electrospinning jet*, in *polymeric nanofibers*. 2006, American Chemical Society. p. 56-73.

50. Hohman, M.M., et al., *Electrospinning and electrically forced jets. II. Applications.* Physics of Fluids, 2001. **13**(8): p. 2221-2236.

51. Hohman, M.M., et al., *Electrospinning and electrically forced jets. I. Stability theory.* Physics of Fluids, 2001. **13**(8): p. 2201-2220.

52. Shin, Y.M., et al., *Experimental characterization of electrospinning: the electrically forced jet and instabilities.* Polymer, 2001. **42**(25): p. 9955-9967.

53. Rayleigh, L., *On The instability of jets.* Proceedings of the London Mathematical Society, 1878. **s1-10**(1): p. 4-13.

54. Burger, C., et al., *Nanofibrous materials and their applications.* Annual Review of Materials Research, 2006. **36**(1): p. 333-368.

55. Koombhongse, S., et al., *Flat polymer ribbons and other shapes by electrospinning.* Journal of Polymer Science Part B-Polymer Physics, 2001. **39**(21): p. 2598-2606.

56. Reneker, D.H., et al., *Nanofiber garlands of polycaprolactone by electrospinning.* Polymer, 2002. **43**(25): p. 6785-6794.

57. Haghi, A.K., et al., *Trends in electrospinning of natural nanofibers.* Physica Status Solidi a-Applications and Materials Science, 2007. **204**(6): p. 1830-1834.

58. Gupta, P., et al., *Electrospinning of linear homopolymers of poly(methyl methacrylate): exploring relationships between fiber formation, viscosity, molecular weight and concentration in a good solvent.* Polymer, 2005. **46**(13): p. 4799-4810.

59.   Casper, C.L., et al., *Controlling surface morphology of electrospun polystyrene fibers: effect of humidity and molecular weight in the electrospinning process.* Macromolecules, 2004. **37**(2): p. 573-578.

60.   Haider, S., et al., *Highly aligned narrow diameter chitosan electrospun nanofibers.* Journal of Polymer Research, 2013. **20**(4).

61.   Pillay, V., et al., *A review of the effect of processing variables on the fabrication of electrospun nanofibers for drug delivery applications.* Journal of Nanomaterials, 2013.

62.   Deitzel, J.M., et al., *The effect of processing variables on the morphology of electrospun nanofibers and textiles.* Polymer, 2001. **42**(1): p. 261-272.

63.   Fong, H., et al., *Beaded nanofibers formed during electrospinning.* Polymer, 1999. **40**(16): p. 4585-4592.

64.   Nezarati, R.M., et al., *Effects of humidity and solution viscosity on electrospun fiber morphology.* Tissue Engineering Part C-Methods, 2013. **19**(10): p. 810-819.

65.   Ki, C.S., et al., *Characterization of gelatin nanofiber prepared from gelatin-formic acid solution.* Polymer, 2005. **46**(14): p. 5094-5102.

66.   Drew, C., et al., *The effect of viscosity and filler on electrospun fiber morphology.* Journal of Macromolecular Science-Pure and Applied Chemistry, 2003. **A40**(12): p. 1415-1422.

67.   Zong, X.H., et al., *Structure and process relationship of electrospun bioabsorbable nanofiber membranes.* Polymer, 2002. **43**(16): p. 4403-4412.

68.   Zhang, C.X., et al., *Study on morphology of electrospun poly(vinyl alcohol) mats.* European Polymer Journal, 2005. **41**(3): p. 423-432.

69.   Sun, Z., et al., *The effect of solvent dielectric properties on the collection of oriented electrospun fibres.* Journal of Applied Polymer Science, 2012. **125**: p. 2585-2594.

70.   Luo, C.J., et al., *Mapping the influence of solubility and dielectric constant on electrospinning polycaprolactone solutions.* Macromolecules, 2012. **45**(11): p. 4669-4680.

71.   Megelski, S., et al., *Micro- and nanostructured surface morphology on electrospun polymer fibers.* Macromolecules, 2002. **35**(22): p. 8456-8466.

72.   Zhao, S.L., et al., *Electrospinning of ethyl-cyanoethyl cellulose/tetrahydrofuran solutions.* Journal of Applied Polymer Science, 2004. **91**(1): p. 242-246.

73.   Zargham, S., et al., *The effect of flow rate on morphology and deposition area of electrospun nylon 6 nanofiber.* Journal of Engineered Fibers and Fabrics, 2012. **7**(4): p. 42-49.

74.   Buchko, C.J., et al., *Processing and microstructural characterization of porous biocompatible protein polymer thin films.* Polymer, 1999. **40**(26): p. 7397-7407.

75.   Lee, J.S., et al., *Role of molecular weight of atactic poly(vinyl alcohol) (PVA) in the structure and properties of PVA nanofabric prepared by electrospinning.* Journal of Applied Polymer Science, 2004. **93**(4): p. 1638-1646.

76.   Wang, X.F., et al., *Formation of water-resistant hyaluronic acid nanofibers by blowing-assisted electro-spinning and non-toxic post treatments.* Polymer, 2005. **46**(13): p. 4853-4867.

77.   Luzio, A., et al., *Electrospun polymer fibers for electronic applications.* Materials, 2014. **7**(2): p. 906-947.

78. Mit-uppatham, et al., *Ultrafine electropsun polyamide-6 fibres: effect of solution condition on morphology and average diameter.* Macromolecular Chemistry and Physics, 2004. **205**: p. 2327 - 2338.

79. Vrieze, S.D., et al., *The effect of temperature and humidity on electrospinning.* Journal of Materials Science 2009. **44**: p. 1357-1362.

80. Ali, A.A. et al., *Hot-pressed electrospun PAN nano fibers: An idea for flexible carbon mat.* Journal of Materials Processing Technology, 2009. **209**(9): p. 4617-4620.

81. Guo, F., et al., *Desalination by membrane distillation using electrospun polyamide fiber membranes with surface fluorination by chemical vapor deposition.* ACS Applied Materials & Interfaces, 2015. **7**(15): p. 8225-8232.

82. Jayasinghe, S.N., *Cell electrospinning: a novel tool for functionalising fibres, scaffolds and membranes with living cells and other advanced materials for regenerative biology and medicine.* Analyst, 2013. **138**(8): p. 2215-23.

83. Sampson, S.L., et al., *Cell electrospinning: an in vitro and in vivo study.* Small, 2014. **10**(1): p. 78-82.

84. Townsend-Nicholson, A., et al., *Cell electrospinning: a unique biotechnique for encapsulating living organisms for generating active biological microthreads/scaffolds.* Biomacromolecules, 2006. **7**(12): p. 3364-3369.

85. Spasova, M., et al., *Electrospun chitosan-coated fibers of poly(L-lactide) and poly(L-lactide)/poly(ethylene glycol): Preparation and characterization.* Macromolecular Bioscience, 2008. **8**(2): p. 153-162.

86. Kost, J., et al., *Responsive polymeric delivery systems.* Advanced Drug Delivery Reviews, 2001. **46**(1-3): p. 125-148.

87. Tansel, B., *Propagation of impacts after oil spills at sea: Categorization and quantification of local vs regional and immediate vs delayed impacts.* International Journal of Disaster Risk Reduction, 2014. **7**: p. 1-8.

88. Gong, Y.Y., et al., *A review of oil, dispersed oil and sediment interactions in the aquatic environment: Influence on the fate, transport and remediation of oil spills.* Marine Pollution Bulletin, 2014. **79**(1-2): p. 16-33.

89. Duong, H.T.T., et al., *Effect of foam density, oil viscosity, and temperature on oil sorption behavior of polyurethane.* Journal of Applied Polymer Science, 2006. **99**(1): p. 360-367.

90. ITOPF, *Fate of marine oil spills.* Technical Information Paper, 2014.

91. Carmody, O., et al., *Adsorption of hydrocarbons on organo-clays - Implications for oil spill remediation.* Journal of Colloid and Interface Science, 2007. **305**(1): p. 17-24.

92. Deschamps, G., et al., *Oil removal from water by selective sorption on hydrophobic cotton fibers. 1. Study of sorption properties and comparison with other cotton fiber-based sorbents.* Environmental Science & Technology, 2003. **37**(5): p. 1013-1015.

93. Sun, X.F., et al., *Acetylation of rice straw with or without catalysts and its characterization as a natural sorbent in oil spill cleanup.* Journal of Agricultural and Food Chemistry, 2002. **50**(22): p. 6428-6433.

94. Wang, X., et al., *Electrospun nanofibrous materials: a versatile medium for effective oil/water separation.* Materials Today, 2016. **19**(7): p. 403-414.

95. Lin, J.Y., et al., *Subtle regulation of the micro- and nanostructures of electrospun polystyrene fibers and their application in oil absorption.* Nanoscale, 2012. **4**(1): p. 176-182.

96.	Wu, J., et al., *Electrospun porous structure fibrous film with high oil adsorption capacity.* ACS Applied Materials & Interfaces, 2012. **4**(6): p. 3207-3212.

97.	Jiang, Z., et al., *Removal of oil from water using magnetic bicomponent composite nanofibers fabricated by electrospinning.* Composites Part B-Engineering, 2015. **77**: p. 311-318.

98.	Ju, H.W., et al., *Wound healing effect of electrospun silk fibroin nanomatrix in burn-model.* International Journal of Biological Macromolecules, 2016. **85**: p. 29-39.

99.	Hsu, F.Y., et al., *Electrospun hyaluronate-collagen nanofibrous matrix and the effects of varying the concentration of hyaluronate on the characteristics of foreskin fibroblast cells.* Acta Biomaterials, 2010. **6**(6): p. 2140-7.

100.	Dong, B., et al., *Electrospinning of collagen nanofiber scaffolds from benign solvents.* Macromolecules Rapid Communication, 2009. **30**(7): p. 539-42.

101.	Kang, M., et al., *Preparation of superhydrophobic polystyrene membranes by electrospinning.* Colloids and Surfaces a-Physicochemical and Engineering Aspects, 2008. **313**: p. 411-414.

102.	Uyar, T., et al., *Self-aligned and bundled electrospun fibers prepared from blends of polystyrene (PS) and poly(methyl methacrylate) (PMMA) with a hairy-rod polyphenylene copolymer.* Materials Letters, 2009. **63**(18-19): p. 1638-1641.

103.	Podzimek, S., *Polymers*, in *light scattering, size exclusion chromatography and asymmetric flow field flow fractionation.* 2011, John Wiley & Sons, Inc. p. 1-36.

104.	Avila, A.F., et al., *A Nano-modified superhydrophobic membrane.* Materials Research-Ibero-American Journal of Materials, 2013. **16**(3): p. 609-613.

105.	Malanga, M., et al., *Historical overview and commercialization of syndiotactic polystyrene*, in *syndiotactic polystyrene.* 2009, John Wiley & Sons, Inc. p. 1-13.

106.	Jiang, L., et al., *A lotus-leaf-like superhydrophobic surface: A porous microsphere/nanofiber composite film prepared by electrohydrodynamics.* Angewandte Chemie-International Edition, 2004. **43**(33): p. 4338-4341.

107.	Liu, X.D., et al., *Preparation and characterization of chitosan derivatives and their application as flame retardants in thermoplastic polyurethane.* Carbohydrate Polymers, 2017. **167**: p. 356-363.

108.	Tabuani, D., et al., *Flame retarded thermoplastic polyurethane (TPU) for cable jacketing application.* Polymer Degradation and Stability, 2012. **97**(12): p. 2594-2601.

109.	Bonab, V.S., et al., *Chemorheology of thermoplastic polyurethane and thermoplastic polyurethane/carbon nanotube composite systems.* Polymer, 2016. **99**: p. 513-520.

110.	Bouvier, M., et al., *In vitro degradation of a poly(ether urethane) by trypsin.* Journal of Biomedical Material Research, 1991. **25**(6): p. 773-89.

111.	Mi, H.Y., et al., *Post-crosslinkable biodegradable thermoplastic polyurethanes: synthesis, and thermal, mechanical, and degradation properties.* Materials & Design, 2017. **127**: p. 106-114.

112.	Huntsman. *A guide to thermoplastic polyurethanes (TPUs).* 2017 [cited 02/08/2017; Available from: http://www.huntsman.com/polyurethanes/Applications/itemrenderer?p_rende

rtitle=Literature&p_renderdate=no&p_renderteaser=no&p_item_id=7991034 25&p_item_caid=1103.

113. Michler, G.H., et al., *Nano- and micromechanics of polymers - structure modification and improvement of properties*. Hanser Publishers.

114. Mathew, M., et al.,*Compatibility studies of polymer-polymer systems by viscometric techniques: nitrile-rubber-based polymer blends.* Polymer, 1998. **39**(25): p. 6235-6241.

115. Wagner, A., et al., *Analysis of porous electrospun fibers from poly(l-lactic acid)/poly(3-hydroxybutyrate-co-3-hydroxyvalerate) blends.* ACS Sustainable Chemistry & Engineering, 2014. **2**(8): p. 1976-1982.

116. Mohamed, A., et al., *Poly(lactic acid)/polystyrene bioblends characterized by thermogravimetric analysis, differential scanning calorimetry, and photoacoustic infrared spectroscopy.* Journal of Applied Polymer Science, 2007. **106**(3): p. 1689-1696.

117. Brostow, W., et al., *Prediction of glass transition temperatures: Binary blends and copolymers.* Materials Letters, 2008. **62**(17-18): p. 3152-3155.

118. Masoodi, R. et al., *Wicking in porous materials: traditional and modern modeling approaches*. 2012: CRC Press.

119. Wenzel, R.N., *Resistance of solid surfaces to wetting by water.* Industrial and Engineering Chemistry, 1936. **28**: p. 988-994.

120. Wolansky, G., et al., *Apparent contact angles on rough surfaces: the Wenzel equation revisited.* Colloids and Surfaces a-Physicochemical and Engineering Aspects, 1999. **156**(1-3): p. 381-388.

121. Cassie, A.B.D.. et al., *Wettability of porous surfaces.* Transactions of the Faraday Society, 1944. **40**(0): p. 546-551.

122. Gao, N.W., et al., *Evaluation of the oleophilicity of different alkoxysilane modified ceramic membranes through wetting dynamic measurements.* Applied Surface Science, 2013. **283**: p. 863-870.

123. Vicente, C.M.S., et al., *Simple measurement of surface free energy using a web cam.* Revista Brasileira De Ensino De Fisica, 2012. **34**(3).

124. Fowkes, F.M., *Attractive forces at interfaces.* Industrial and Engineering Chemistry, 1964. **56**(12): p. 40-&.

125. Owens, D.K., et al., *Estimation of surface free energy of polymers.* Journal of Applied Polymer Science, 1969. **13**(8): p. 1741-&.

126. Neumann, A.W., et al., *Equation-of-state approach to determine surface tensions of low-energy solids from contact angles.* Journal of Colloid and Interface Science, 1974. **49**(2): p. 291-304.

127. Ahmad, J., et al., *Wetting, solubility and chemical characteristics of plasma-polymerised 1-isopropyl-4-methyl-1,4-cyclohexadiene thin films.* Coatings, 2014. **4**(3): p. 527-552.

128. Carroll, B.J., *Accurate measurement of contact-angle, phase contact areas, drop volume, and laplace excess pressure in drop-on-fiber systems.* Journal of Colloid and Interface Science, 1976. **57**(3): p. 488-495.

129. McHale, G., et al., *Wetting of a high-energy fiber surface.* Journal of Colloid and Interface Science, 1997. **186**(2): p. 453-461.

130. McHale, G., et al., *Global geometry and the equilibrium shapes of liquid drops on fibers.* Colloids and Surfaces a-Physicochemical and Engineering Aspects, 2002. **206**(1-3): p. 79-86.

131. Hughes, T.A., *Measurement and Control Basics*. 2015: International Society of Automation (ISA).

132. Ward-Smith, J., *Mechanics of fluids, Ninth Edition*. 2011, London, UNKNOWN: CRC Press.

133. Loh, Q.L., et al., *Three-dimensional scaffolds for tissue engineering applications: role of porosity and pore size.* Tissue Engineering Part B-Reviews, 2013. **19**(6): p. 485-502.

134. Li, H.Y., et al., *Polypropylene fibers fabricated via a needleless melt-electrospinning device for marine oil-spill cleanup.* Journal of Applied Polymer Science, 2014. **131**(7).

135. Wang, Y., et al., *Scanning electron microscopy*, in *nanotechnology research methods for foods and bioproducts*. 2012, Wiley-Blackwell. p. 103-126.

136. Gallignani, M., et al., *Infrared detection in flow analysis - developments and trends (review).* Talanta, 2004. **64**(5): p. 1127-1146.

137. Crompton, T.R., *Thermal methods of polymer analysis*. Smithers Rapra Technology.

138. Materials, A.S.f.T.a., *ASTM D882-12 Standard test method for tensile properties of thin plastic sheeting, ASTM International, West Conshohocken, PA, 2012*. 2012. p. 12.

139. Young, T.J., et al., *The use of the PeakForce (TM) quantitative nanomechanical mapping AFM-based method for high-resolution Young's modulus measurement of polymers.* Measurement Science and Technology, 2011. **22**(12).

140. Pittenger, B., et al., *Quantitative mechanical mapping at nanoscale with peakforce QNM*. Application Note 128 [cited 2017 05/02/2017]; Available from: https://www.bruker.com/products/surface-and-dimensional-analysis/atomic-force-microscopes/afm-application-notes.html.

141. ASTM, *ASTM F726-12 Standard Test Method for Sorbent Performance of Adsorbents, ASTM International, West Conshohocken, PA, 2012*. 2012.

142. Dong, T., et al., *Adsorption and adhesiveness of kapok fiber to different oils.* Journal of Hazardous Materials, 2015. **296**: p. 101-111.

143. Fang, J., et al., *Needleless melt-electrospinning of polypropylene nanofibres.* Journal of Nanomaterials, 2012.

144. Dalton, P.D., et al., *Electrospinning of polymer melts: Phenomenological observations.* Polymer, 2007. **48**(23): p. 6823-6833.

145. Khanlou, H.M., et al., *Prediction and optimization of electrospinning parameters for polymethyl methacrylate nanofiber fabrication using response surface methodology and artificial neural networks.* Neural Computing & Applications, 2014. **25**(3-4): p. 767-777.

146. Lin, J.Y., et al., *Direct fabrication of highly nanoporous polystyrene fibers via electrospinning.* ACS Applied Materials & Interfaces, 2010. **2**(2): p. 521-528.

147. Bosworth, L.A., et al., *Acetone, a sustainable solvent for electrospinning poly(epsilon-caprolactone) fibres: effect of varying parameters and solution concentrations on fibre diameter.* Journal of Polymers and the Environment, 2012. **20**(3): p. 879-886.

148. Uyar, T., et al., *Electrospinning of uniform polystyrene fibers: The effect of solvent conductivity.* Polymer, 2008. **49**(24): p. 5336-5343.

149. Jarusuwannapoom, T., et al., *Effect of solvents on electro-spinnability of polystyrene solutions and morphological appearance of resulting electrospun polystyrene fibers.* European Polymer Journal, 2005. **41**(3): p. 409-421.

150. Wang, N., et al., *Tailored fibro-porous structure of electrospun polyurethane membranes, their size-dependent properties and trans-membrane glucose diffusion.* Journal of Membrane Science, 2013. **427**: p. 207-217.

151. Cha, D.I., et al., *Mechanical behaviors and characterization of electrospun polysulfone/polyurethane blend nonwovens.* Macromolecular Research, 2006. **14**(3): p. 331-337.

152. Carroll, B.J., *The equilibrium of liquid-drops on smooth and rough circular-cylinders.* Journal of Colloid and Interface Science, 1984. **97**(1): p. 195-200.

153. Mazoochi, T., et al., *Chitosan nanofibrous scaffold fabricated via electrospinning: the effect of processing parameters on the nanofiber morphology.* International Journal of Polymer Analysis and Characterization, 2011. **16**(5): p. 277-289.

154. Zhou, X.Y., et al., *Fabrication of unidirectional diffusion layer onto polypropylene mat for oil spill cleanup.* Industrial & Engineering Chemistry Research, 2015. **54**(47): p. 11772-11778.

155. Chatterjee, A., et al., *Studies of wicking behaviour of polyester fabric.* Journal of Textiles, 2014. **2014**.

156. ITOPF, *Use of sorbent materials in oil spill response.* Technical Information Paper, 2012: p. 12.

157. Chapman, H., et al., *The use of chemical dispersants to combat oil spills at sea: A review of practice and research needs in Europe.* Marine Pollution Bulletin, 2007. **54**(7): p. 827-838.

158. Hejda, F.S., et al.,. *Surface free energy determination by contact angle measurements - A comparison of various approaches.* in *WDS`10*. 2010.

159. Cassie, A.B.D., et al., *Wettability of porous surfaces.* Transactions of the Faraday Society, 1944. **40**: p. 0546-0550.

160. Chibowski, E., et al., *Surface free energy of polypropylene and polycarbonate solidifying at different solid surfaces.* Applied Surface Science, 2009. **256**(5): p. 1573-1581.

161. Vargaftik, N.B., et al., *International tables of the surface-tension of water.* Journal of Physical and Chemical Reference Data, 1983. **12**(3): p. 817-820.

162. Ross, S., *Variation with temperature of surface tension of lubricating oils*, N.A.C.f. Aeronautics, Editor. 1950: Washington.

163. Chun, K.S., et al., *Utilization of cocoa pod husk as filler in polypropylene biocomposites: effect of maleated polypropylene.* Journal of Thermoplastic Composite Materials, 2015. **28**(11): p. 1507-1521.

164. Eral, H.B., et al., *Drops on functional fibers: from barrels to clamshells and back.* Soft Matter, 2011. **7**(11): p. 5138-5143.

165. Lillard, J.G., et al., *Molecular structure and properties of lubricating oil components.* Industrial and Engineering Chemistry, 1952. **44**(11): p. 2623-2631.

166. Jamieson, G.S.B., et al., *The chemical composition of sunflower-seed oil.* Journal of the American Chemical Society, 1920. **44**(12): p. 2952.

167. Shin, C., *Filtration application from recycled expanded polystyrene.* Journal of Colloid and Interface Science, 2006. **302**(1): p. 267-271.

168. Shin, C., et al., *Recycled expanded polystyrene nanofibers applied in filter media.* Colloids and Surfaces a-Physicochemical and Engineering Aspects, 2005. **262**(1-3): p. 211-215.

169. Bianco, A., et al., *Electrospun PHBV/PEO co-solution blends: microstructure, thermal and mechanical properties.* Materials Science & Engineering C-Materials for Biological Applications, 2013. **33**(3): p. 1067-1077.

170. Islam, M.S., et al., *Fabrication and characterization of poly(vinyl alcohol)/alginate blend nanofibers by electrospinning method.* Colloids and Surfaces a-Physicochemical and Engineering Aspects, 2010. **366**(1-3): p. 135-140.

171. Dasdemir, M., et al., *Electrospinning of thermoplastic polyurethane microfibers and nanofibers from polymer solution and melt.* Journal of Applied Polymer Science, 2013. **127**(3): p. 1901-1908.

172. Wang, N., et al., *Tortuously structured polyvinyl chloride/polyurethane fibrous membranes for high-efficiency fine particulate filtration.* Journal of Colloid and Interface Science, 2013. **398**: p. 240-246.

173. Lee, K.H., et al., *Mechanical behavior of electrospun fiber mats of poly(vinyl chloride)/polyurethane polyblends.* Journal of Polymer Science Part B-Polymer Physics, 2003. **41**(11): p. 1256-1262.

174. *Safety Data Sheet for Pellethane 2363 80AE TPU*, Lubrizol, Editor. 2017.

175. SigmaAldrich, *Safety Data Sheet for Polystyrene.* 2017.

176. Uyar, T., et al., *The formation and characterization of cyclodextrin functionalized polystyrene nanofibers produced by electrospinning.* Nanotechnology, 2009. **20**(12).

177. Huang, C., et al., *Needleless electrospinning of polystyrene fibers with an oriented surface line texture.* Journal of Nanomaterials, 2012.

178. Tanzi, M.C., et al., *Chemical stability of polyether urethanes versus polycarbonate urethanes.* Journal of Biomedical Material Research, 1997. **36**(4): p. 550-9.

179. Miller, J.A., et al., *Properties of polyether polyurethane block copolymers - effects of hard segment length distribution.* Macromolecules, 1985. **18**(1): p. 32-44.

180. Sas, I., et al., *Literature review on superhydrophobic self-cleaning surfaces produced by electrospinning.* Journal of Polymer Science Part B-Polymer Physics, 2012. **50**(12): p. 824-845.

181. Bognitzki, M., et al., *Preparation of fibers with nanoscaled morphologies: electrospinning of polymer blends.* Polymer Engineering and Science, 2001. **41**(6): p. 982-989.

182. Uyar, T., et al., *Electrospun polystyrene fibers containing high tempetature stable volatile fragrance/flavor facilitated by cyclodextrin inclusion complexes.* Reactive & Functional Polymers, 2009. **69**(3): p. 145-150.

183. Huang, C., et al., *Needleless Electrospinning of Polystyrene Fibers with an Oriented Surface Line Texture.* Journal of Nanomaterials, 2012. **2012**: p. 7.

184. Lei, X.F., et al., *Synthesis and Electrochemical Performance of Aluminum Based Composites.* Journal of the Brazilian Chemical Society, 2010. **21**(2): p. 209-213.

185. Mrad, O., et al., *A comparison of plasma and electron beam-sterilization of PU catheters.* Radiation Physics and Chemistry, 2010. **79**(1): p. 93-103.

186. Dutta, J., et al., *Investigation of morphology, mechanical, dynamic mechanical and thermal behaviour of blends based on ethylene vinyl acetate (EVA) and thermoplastic polyurethane (TPU).* RSC Advances, 2014. **4**(105): p. 60831-60841.

187. Kannan, M., et al., *Thermogravimetric analysis and differential scanning calorimetric studies on nanoclay-filled TPU/PP blends.* Journal of Thermal Analysis and Calorimetry, 2013. **112**(3): p. 1231-1244.

188. Han, J.H., et al., *CNT buckypaper/thermoplastic polyurethane composites with enhanced stiffness, strength and toughness.* Composites Science and Technology, 2014. **103**: p. 63-71.

189. Pittenger, B.E., et al., *Quantitative mechanical property mapping at the nanoscale with peakforce QNM.* Bruker Application Note, 2009. **128**: p. 1 - 12.

190. Croisier, F., et al., *Mechanical testing of electrospun PCL fibers.* Acta Biomaterials, 2012. **8**(1): p. 218-24.

191. Thomas, V., et al., *Mechano-morphological studies of aligned nanofibrous scaffolds of polycaprolactone fabricated by electrospinning.* Journal of Biomaterial Science Polymer Edition, 2006. **17**(9): p. 969-84.

192. Radetic, M., et al., *Efficiency of recycled wool-based nonwoven material for the removal of oils from water.* Chemosphere, 2008. **70**(3): p. 525-30.

193. Rengasamy, R.S., et al., *Study of oil sorption behavior of filled and structured fiber assemblies made from polypropylene, kapok and milkweed fibers.* Journal of Hazardous Materials, 2011. **186**(1): p. 526-532.

194. Xiang, C.H., et al., *Increasing mechanical properties of 2-d-structured electrospun nylon 6 non-woven fiber mats.* Materials, 2016. **9**(4).

195. Ma, Z.W., et al., *Surface modified nonwoven polysulphone (PSU) fiber mesh by electrospinning: A novel affinity membrane.* Journal of Membrane Science, 2006. **272**(1-2): p. 179-187.

196. Shirazi, M.J.A., et al., *Coalescing filtration of oily wastewaters: characterization and application of thermal treated, electrospun polystyrene filters.* Desalination and Water Treatment, 2013. **51**(31-33): p. 5974-5986.

197. Shirazi, M.M.A., et al., *Characterization of electrospun polystyrene membrane for treatment of biodiesel's water-washing effluent using atomic force microscopy.* Desalination, 2013. **329**: p. 1-8.

198. Shi, W., et al., *Mechanism of Ultrasonic Joining of Textile Materials.* International Journal of Clothing Science and Technology, 2000.

199. Kayar, M., *Analysis of Ultrasonic Seam Tensile Properties of Thermal Bonded Nonwoven Fabrics.* Journal of Engineered Fibers and Fabrics, 2014. **9**(3): p. 8-18.

200. Kocak, D., et al., *Effects of chemical modifications on mechanical properties of luffa cylindrica.* Asian Journal of Chemistry, 2013. **25**(2): p. 637-641.

201. Zong, X.H., et al., *Structure and morphology changes during in vitro degradation of electrospun poly(glycolide-co-lactide) nanofiber membrane.* Biomacromolecules, 2003. **4**(2): p. 416-423.

202. Zhang, L., et al., *Effects of heat treatment on the morphology and performance of psu electrospun nanofibrous membrane.* Journal of Engineered Fibers and Fabrics, 2012. **7**: p. 7-16.

203. Ma, Z.W., et al., *Electrospun cellulose nanofiber as affinity membrane.* Journal of Membrane Science, 2005. **265**(1-2): p. 115-123.

204. Homaeigohar, S.S., *Functional electrospun nanofibrous membrane for water filtration.* 2011, PhD Thesis. University of Kiel.

205. Na, H., et al., *Effect of hot-press on electrospun poly(vinylidene fluoride) membranes.* Polymer Engineering and Science, 2008. **48**(5): p. 934-940.

206. Peng, P., et al., *Phase morphology and mechanical properties of the electrospun polyoxymethylene/polyurethane blend fiber mats.* Journal of Polymer Science Part B-Polymer Physics, 2009. **47**(19): p. 1853-1859.

207. Zhou, Y., et al., *Micro- and macromechanical properties of materials.* 2013: CRC Press.

208. Kayar, M., et al., *Analysing effect of the factors on ultrasonic seam tensile properties of nonwoven fabrics by nested anova design.* International Journal of Clothing Science and Technology, 2015. **27**(6): p. 803-817.

209. Tassaing, T., et al., *Spectroscopic study of the polystyrene//CO2/ethanol system.* Industrial & Engineering Chemistry Research, 2000. **39**(12): p. 4470-4475.

210. Horinouchi, A., et al., et al., *Aggregation states of polystyrene at nonsolvent interfaces.* Langmuir, 2014. **30**(22): p. 6565-6570.

Appendix

I.) Drop on fibre

```
x_2=24.5225;
x_1=4.2345;
theta=32.17;
y_sv=0.04345;
y_lv=0.03167;
n=x_2/x_1
a=(n*cos(theta)-1)/(n-cos(theta));
k=sqrt(1-(a^2/n^2));
t_1=sqrt((n^2-1)/(a*n)^2);
ellipticF(t_1,k);
ellipticE(t_1,k);
L=2*((a*ellipticF(t_1,k))+(n*ellipticE(t_1,k)));
L
V=(0.667*pi*n)*((((2*a^2)+(3*n*a)+(2*n^2))*ellipticE(t_1,k))-
((a^2)*(ellipticF(t_1,k))-((1/n)*((1-a^2)*(n^2-1))^0.5)))-pi*L;
V
A_sl=2*pi*L;
A_lv=4*pi*n*(a+n)*ellipticE(t_1,k);
E=y_lv*(A_lv-(A_sl*cos(theta)));
E
V_act=(((x_1/1000000)^3)*V)*1000000000
E_act=(((E-(y_lv*A_lv))/A_sl)+y_sv)*A_sl*1e-12
```

II.) Stress-strain Curve

a.)

| PS CD | PS MD |

b.)

| PSPU 82 CD | PSPU 82 MD |

c.)

| PSPU 64 CD | PSPU 64 MD |
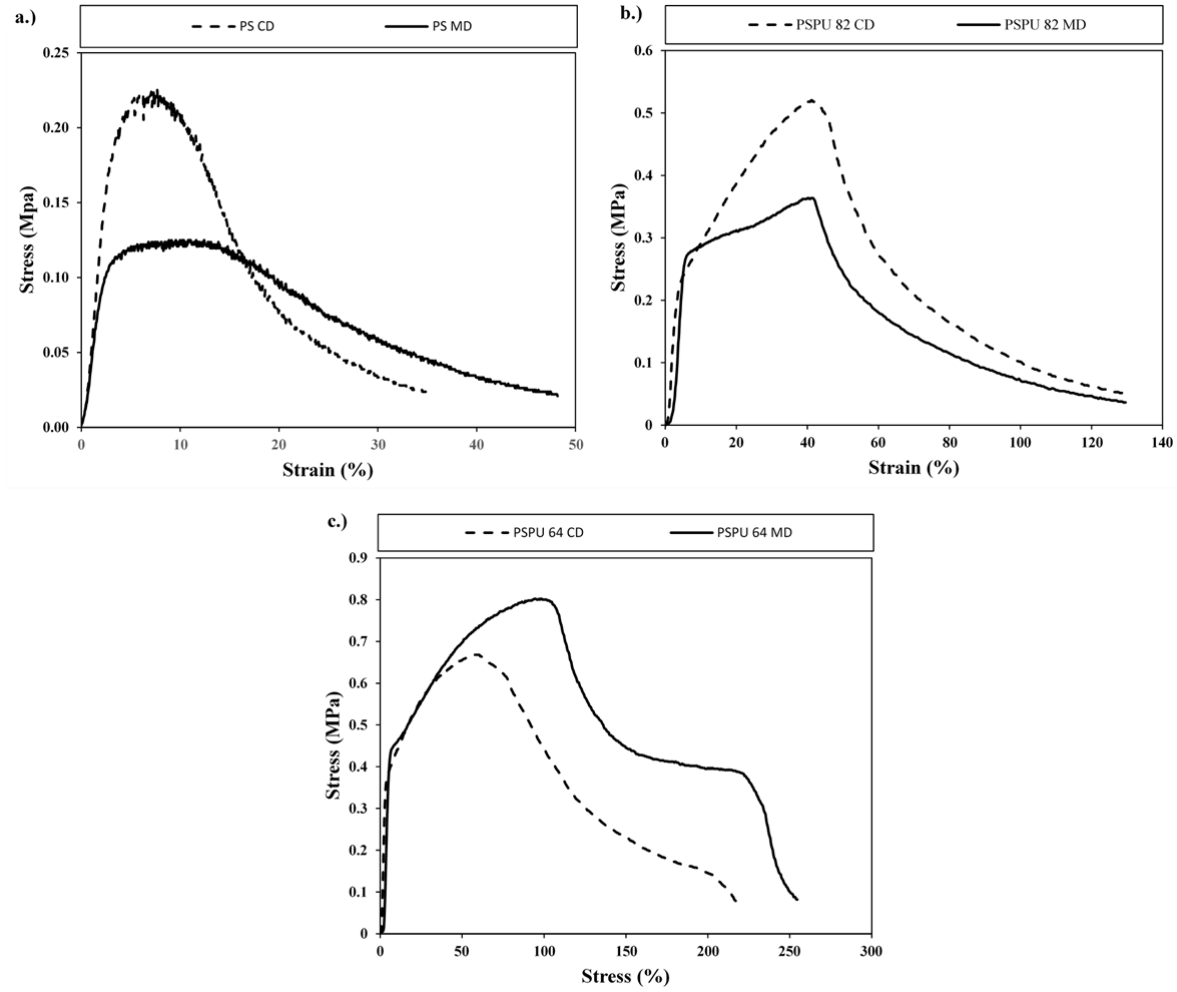
III.) Mat thickness of Ultrasonic treat mat

Sample	PS Untreated	50% EtOH No UT	50% EtOH UT 5min	50% EtOH UT 10min
Mat Thickness (µm)	1200	1090	1090	1090